Defence Research and Development Canada
Recherche et développement pour la défense Canada

DEFENCE R&D DÉFENSE

Study of a Waveguide Antenna Implemented in Laminated Material

Jack O. Litzenberger, Michel Clénet, Gilbert A. Morin and Yahia M. M. Antar

DISTRIBUTION STATEMENT A
Approved for Public Release
Distribution Unlimited

Defence R&D Canada - Ottawa
TECHNICAL REPORT
DRDC Ottawa TR 2002-132
December 2002

Canada

20030320 006

Study of a waveguide antenna implemented in laminated material

Jack O. Litzenberger
Royal Military College of Canada

Michel Clénet
DRDC Ottawa

Gilbert A. Morin
DRDC Ottawa

Yahia M. M. Antar
Royal Military College of Canada

Defence R&D Canada - Ottawa

Technical Report

DRDC Ottawa TR 2002-132

December 2002

AQ F03-06-1358

© Her Majesty the Queen as represented by the Minister of National Defence, 2002

© Sa majesté la reine, représentée par le ministre de la Défense nationale, 2002

Abstract

This document presents the investigation of a novel end-fire antenna implemented in laminated material. This study is related to the development of a phased array for the AEHF Military Satellite Communication Systems. This work includes theoretical analysis, computation of the developed models and measurement of the realised prototypes at 20.7GHz. The antenna element consists of a radiating rectangular waveguide. As a laminated dielectric material, like LTCC material, is supporting the antenna, the vertical walls need to be formed with vias of specific pitch. An effective coaxial-to-waveguide transition has also been developed to feed the radiating element. The results show that this laminated waveguide can be used as an integrated radiating element in the AEHF band for military satellite communications. A five-element array has also been prototyped. Although the results show low mutual coupling between the elements, additional work needs to be carried out to improve the array radiation characteristics.

Résumé

Ce document présente l'étude d'une nouvelle antenne à rayonnement longitudinal implantée dans un matériau laminé. Cette étude est relié au développement d'un réseau à déphasage pour les systèmes de communications militaires par satellites. Ce travail inclus l'analyse théorique, la simulation des modèles développés et la mesure des prototypes réalisés à 20.7GHz. L'antenne élémentaire consiste en un guide d'onde rectangulaire rayonnant. Comme un matériau diélectrique laminé, tel que le "LTCC", sert de support à l'antenne, les parois verticales du guide sont réalisées avec des trous métallisés. Les résultats montrent que ce guide d'onde laminé peut être utilisé comme élément rayonnant dans la bande AEHF. Un réseau de cinq éléments a également été fabriqué. Bien que le couplage mutuel entre les éléments soit faible, une étude supplémentaire est requise afin d'améliorer les caractéristiques de rayonnement du réseau.

This page intentionally left blank.

Executive summary

The requirement for greater bandwidth in military satellite communication systems has resulted in research for systems that can be used in the Extremely High Frequency (EHF) band. To support this requirement, the Department of National Defence has sponsored the development of unique Canadian technology under the Canadian Military Satellite Communications (CMSC) Project. This is part of the Canadian commitment to the United States Advanced Extremely High Frequency (AEHF) Military Satellite Communications project. The end goal is to provide the Canadian Military with worldwide military satellite communications to support Canadian Forces operations.

In collaboration with DRDC Ottawa (formerly Defence Research Establishment Ottawa), the Royal Military College of Canada (RMC) investigated an antenna element for the CMSC project. The antenna was designed to operate in the AEHF band with a broad beamwidth such that it could be integrated into an array. Laminated packaging technology was used to enable packaging of active and passive RF components within a low-loss material in multi-layer topologies.

The antenna element investigated consists of a radiating rectangular waveguide. As the vertical walls of the waveguide are implemented with *vias*, this waveguide is known as a laminated waveguide. Although research has been conducted with laminated waveguides as low-loss microwave transmission, such waveguides have not yet been utilised to realise an integrated radiating rectangular waveguide antenna.

The goal of this project was to develop a single-element prototype antenna and feed system in laminated packaging technology. As a preliminary study the antenna is investigated at the operating frequency of 20.7 GHz. The design utilised a novel coaxial- to-laminated waveguide transition feed system and aperture impedance matching network implemented into a radiating element using laminated packaging technology.

Various prototypes were fabricated and tested to determine the performance of the transition and the antenna. The first prototypes, known as non-radiating laminated waveguides, consist of coaxial transitions at each end of the laminated waveguide. These transitions had very low losses with a bandwidth of 35% of the centre frequency. The remaining prototypes, known as radiating laminated waveguide antenna, consist of a single coaxial transition feeding an open ended laminated waveguide. One of these prototypes had broad beamwidth with the required 1 GHz bandwidth and a maximum gain of 3.65 dB.

This project demonstrates the feasibility for a laminated waveguide to be used as an integrated radiating element in the AEHF band. A low loss broadband coaxial to laminated waveguide transition was also successfully developed as a feed system to the antenna. This very effective transition can be used for any future laminated waveguide devices. To demonstrate the use of the antenna in an array, a five-element laminated waveguide array was prototyped and tested. Although additional work is required in improving the array radiation pattern, the mutual coupling between adjacent antenna elements was quite low.

Litzenberger, J.O., Clénet, M., Morin, G.A., Antar Y.M.M. 2002. Study of a waveguide antenna implemented in laminated material. DRDC Ottawa TR 2002-132. Defence R&D Canada - Ottawa

Sommaire

La demande d'élargissement de la bande passante pour les communications militaires par satellite a engendré l'étude de systèmes de communications opérant en bande EHF. Le Département de la Défense Nationale a donc initié le développement d'une technologie canadienne unique dans le cadre d'un projet de réalisation de systèmes de communications militaires canadiennes par satellite. Ce projet canadien est une partie intégrante du projet américain de communications militaires par satellite en bande EHF, appelé AEHF SatCom.

Le Collège Royal Militaire, en collaboration avec RDDC Ottawa (appelé CRDO précédemment) a développé une antenne élémentaire pour ce projet. Cette antenne a été réalisée pour fonctionner en bande AEHF. Elle possède une large ouverture à mi-puissance, permettant son utilisation en réseau. L'antenne est étudiée en considérant un matériau diélectrique laminé, permettant son intégration avec des composants RF passifs et actifs dans une structure multicouche.

L'antenne élémentaire considérée est un guide d'onde rectangulaire rayonnant. Comme les parois verticales du guide d'ondes sont réalisées par des trous métallisés au travers du matériau multicouche, ce type de guide d'onde est appelé guide d'ondes laminé. Bien que des études aient été effectuées sur les guides d'ondes laminés pour des applications de transmission micro-onde à faibles pertes, ils n'ont encore pas été utilisés en tant qu'élément rayonnant.

Le but de cette étude était de développer une antenne élémentaire et son système d'alimentation en utilisant un matériau multicouche. L'antenne est étudiée à 20,7 GHz. L'étude du système d'alimentation est basée sur la réalisation d'une nouvelle transition câble coaxial-guide d'ondes. Des méthodes classiques d'adaptation d'impédance pour guides d'ondes conventionnels ont été adaptées aux guides d'ondes laminés.

Plusieurs prototypes ont été réalisés et testés afin d'évaluer les performances des différentes composantes. Les premiers prototypes, appelés guides d'ondes laminés non-rayonnants, sont composés d'une transition câble coaxial-guide d'onde à chaque extrémité d'un guide d'onde laminé. Ces transitions génèrent de très faibles pertes, et fonctionnent sur une bande passante de 35%. Les prototypes suivants sont composés d'une transition associée à un guide d'ondes laminé ouvert. Un de ces prototypes présente une large ouverture à mi-puissance, la bande passante requise de 1 GHz, et un gain de 3.65 dB.

Cette étude démontre la possibilité d'utiliser comme élément rayonnant en bande AEHF des guides d'ondes réalisés avec des matériaux laminés. La transition câble coaxial-guide d'onde développée, possède de faibles pertes, et se révèle un système d'alimentation efficient pour cette antenne. Cette transition peut être utilisée pour tout futur élément employant des guides d'ondes laminés. Pour évaluer le fonctionnement de l'antenne en réseau, un réseau de cinq guides d'ondes laminés rayonnants a été conçu et mesuré. Il apparaît que le couplage entre les éléments est très faible. Une étude approfondie est nécessaire pour améliorer les caractéristiques de rayonnement du réseau.

Litzenberger, J.O., Clénet, M., Morin, G.A., Antar Y.M.M. 2002. Study of a waveguide antenna implemented in laminated material. DRDC Ottawa TR 2002-132. R & D pour la défense Canada - Ottawa

Table of contents

List of figures

List of tables

Acknowledgements

This project could not have been completed without the assistance of the Communication Research Centre (CRC).

A substantial effort was undertaken by the CRC, Mr. David Lee in particular, in the fabrication and testing of the circuits designed for this project. The quality of the fabrication and attention to detail is evident in the results. The final designs were very near the limits for tolerances at the CRC model shop, but the staff met the challenge.

1. Introduction

Satellite communication systems can provide the military with the capability of worldwide connectivity. The desire for increased amounts of information and real time data from deployed Canadian Forces (CF) units has resulted in systems that require a large bandwidth. With a large bandwidth, communication systems can provide information from the simple form of Teletype data to real time video conferencing. However, this large bandwidth requirement results in satellite communication systems that operate in higher frequency bands than are currently available. This has resulted in research in communication systems that operate in the Extremely High Frequency (EHF) band.

An additional advantage of operating at higher frequency is miniaturisation. As the frequency increases, the size of the circuitry required decreases in size. This can be easily demonstrated by comparing the systems used for satellite TV. The first satellite systems used for television had parabolic satellite dishes (antennas) with a relatively large diameter (2-3m) because they operated in the UHF band. Today, satellite television (DTV) operates at the Super High Frequency (SHF) band, and therefore requires a much smaller satellite dish size.

One of the key components to a communication system is the antenna. This is a device that can radiate or receive radio waves [1]. Careful attention must be made in designing the antenna, so as not to degrade the performance of the entire system. The antenna is the first device in a chain of components so the antenna specifications must meet or exceed all of the other component specifications.

A principle requirement is always the cost of fabrication. Components must be designed utilising fabrication techniques such that it can be mass-produced at a low cost. Just as research is conducted to improve communication systems, a great deal of research into new packaging techniques provides circuit designers with new material and techniques to realise their circuits. This project utilised a technique known as multi-layer packaging technology to reduce the potential costs of any post prototype fabrication.

This project investigates a new antenna that can be implemented using multi layer packaging technology. This research was completed for the Advanced EHF Satellite Communications Project, referred to as AEHF throughout this project, under the auspices of the Canadian Military Satellite Communications Project (CANMILSATCOM). Although the antenna element investigated in this project is envisioned for future integration into an array, the project focused on the design and prototyping of a single antenna element. Defence Research and Development Canada – Ottawa (DRDC Ottawa) provided the single element specifications and funded the fabrication and testing of all of the prototypes.

1.1. CANMILSATCOM and AEHF

The CANMILSATCOM project was created to provide worldwide secure communication for Canadian Forces personnel. This project is in collaboration with the United States (US) Department of Defence (DoD) and encompasses the Canadian Commitment to the US AEHF project and Military Satellite Communications (MILSATCOM). Through this shared initiative with the US, Canada will have guaranteed access to the worldwide AEHF satellite system.

The satellite system will be comprised of a minimum of five satellites in low inclined geosynchronous orbits with communications in the military EHF band. This band covers both the SHF and EHF bands with an uplink frequency of 43.5-45.5 GHz (EHF) and a downlink

frequency of 20.2-21.2 GHz (SHF). There are a number of advantages to operating military communications in the EHF band.

The first advantage is in the reduction of the physical size of the components. As the frequency increases, the size of the microwave components is reduced. This results in a decreased size for the ground terminals used in the AEHF system. EHF systems also tend to have very narrow beamwidths that result in security benefits such as prevention of jamming, detection and unwanted interception. The EHF band will also allow sufficient bandwidth to provide all of the information management applications and command and control links between ships, submarines, aircraft and ground-based vehicles.

1.2. Laminated packaging technology

Laminated packing technology allows for the creation of multi-level microwave integrated circuits. This technology enables the vertical stacking of components and thus increases the functional density of the circuits. Furthermore, it allows the creation of 3D structures within an integrated circuit. This degree of freedom, in the vertical axis, allows the designer to integrate passive components within the dielectric material.

Two types of laminated packaging materials were investigated for this project. The original project from DRDC specified the use of Low Temperature Co-fired Ceramic (LTCC) for the construction of the antenna.

LTCC is a packaging technology that allows for electronics circuitry to be greatly reduced in size. This is accomplished by stacking components on various levels and by using a moderate dielectric permittivity to reduce the electrical size of the components. Components, such as resistors and capacitors, can be directly integrated within the substrate thus eliminating the requirement for solder joints or wire bonds. Furthermore, as the ceramic substrate is a relatively good insulator, both digital and microwave circuitry can be alternately stacked and integrated within the same package [2]. However, implementation of circuits in LTCC requires a foundry and can be cost prohibitive for prototyping limited runs. Furthermore, the prototype fabrication facility at CRC was not able to implement the circuit in LTCC; therefore a different laminated packaging material was used.

For the purposes of this project, the laminated packaging process of LTCC can be replicated by PCB (Printed Circuit Board) fabrication techniques that allows for the stacking and bonding of various layers of dielectric material. For example, the company ARLON© provides a ceramic dielectric laminate and bonding material that have the same dielectric properties that can be processed using conventional PCB fabrication techniques. However, as LTCC was specified for the final project implementation, the LTCC foundry design guidelines should be followed to allow the design to be converted for future fabrication using the LTCC process.

1.3. Arrays and array architecture

Due to the vast distances between the satellite and ground terminal, antennas used in satellite communication are normally designed with very large gains. For a given antenna, the gain can only be increased by "increasing the electrical size of the antenna" [3]. This can be accomplished by increasing the physical size of an antenna, as seen in the parabolic dishes used in radio astronomy. Such large antennas may not be practical for military use where portability is required. However, the same effect can result from arranging a single antenna element into an array of elements. Such an arrangement is called an array. Although a synopsis of array theory is presented in chapter 2, a general description of array architecture follows.

Array architectures can be generally categorised into one of two types: brick or tile [4]. The two configurations for combining the individual antenna elements into an array are shown in

Figure 1. Brick architecture has some advantages over the tile. First of all, the circuitry required before the antenna (phase shifters, amplifiers, etc.) can be fit within the brick. With the tile architecture, these elements must be fit into additional layers located behind the tiled array and can result in problems of board alignment and dissipation of heat.

As the frequency increases, components become smaller in size and more devices can be placed on the same substrate. This component density can result in heat dissipation problems, which can be overcome with the brick architecture. As seen in Figure 1, brick architecture offers a greater surface area for heat loss than the tile architecture. Therefore, for the EHF band, the brick architecture becomes more practical than the tile architecture [5].

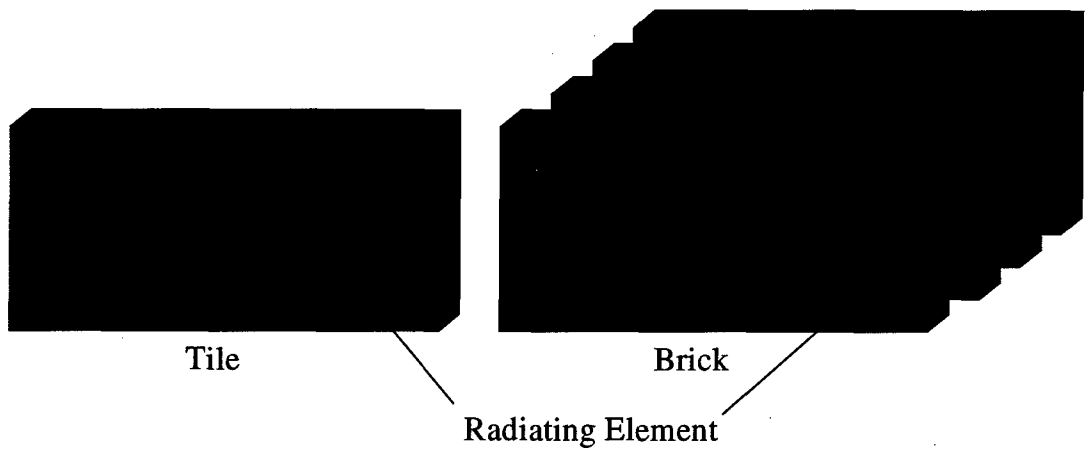

Figure 1. Array Architecture

1.4. Antenna types suitable for brick architecture

Given its suitability for EHF antennas, Brick architecture has been specified as a requirement by DRDC for the AEHF project. However, only certain antenna types, known as end fire radiators, are compatible with this architecture. A brief description of some of these antenna types follows.

1.4.1. Printed dipole antennas

The printed dipole antenna is a monolithic dipole realised on a substrate. In general, it can be treated as a narrow rectangular microstrip patch [6]. For that reason, the radiation pattern will be similar to the microstrip patch with the maximum radiation intensity normal to the dielectric. If the shape of the strip is modified from a rectangular strip to a triangular strip, then

the radiation pattern will be significantly different and the antenna is known as a bow tie antenna. This change in shape results in an increase in the bandwidth of the dipole antenna. Unfortunately, both the bow tie and dipoles have significant radiation in both the forward and backward directions. This would make the antenna undesirable when used in a brick array configuration.

1.4.2. Tapered slot antennas

A tapered slot antenna (TSA) consists of a slot line in which the slot width is gradually increased in order to form an open circuit. This results in a gradual taper of the metal material to form the open end, thus the name, Tapered Slot. In general, a slot line open circuit produces a significant amount of radiation [7], which makes the tapered slot an effective radiator. The Vivaldi configuration, in which the taper is of an exponential form, is shown in Figure 2.

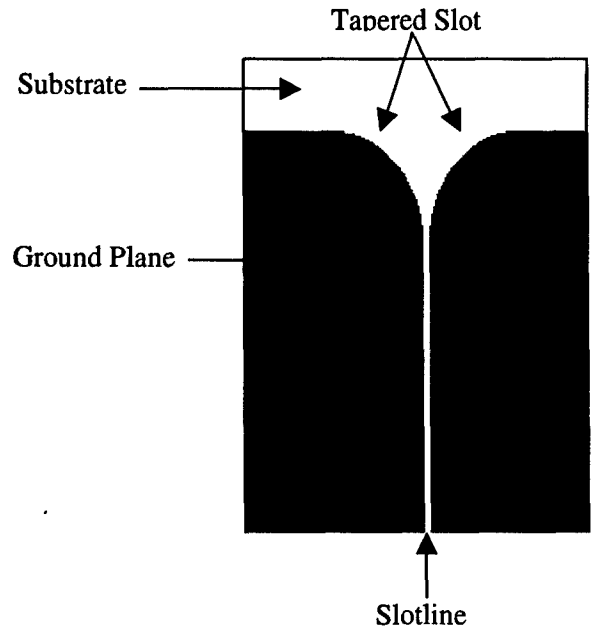

Figure 2. Vivaldi Antenna

The TSA is an end fire travelling wave antenna. Its radiation mechanism consists of a wave that propagates along the slot and then radiates from the discontinuity (open circuit end) of the slot line. Because of this, the radiation will be linearly polarised in the same plane as the slot. As a travelling wave antenna, TSA's are inherently wide band, and are commonly used for satellite communication and phase arrays [8]. Although such an antenna type could be used for the AEHF project, DRDC Ottawa selected two other antenna types for potential AEHF candidates.

1.4.3. Quasi-Yagi antenna

The Yagi-Uda antenna is another end-fire radiator and is essentially an array of dipoles (Figure 3). It is a commonly used antenna for VHF/UHF bands and can be seen on many rooftops as a TV antenna. In its basic form, the antenna is comprised of a reflector, a linear dipole and a number of parallel directors. These antennas are simple to construct and able to be used for a wide variety of applications. In general, a front–to-back ratio (defined as the ratio of forward to backward gain) of 15 dB [9] can be attained with an overall gain of 15-17 dB.

The classical Yagi dipole antenna can also be implemented in monolithic form and used an end-fire radiator for brick architecture arrays. Recent work [10] has been completed to demonstrate the capability of such an element in an array. DRDC Ottawa is currently investigating this antenna type as a potential candidate for the uplink frequency (43.5-45.5 GHz).

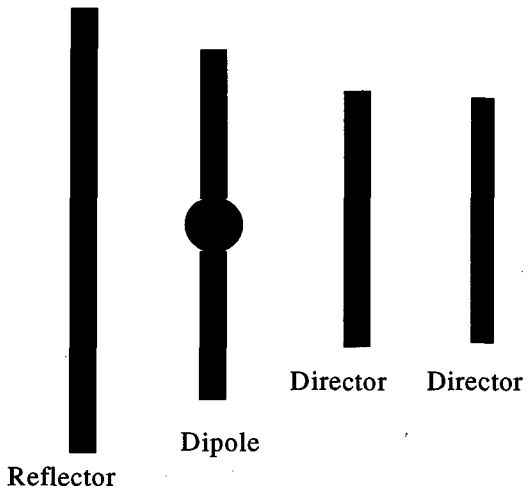

Figure 3. Basic Yagi Antenna Configuration

1.4.4. Aperture antennas

Aperture antennas are widely used at microwave frequencies. They are typically an extension of a round or square waveguide and include antennas that are slots, waveguides, horns, reflectors and lenses. They can be used in both tile or brick array architectures.

The most commonly used shape of aperture at microwave frequencies is square [9]. It is implemented as either a radiating rectangular waveguide, the main focus of this project, or with flared walls to increase the aperture size. Either type is known as a horn. The specific type of horn is defined by the manner in which the walls are flared, given in Figure 4 [11]. If the flare is in the plane of the Electric field, it is known as an E-plane horn. With a flare in the plane perpendicular to the Electric field, the horn is called an H-plane horn. Where there is a flare in both planes, the horn is called pyramidal. The purpose of this flare is to control the beam pattern, aperture impedance and/or gain. When there is no flare, the antenna is a radiating waveguide.

Horn antennas are widely used because of large gain, low Standing Wave Ratio (SWR), wide bandwidth, controllable beamwidth and ease of excitation. However, a horn antenna had not yet been implemented in laminated packaging technology. This made the horn antenna an ideal candidate for DRDC Ottawa sponsored research as a potential candidate for the downlink frequency of the AEHF project.

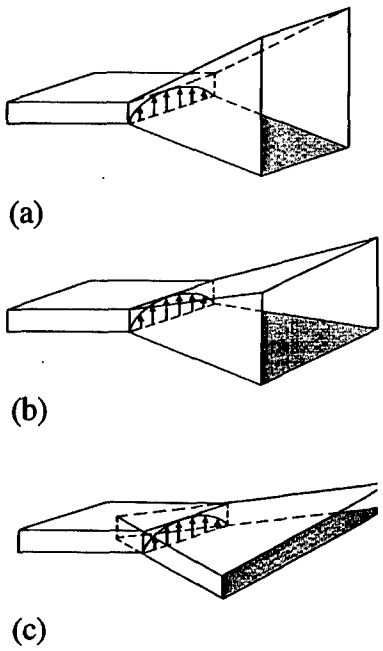

Figure 4. (a) E-plane, (b) Pyramidal and (c) H-plane Horn Configurations

The horns in Figure 4 are extensions of a rectangular waveguide (RWG) with solid vertical walls and thus cannot be realised within a substrate. However, it is possible to implement a RWG with laminated packaging technology. The vertical walls can be replaced by a series of metal posts known as *vias*. Drilling holes in the substrate and then plating the holes with metal form these vias. The bottom and top of the RWG are formed with metal cladding on the substrate. This type of RWG realised within a substrate is known as a laminated waveguide (LWG). A diagram of such a LWG, of width a and height b, is shown in Figure 5. The theory and background of the LWG are presented in Chapter 2.

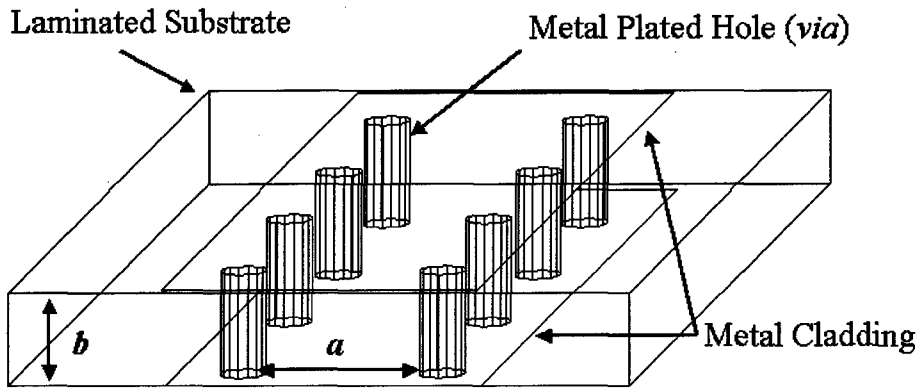

Figure 5. Laminated Waveguide

1.5. Project objectives

The purpose of the project is to determine if a horn antenna could be implemented with laminated packaging technology for use in the AEHF SATCOM project. DRDC Ottawa provided the antenna specifications detailed in Table 1.

Table 1. Single Element Antenna Specifications

Antenna type	Horn or radiating waveguide
Packaging Material	CLTE
Directivity	> 3 dB
Beamwidth	+/- 60 degrees
Bandwidth (SWR < 2)	20.2 to 21.2 GHz
	43.5 to 45.5 GHz

Although there were two possible bands of operation (uplink and downlink), this project investigates the feasibility of realising an antenna in the lower band (uplink) due to the limitations of the testing facilities. Furthermore, to ensure a cost-effective and timely completion of the project, the prototypes were fabricated with another suitable laminated packaging technology and not LTCC.

The primary goal of the project, developing an antenna prototype that meets the specifications, can be characterised by three basic objectives. First of all, it was necessary to determine if a horn antenna could be designed to meet the single element specifications. Then, it was necessary to verify the methods by which an antenna design could be realised in a laminated packaging technology. Finally, a number of prototypes were fabricated and tested.

A number of steps were followed in order to reach these objectives. The first step was to research the radiation mechanism of apertures. This provided the necessary background theory to develop an analytical model of the radiating aperture that could then be realised in the LWG antenna. Given the analytical model, the radiating aperture dimensions of the horn could be determined to meet the gain and beamwidth specifications.

The next step was to develop a more robust model using a modern electromagnetic software package, the High Frequency Structure Simulator (HFSS). This model was then used to take into account certain effects, such as diffraction, not included in the analytical expressions. As well as determining the directivity and gain of the aperture, the HFSS model provided a method of accurately determining the impedance of the LWG and its aperture. This information was required to design the impedance matching circuitry.

There were two difficult impedance matching challenges to overcome. The first was to design an impedance matching network for the aperture using components that could be implemented with laminated packaging technology. This put a design constraint on the types of components and techniques that could be used. Furthermore, a LWG had never been used to implement a radiating RWG within a substrate, so it was not known if matching techniques commonly used for horns and RWG were applicable.

Once the aperture-matching problem was resolved, it was then necessary to design a feed system to excite the desired mode in the LWG. Although there are well known techniques used for feeding RWG, there was limited work published on feed systems for LWG. In fact, to the knowledge of this author, there was no previous published work on coaxial-to-LWG transitions so a completely novel concept had been developed as part of this project.

The final steps were fabrication of the prototypes and subsequent measurement at CRC. Laminated waveguide prototypes with dual coaxial feeds were fabricated in order to demonstrate the performance of the coaxial-to-LWG transition. Various radiating LWG antennas, including an array, were also prototyped to validate the analytical and HFSS models.

1.6. Project organisation

The layout of the project essentially follows the steps described in the previous section. Chapter 2 provides the background theory required to develop the analytical model of the radiating rectangular aperture of the RWG. This is used to determine the directivity of the single element radiator and that of an array of rectangular radiators. Also included in the chapter are the analytical expressions for determining the bandwidth, losses and characteristic impedance of the RWG as well as the necessary background for impedance matching. The final section contains the analytical model for an array of radiating apertures.

Given the necessary theory, the design of the LWG is detailed in Chapter 3. This includes determining the aperture dimensions to meet the beamwidth specifications and a comparison of the analytical and finite element based (HFSS) models. The procedure for designing a LWG and the impedance matching circuitry is provided in detail resulting in specifications for the prototypes.

The fourth chapter contains the main objective of the project. Measured results are compared to the various models in order to validate the various hypotheses and to determine if the single radiating element specifications can be met. Analysis of the array is also provided.

In the final chapter the performance of the prototypes is discussed with an emphasis on the future work required with LWG antennas before use in the AEHF project is possible. To assist in this future work, additional designs are provided to convert the prototype design for use with LTCC fabrication technology. The final section summarises the various accomplishments of

this project. Measured data and some additional prototype analysis are provided in the appendices.

2. WAVEGUIDE THEORY

2.1. Introduction

To understand the method to design a radiating waveguide that is integrated into a laminated substrate requires some background theory. However, before describing the theory behind LWG design, it is first necessary to understand the fundamental hypothesis of this project; the behaviour of the fields of a LWG is the same as a RWG of the same dimensions. Therefore the LWG behaviour can be described by the general solutions to Maxwell's equations for a waveguide.

Assuming that one has a good background into Electromagnetic (EM) Theory, the following sections provide the theoretical background specific to the LWG antenna design and include the theory of:

a. Waveguide Transmission Line (Rectangular only)
b. Radiating Apertures
c. Laminated waveguides
d. Impedance matching and transformation, and
e. Arrays

2.2. Rectangular waveguide

The rectangular waveguide was one of the first microwave transmissions lines and is still widely used. A typical waveguide is fabricated with a hollow conductor. These structures have solid walls, and could not be constructed with laminated packaging techniques. This has resulted in the fabrication of microwave circuitry that tended toward the monolithic variety, known as Monolithic Microwave Integrated Circuits (MMIC), of planar transmission lines (microstrip, stripline, slot line) [12]. However, planar transmission lines leak or radiated EM radiation, especially at discontinuities. Therefore, the best possible transmission line characteristics are obtained from waveguides [13].

In the hollow rectangular waveguide of Figure 6 [14], only traverse electric (TE) or transverse magnetic (TM) waves can exist. Since there is only one conductor, the transverse electromagnetic (TEM) wave cannot propagate in the rectangular waveguide. The TE and TM waves can exist in an infinite number of modes. These modes correspond to the number of standing wave maxima that occur in the directions perpendicular to the direction of propagation [15]. The modes that can propagate are dependent on the geometry of the waveguide.

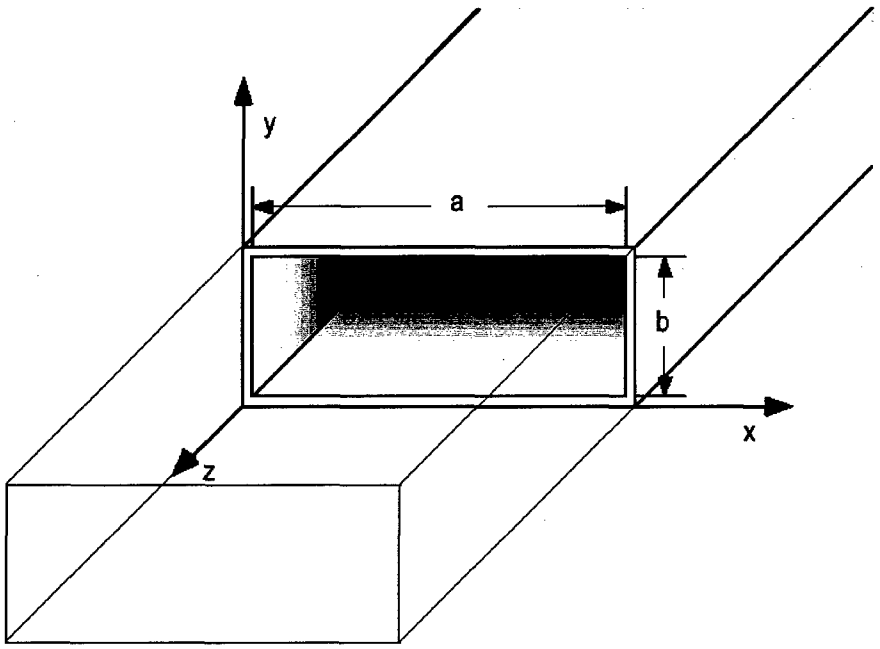

Figure 6. Rectangular Waveguide

For any source free transmission line, Maxwell's curl equations take the form [16]:

$$\nabla \times \vec{E} = -j\omega\mu\vec{H}, \qquad \nabla \times \vec{H} = j\omega\varepsilon\vec{E} \tag{2.1}$$

Using a vector identity the equations can be represented as the Helmholtz Equations

$$\nabla^2\vec{E} + k^2\vec{E} = 0, \qquad \nabla^2\vec{H} + k^2\vec{H} = 0 \tag{2.2}$$

where the wave number $k = 2\pi f\sqrt{\mu\varepsilon}$, with f the frequency, μ the permeability and ε the permittivity.

The solutions of these equations for the TE and TM fields yield the classic results of the propagation modes given at the references [12] [15].

When the mode of propagation is TE, the axial component of the electric field, $\mathbf{E}_z$, must be zero. This will result in the propagation constant

$$\beta = \sqrt{k^2 - k_c^2} \tag{2.3}$$

where k_c is the cut-off wave number given by

$$k_c = \sqrt{(m\pi/a)^2 + (n\pi/b)^2} \tag{2.4}$$

If the wave is to propagate then the phase constant, β, must be real. This is true for $k > k_c$. This results in a cut-off frequency for each mode (m,n) given by:

$$f_{c_{mn}} = \frac{1}{2\pi\sqrt{\mu\varepsilon}}\sqrt{(\frac{m\pi}{a})^2 + (\frac{n\pi}{b})^2} \qquad (2.5)$$

Frequencies below the cut-off will result in fields with an imaginary propagation constant that will attenuate exponentially. These waves are known as evanescent waves.

In general, waveguides are designed for the propagation of one mode, known as the dominant mode. This will simplify the design of elements used to couple energy to and from the waveguide [15]. If more than one mode propagates, the waveguide is said to be overmoded. This is an undesirable condition and results in unwanted losses in the waveguide. Furthermore, as will be seen later, if the waveguide is used as an antenna element, single mode propagation allows for formation of the desired far-field radiation pattern. The dominant mode in a rectangular waveguide is the TE10 mode.

As waveguides do not leak, there are only two loss mechanisms: dielectric losses and losses due to finite conductivity. The losses due to the dielectric in a rectangular waveguide with TE or TM modes are given by [12]:

$$\alpha_d = \frac{k^2 \tan\delta}{2\beta} \qquad (2.6)$$

The losses due to the finite conductivity of the wall conductors (σ_c,) for the fundamental TE10 mode are calculated by:

$$\alpha_c = \frac{\sqrt{\frac{\omega\mu}{2\sigma}}}{a^3 b\beta k\eta}(2b\pi^2 + a^3k^2) \qquad (2.7)$$

The total attenuation constant for the rectangular waveguide is the sum of both coefficients [12].

$$\alpha = \alpha_d + \alpha_c \qquad (2.8)$$

The concept of impedance for a waveguide can often be confusing and requires some additional clarification. When discussing waveguide impedance, two terms are often used: wave impedance and characteristic impedance (Z_o). For any propagating mode, the ratio of the transverse components of the E- and H-fields is defined as the wave impedance [17]. In the TEM mode, the wave impedance is the same as the intrinsic impedance of the medium ($\sqrt{\frac{\mu}{\varepsilon}}$) [17]. For the TE mode, the wave impedance is given by [17]

$$Z_{TE} = \frac{j\omega\mu}{\gamma} \qquad (2.9)$$

The wave impedance is different from the characteristic impedance. In a transmission line the characteristic impedance is a function of the transmission line geometry, dielectric material in the line, and the relation between the incident voltage and current [18]. With a RWG, the characteristic impedance can be defined in terms of voltage, current and power (Z_{VI}, Z_{PV} and Z_{PI}). All three definitions result in the same equation, but differ by a constant. For the purposes of this project, the power current definition is used and is given by [19]

$$Z_{PI} = Z_{TE}\frac{\pi^2 b}{8a} \tag{2.10}$$

2.3. Laminated waveguides

The idea of forming an integrated waveguide within an MIC substrate was first postulated in [20] [13]. The laminated waveguide vertical walls are formed by a series of vias connecting the upper and lower ground planes. This forms a rectangular waveguide within the dielectric substrate as shown in Figure 5 of Chapter 1.

In a RWG propagating the dominant TE10 mode, there is only a vertical component of the electric field. Utilising the coordinates as defined in Figure 2.1, the E-field would only have a component in the y direction. This means that to guide the travelling wave in the z direction, the walls must be able to provide a current flow in the vertical (y) axis to reflect this electric field. This path for the current flow is provided by the vias of the LWG. However the spacing between vias, known as pitch, must be kept sufficiently small such that the guided wave does not leak between the vias [13].

It has been demonstrated [13] [21] that the amount of leakage between the vias increases with via pitch. The leakage, and subsequent losses, increase suddenly when the via pitch exceeds $\lambda/4$ [16]. This forms the fundamental limit for via pitch when designing laminated waveguides. Furthermore, the via pitch should be kept sufficiently small such that the losses from the laminated waveguide are less than that of a planar transmission line, otherwise there would be no advantage in using the laminated waveguide as a transmission line. Both the RWG and LWG can be designed to have lower losses than a planar transmission line in the SHF band (30GHz) [21]. However, the determination of the minimum via pitch is entirely dependent on the capability of the fabrication process.

Although there is no direct analytical solution for calculating the leakage as a function of via pitch, two numerical methods have been successfully used. The first method utilises the Galerkin's method of moments [20] to determine the waveguides attenuation constant as a function of via spacing (pitch). The other commonly used approach involved the use of a commercial Finite Element Base modelling package to estimate the insertion loss for various via pitch configurations [13][21]. The fundamental result of both methods is that the losses increased with via pitch. The FEM with HFSS, detailed in Chapter 3, is used for this project.

2.4. Radiation from rectangular apertures

The dimensions of the aperture and the field distribution of the aperture determine the far-field radiation pattern. Of particular interest, is to determine the dimensions of the aperture (a and b) in order to meet the beamwidth requirements of the specifications. Before detailing the equations and methodology used, it is first necessary to understand some of the basic assumptions.

First and foremost, the aperture of the LWG is assumed to be rectangular defined by the inner bounds of the vias and ground planes. Secondly, it is also reasonable to assume that the far-field radiation pattern between the aperture in an infinite ground plane and that of an aperture in free space would have the same beamwidth and directivity. Finally, the behaviour of the fields inside the LWG is the same as a RWG with solid walls such that the field distribution at the end of the LWG would be TE10. Given these assumptions, the classical technique of the field equivalence principle, detailed below, can be used to determine the far-field radiation characteristics of the radiating LWG.

The field equivalence principle essentially states that the actual sources, such as an antenna, of EM fields can be replaced with equivalent sources within a region when they produce the same fields within that region [9]. This technique is used to determine the fields radiated outside the rectangular aperture. So, the first step in the aperture radiation problem is to select a region where the fields are known. Within the conductor of the Radiating aperture at Figure 2.1, the field distribution is that of TE10 mode given by:

$$\mathrm{E} = \hat{a}_y E_o \cos\left(\frac{\pi}{a}x\right) \quad \begin{cases} -a/2 \le x \le a/2 \\ -b/2 \le y \le b/2 \end{cases} \tag{2.11}$$

where E_o is a constant.

The next step is to replace the actual sources with equivalent sources, electric (J) and magnetic current (M) densities, with the region. For an aperture in an infinite ground plane [9]:

$$\mathrm{M}_s = \begin{cases} -2\hat{n}\times\mathrm{E} \begin{cases} -a/2 \le x \le a/2 \\ -b/2 \le y \le b/2 \end{cases} \\ 0 \end{cases} \tag{2.12}$$

$$J_s = 0$$

Once the sources are uniquely specified over the region, the radiated E and H are given by Maxwell's equations. These equations are normally solved by a two-step process [22]:

a. Determine the magnetic (**F**) and electric (**A**) vector potentials from M and J; then

b. Calculate **E** and **H**.

Although the specifics of the derivations can be found [9], only the solutions are provided here [23].

$$E_\theta = \frac{jkab}{4r} E_o e^{-jkr} \sin\phi \frac{\sin v}{v} \frac{\cos u}{(\pi/2)^2 - u^2} \tag{2.13}$$

$$E_\phi = \frac{jkab}{4r} E_o e^{-jkr} \cos\phi\cos\theta \frac{\sin v}{v} \frac{\cos u}{(\pi/2)^2 - u^2} \tag{2.14}$$

where

$$v = (kb/2)\sin\theta\sin\phi,$$

$$u = (ka/2)\sin\theta\cos\phi$$

Once the far zone fields are known, the radiation intensity and directivity can be determined.

$$U(\theta,\phi) = \frac{r^2}{2\eta}\left(|E_\theta|^2 + |E_\phi|^2\right) \tag{2.15} [24]$$

$$D(\theta,\phi) = \frac{4\pi U(\theta,\phi)}{P_{rad}} \tag{2.16} [23]$$

$$P_{rad} = ab\frac{|E_o|^2}{4\eta} \tag{2.17} [11]$$

Combining the above equations, the maximum Directivity is then given by:

$$D_o = \frac{8}{\pi^3} abk^2 \tag{2.18}$$

It is then possible to predict the E- and H-plane directivity patterns for a radiating rectangular aperture.

E-plane

$$D(\theta, \pi/2) = D_o \left| \frac{\sin v}{v} \right|^2 \tag{2.19}$$

H-plane

$$D(\theta, 0) = \frac{\pi}{2} abk^2 \left| \frac{\cos\theta \cos u}{(\pi/2)^2 - u^2} \right|^2 \tag{2.20}$$

The above result does not include the effects of diffraction at the waveguide edges nor the far-field contribution from field distribution on the outer portions of a radiating waveguide. In the case where the aperture dimensions are much greater than the wavelength, the half-power beamwidth can be approximated by [9]:

E-plane

$$BW = \frac{50.6}{b/\lambda} \tag{2.21}$$

H-plane

$$BW = \frac{68.8}{a/\lambda} \tag{2.22}$$

2.5. Impedance matching

One of the most important elements in microwave circuit design is ensuring that all of the available power is delivered to the load. For an antenna, all of the power from the generator is passed through the transmission line to and from the antenna. This occurs when the transitions between the generator, transmission line and antenna are matched and no energy is reflected at these transitions. To eliminate the reflections at the transitions, matching networks are used.

The type of matching network selected depends on a number of factors [25]. First of all, simple is better. Complex networks are more costly and less reliable. For antenna systems, bandwidth is another important criteria of the matching network. Given the type of transmission line, only certain types of networks will be applicable due to fabrication limits. Finally, the matching network should be variable and thus allow for fine-tuning of the impedance match. [25].

Impedance networks can be constructed utilising reactive elements, lumped elements or impedance transformers. Given the geometry of a LWG, reactive elements are relatively easy to fabricate. Impedance transformers require a specific length of transmission line to implement and it is desirable to keep the antenna element as short as possible. For these reasons, only reactive element matching techniques are discussed.

When tuning, or impedance matching, with reactive elements it is important to design the impedance-matching network by matching the generator to the transmission line and by matching the transmission line to the load [26]. This results in two matching networks, but ensures that the

load and generator matches are independent of each other. The purpose of this is to reduce the frequency selectivity of the matching network.

In keeping with this design philosophy, the design of a matching network for a radiating waveguide has two parts. First it is necessary to excite the waveguide (the generator) in the desired mode. Then, the waveguide transmission line must be matched to the load or aperture. The techniques for accomplishing this are described below.

2.5.1. Aperture match

Given any load, so long as it has a non-zero real part, it is possible to find a matching network [25]. As the waveguide is radiating into free space or air, this condition will always be met. The difficulty is in selecting the reactive elements of the matching network that meet the constraints of the fabrication technique.

A portion of the transmission line itself, in the form of a short or open circuit stub can be used. Given a segment of transmission line with characteristic impedance Zo, length l, propagating a wave with a propagation constant $\gamma = \alpha + j\beta$, and terminated with a load Z_l, the impedance is given by [27]:

$$Z = Z_o \frac{Z_l + Z_o \tanh(\gamma l)}{Z_o + Z_l \tanh(\gamma l)} \tag{2.21}$$

For a short circuited stub, the impedance is then

$$Z = Z_o \tanh(\gamma l) \tag{2.22}$$

When the losses are negligible, it can be seen from the above equation that the short circuit stub can be used as an inductance or capacitance depending on the length such that the normalised impedance is

$$\frac{Z}{Z_o} = \bar{Z} = j\tan(\beta l) \tag{2.23}$$

For any waveguide supporting the dominant TE10 mode, there are a number of elements located within the waveguide that can be used for matching. These elements include the:

a. iris;

b. cylindrical post; and

c. diaphragm.

All of these elements, or discontinuities, result in modes other than TE10 being generated in the waveguide. Energy is stored in the fields of the modes and results in the discontinuity behaving as an equivalent inductance or capacitance. If the energy stored is predominantly from the magnetic field, then the discontinuity is inductive [26]. When the energy is mostly in the electric field, the discontinuity is capacitive. With the fabrication of a LWG, only the post and diaphragm discontinuities are physically realisable as vias.

The cylindrical post is a thin conducing rod that is placed inside the waveguide in the direction of the E-field. When excited by a TE10 mode, the post behaves like an inductance. For a thin post located in the centre of the waveguide, the normalised shunt inductance is given in various texts [26] [28]. However, the post thickness must be less than 5% of the waveguide width [28] and this may not be realisable with standard PCB fabrication techniques.

When the post of finite thickness is in a waveguide, the behaviour depends on the penetration depth [28]. If the depth is less than 70% of the waveguide height, then the post is

capacitive. If the depth is greater, the post behaves like an inductance. There are no simple analytical expressions for reactance of the finite thickness post. However, measured data and the equivalent circuits can be found [28].

Symmetric diaphragms can also be realised in LWG. In a RWG, a diaphragm is a thin conducting sheet that reduces the width of the waveguide. With a LWG, the diaphragm can be realised by vias that are formed close to the waveguide walls, thus forming a narrowing within the waveguide. An approximate expression for the normalised susceptances of a diaphragm of width d in a RWG is given by [26]

$$\overline{B} = \frac{2\pi}{\beta a}\cot^2\left(\frac{\pi d}{2a}\right)\left(1+\csc^2\left(\frac{\pi d}{2a}\right)\right) \qquad (2.24)$$

Once the aperture load has been determined, there are various techniques to tune the load to the transmission line with the simplest being the single stub. As can be seen from Equation 2.21 above, any load impedance can be transformed by moving a distance l from the load. To match with a single stub, or element, the load is transformed to a point where the normalised input admittance is given by

$$\overline{Y_{in}} = 1 \pm j\overline{B} \qquad (2.25)$$

At that point, a shunt susceptance is added such that the admittance $\overline{Y_{in}} = 1$. The transmission line will then be matched to the load.

2.5.2. Coaxial to rectangular waveguide transition.

The matching of the generator to the waveguide is more complicated than that of matching a generator to a transmission line that supports a TEM wave. This is because it is possible to excite more than one mode within the waveguide. Excitation of non-propagating modes is undesirable and results in a waste of energy.

In general, probes, loops or apertures may be used to excite waveguides. Probes are easily implemented in a LWG with vias, and previous work [13] demonstrated that a LWG could be excited by means of a probe. As it is the transition selected for this project, only the probe coupling theory will be covered.

A typical coaxial probe to waveguide transition, shown in Figure 7, consists of a number of elements that can be adjusted to achieve the maximum power transfer. The radiation resistance of the probe (R_o) is determined by its penetration depth (d) and distance from the end of the waveguide (l) as per Equation (2.26) below.

$$R_o = \frac{\eta}{2ab\beta k}\left|1-e^{-2j\beta l}\right|^2 \tan^2\left(\frac{kd}{2}\right) \qquad (2.26)$$

These parameters can be adjusted until the radiation resistance is equal to the characteristic impedance of the coaxial line [26]. This results in the maximum power transfer and the lowest reflection coefficient.

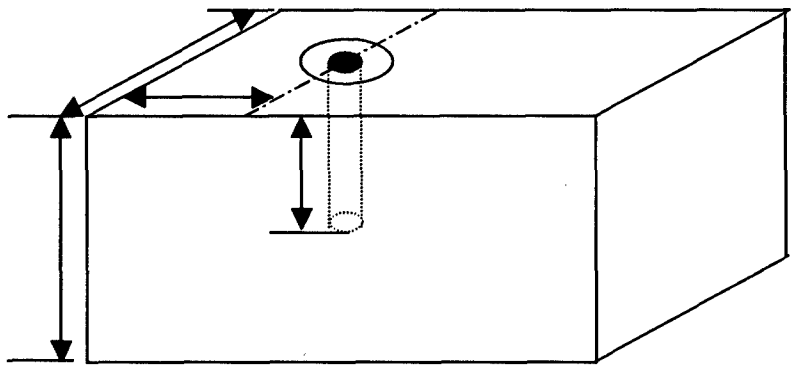

Figure 7. Probe to RWG Transition

Probe transitions are typically narrowband [29], however, there are techniques that can result in a larger bandwidth. It has been demonstrated [29] that using electrically large coaxial line apertures with a probe offset from the centre of the waveguide can result in a significant increase in the bandwidth. The length of the probe and distance from the short circuit can be used for tuning the transition. Unfortunately, adjusting these parameters increases the bandwidth, but at the expense of the minimum SWR in the pass band [29] as describe in the following section.

2.5.3. Bode Fano criterion

As previously discussed, there are a number of techniques and elements that can be used for tuning both the load and generator to the transmission line. Although it is possible to obtain a near perfect match at a single frequency, the antenna must be able to operate over the specified pass band at a minimum SWR. The Bode Fano Criterion gives the relation between the minimum SWR and the maximum possible bandwidth.

This criterion sets the limit on bandwidth, given a minimum reflection coefficient, for any loss less matching network [25]. For series load given by $Z_L = R + jwL$, the Bode Fano Criterion states that the maximum possible bandwidth, $\Delta\omega$, for the reflection coefficient, Γ_m, is given by [25]

$$\Delta\omega \ln\frac{1}{\Gamma_m} \leq \frac{\pi R}{L} \qquad (2.27)$$

The limits for other loads (parallel or series R, L, and C combinations) can be found at the reference [25]. It is important to note that the limit demonstrates an important characteristic for designing matching networks. The bandwidth for a given load can only be increased at the expense of the minimum reflection coefficient in the pass band [25].

2.6. Array theory

The end goal of the CMSC project is to develop an array. Arranging the individual elements in an array has two principle benefits. First of all, by selecting the proper geometry, phase and amplitude excitation of the elements, the directivity can be significantly increased. This is necessary for satellite communication due to the vast distances that the signal must propagate. Secondly, it is possible to electronically steer the beam (main lobe) of the array by controlling the element's phase. This eliminates the requirement for structures and components to mechanically steer the antenna.

The fundamental basis for array theory is that the electric field of an array is the resultant sum of the electric fields from all of the elements. Thus the radiation pattern of an array is comprised of the constructive and destructive interference patterns of the element fields. The result of this is known as the principle of pattern multiplication, which states, "the far-zone field of an array of identical elements is product of the field of a single element and the array factor"[30] which is true if there is negligible mutual coupling between the elements. The array factor depends on the geometry of the array and the relative amplitudes and phases of the excitation of the elements.

For an array of N radiating elements that are uniformly spaced along the x-axis, the array factor (AF) is given by [31]

$$AF = \sum_{m=1}^{N} I_m e^{j(m-1)(kd_x \sin\theta\cos\phi+\beta_x)} \tag{2.28}$$

where I_m is the amplitude coefficient of the element, d_x the spacing between each element and β_x the progressive element phase shift. The resultant radiation intensity of the array from the pattern multiplication principle is then

$$U(\theta,\phi) = \frac{r^2}{2\eta}\left(\left|E_\theta\right|^2 + \left|E_\phi\right|^2\right)\left|AF\right|^2 \tag{2.29}$$

A numerical integration technique can then be used to calculate the total power radiated (P_{rad}) in order to determine the array directivity from Equation (2.16). Analytically, the total radiated power can be found by [24]

$$P_{rad} = \int_0^{2\pi}\int_0^{\pi} U(\theta,\phi)\sin(\theta)\,d\theta\,d\phi \tag{2.30}$$

When an analytical solution cannot be obtained, a series approximation can be used to estimate the above integral. The total radiated power can then be calculated from [24]

$$P_{rad} = \left(\frac{\pi}{L}\right)\left(\frac{2\pi}{M}\right)\sum_{j=1}^{M}\left[\sum_{i=1}^{L} U(\theta_i,\phi_j)\sin\theta_i\right] \tag{2.31}$$

where

$$\theta_i = i\left(\frac{\pi}{L}\right) \qquad i = 1, 2, 3, \ldots L$$

and

$$\phi_j = j\left(\frac{2\pi}{M}\right) \qquad j = 1, 2, 3, \ldots M$$

2.7. Summary

A number of analytical expressions for the RWG were presented in the previous sections. These expressions are used to design a waveguide for the propagation of a wave at a desired mode and frequency, calculate the impedance, and compute the directivity of the aperture formed by the end of the RWG. Also included were the expressions for designing impedance matching networks and probe to RWG transitions. All of these expressions were for a solid walled RWG with the fundamental hypothesis of this chapter being that the RWG expressions are valid for the LWG.

The next chapter uses the formula developed in Chapter 2 to design a LWG antenna. This design is then used to confirm the hypothesis through a finite element based model (HFSS). The design includes an aperture-matching network utilising vias to realise reactive elements and a broadband coaxial probe to LWG transition

3. LAMINATED WAVEGUIDE DESIGN

3.1. Introduction

This section deals with the application of the theory and modelling for the design of a radiating LWG in the lower portion of the AEHF band. In the beginning of the design process and as described in the previous chapter's hypothesis, it was assumed that a radiating rectangular aperture could approximate the fields formed by a LWG aperture. This provides the basic aperture dimensions that would have to be realised by the LWG.

Once the dimensions for the open end of the waveguide are determined, the laminated waveguide can be designed. This requires consideration of the materials available, fabrication limits, and optimisation of via spacing to realise the waveguide within the substrate.

The final step of the design process is to develop the impedance matching networks. This is done in two steps, firstly to match the aperture to the waveguide and, secondly, to match the waveguide to the coaxial probe. Additional designs can then be made to estimate the effect of fabrication tolerances on the matching networks.

3.2. Aperture design

The radiating element specifications, given in Table 1, require an optimum beamwidth of 120 degrees in both the E and H-planes. For a rectangular aperture, the E-plane and H-plane beamwidths are inversely proportional to the dimensions of the aperture [9]. Therefore the broadest beam pattern results from the smallest possible aperture dimensions.

As the aperture is fed by a waveguide, the dimensions of the waveguide must be selected such that only the dominant TE10 mode propagates. The cut-off frequency for this mode will define the lower limit of the pass band with the cut-off frequency of the next higher mode defining the upper pass band limit. When a rectangular waveguide is designed to be used as a transmission line, the dimensions width a and height b, as per Figure 6, are selected to minimise the losses and allow sufficient bandwidth in the dominant mode. There is a compromise between the bandwidth and attenuation so the width is normally selected to be in the order of twice the height [33]. This results in the first two operating modes being TE10 and TE20. In this case, there is a basic rule of thumb that the frequency of operation for the waveguide, in relation to the cut-off frequencies of the dominant mode (f_{c10}), is given by [32]:

$$1.2 f_{c10} < f < 1.8 f_{c10} \tag{3.1}$$

For a radiating aperture, the height and width must also be selected to achieve the desired beamwidth. As it was desirable to have the E- and H-plane patterns as symmetrical as allowable, Equations 2.19 and 2.20 can be used to show that $\frac{a}{b} < 2$. This results in the first two propagating modes being TE10 and TE01. Utilising Equation 2.5, the dimensions of the waveguide can be calculated as follows.

$$a = \frac{1}{2 f_{c10} \sqrt{\mu\varepsilon}} \tag{3.2}$$

$$b = \frac{1}{2 f_{c01} \sqrt{\mu\varepsilon}} \tag{3.3}$$

Given the above equations, the dimensions of the waveguide can be determined such that only the dominant mode propagates. The next step is to establish the cut off frequencies. The waveguide rule of thumb indicates that the centre frequency should be at least 20% of the centre frequency from the cut-off frequency of the dominant mode. Applying this 20% guideline results in the cut-off frequency for the two modes (TE10 and TE01) being at 17 and 25 GHz respectively. This results in aperture dimensions with the broadest possible beam pattern for a minimum 20% pass band.

3.2.1. Selection of the material

Initially, the project was to be implemented with LTCC. However cost and time constraints led to the decision to find another type of material that could be used to prototype the final design. CRC had some experience with fabricating microwave circuits with laminated copper clad dielectric. There was bonding material (CLTE-P) that could be used with a variety of dielectric materials, but CRC recommended using CLTE laminate. This laminate and bonding material were specifically designed to be used together and had the same dielectric properties. CLTE was chosen for the following reasons:

a. CRC had successfully fabricated laminates up to 50 sheets thick.

b. The bonding material and substrate had the same dielectric constant so the final laminate would be essentially homogenous, similar to LTCC.

c. Both the laminate and bonding material were provided at no cost by ARLON©.

The laminate and bonding material could be drilled before and after lamination.

Table 2. CLTE Material Properties

Property	Value
Dielectric Constant	2.94
Loss Tangent	0.0025

Once the material is selected, it is possible to determine the dimensions of the waveguide for a 20% pass band between the two cut-off frequencies.

a=5.14mm (202.5 mil)

b=3.48mm (137 mil)

(Note: Although it is not the standard, mils (1/1000") had to be used as the units for the design since the PCB fabrication facilities used imperial units.)

CLTE is available in a variety of dielectric thickness from 0.254 mm (10 mil) to 3.175 mm (125 mil) with a bonding material thickness of 0.061 mm (2.4 mil). As the goal was to emulate the LTCC process and provide the greatest degree of flexibility in thickness, the 0.254 mm substrate was selected. However, to simplify the fabrication process, models could be constructed with two layers (3.175 mm and 0.254 mm), thus realising a 3.48 mm (137 mil) thick dielectric.

To determine the number of layers with the thin dielectric requires a relatively simple calculation. The waveguide height (b) is the same as the thickness of the substrate and a TE01 cut-off frequency of 25 GHz requires b= 3.50 mm. With the finite thickness defined by the 0.254

mm for the dielectric and 0.061 mm for the bonding material, there are two possible configurations:

a. 11 layers of dielectric and 10 layers of bonding films results in a final thickness of 3.40 mm; or

b. 12 layers of dielectric and 11 layers of bonding film with a final thickness of 3.72 mm.

Using the 11-layer configuration resulted in a TE01 cut-off of 23.5 GHz; therefore the 10-layer configuration was selected (TE01 cut-off of 25.7 GHz), thus maintaining the desired 20% bandwidth.

3.2.2. Aperture directivity.

The first method used to determine the directivity is through the analytical equations presented in the previous chapter. Given the aperture dimension of 3.40 mm by 5.13 mm (134 by 202 mil) for a CLTE filled waveguide at 20.7 GHz, the resultant directivity obtained form Equation 2.18 is $D_o = \frac{8}{\pi^3} abk^2 = 2.49 = 3.96dB$.

The E and H-plane plots, from Equations 2.19 and 2.20 are provided below in Figure 8.

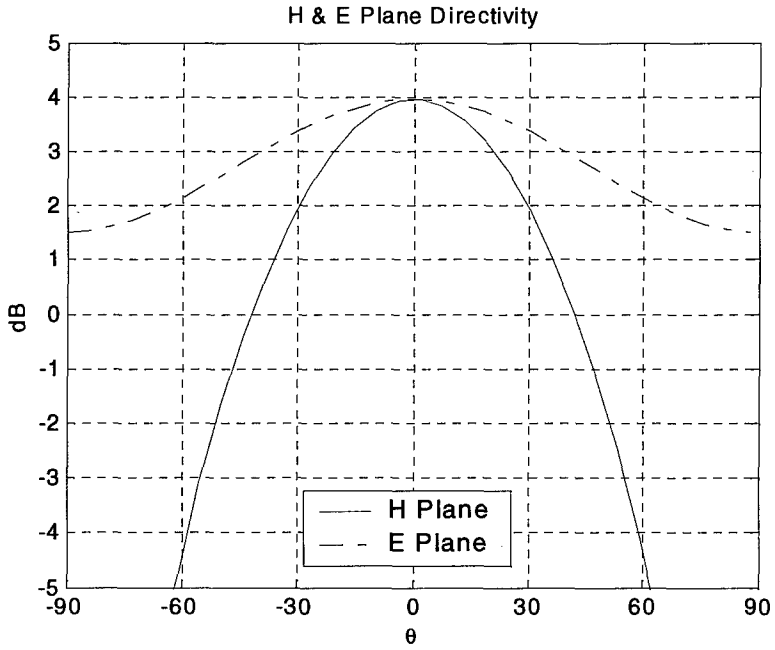

Figure 8. Radiating Aperture Directivity

Another method for calculating directivity is by using commercial EM Simulation packages. In the design for this project, the ANSOFT © HFSS software, referred to as HFSS, was used. HFSS is a FEM based that calculates S-parameters and full-wave fields for arbitrarily shaped 3D passive structures [34]. This software was selected as the FEM can be used for structures with finite dielectrics that occur in dielectric filled radiating waveguides.

Using the same dimensions and material properties as in the analytical expression, a radiating RWG was modelled using HFSS. The simple HFSS model consists of an open-ended RWG, filled with the CLTE dielectric, radiating into free space. The results for maximum directivity are compared in Table 3, and the E- and H-plane radiation patterns in Figure 9. The E-plane and H-plane radiation patterns, obtained analytically and with HFSS, are compared in Figure 10.

Table 3. Directivity Comparison

Method	Directivity (dB)
Analytical	3.96
HFSS	3.82

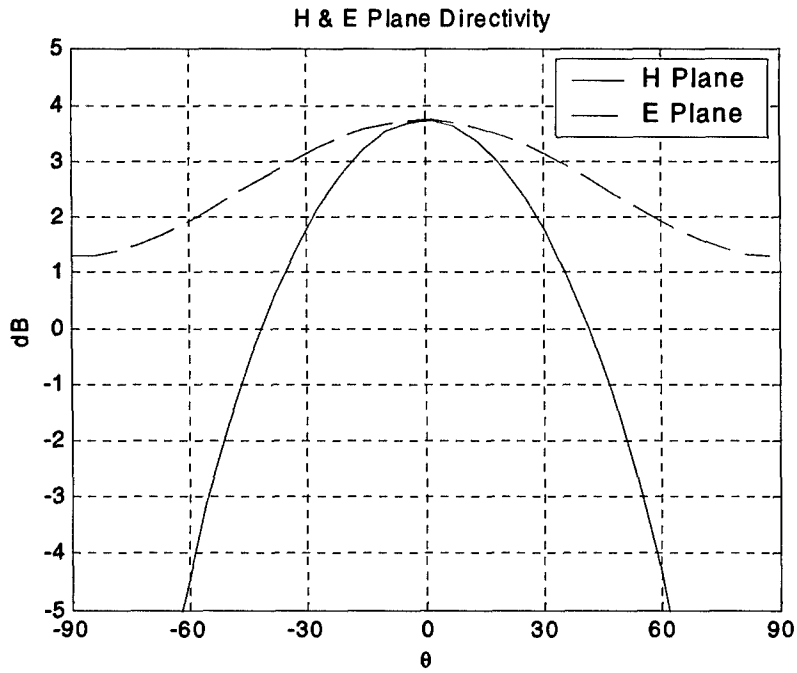

Figure 9. ADP Radiating RWG in HFSS

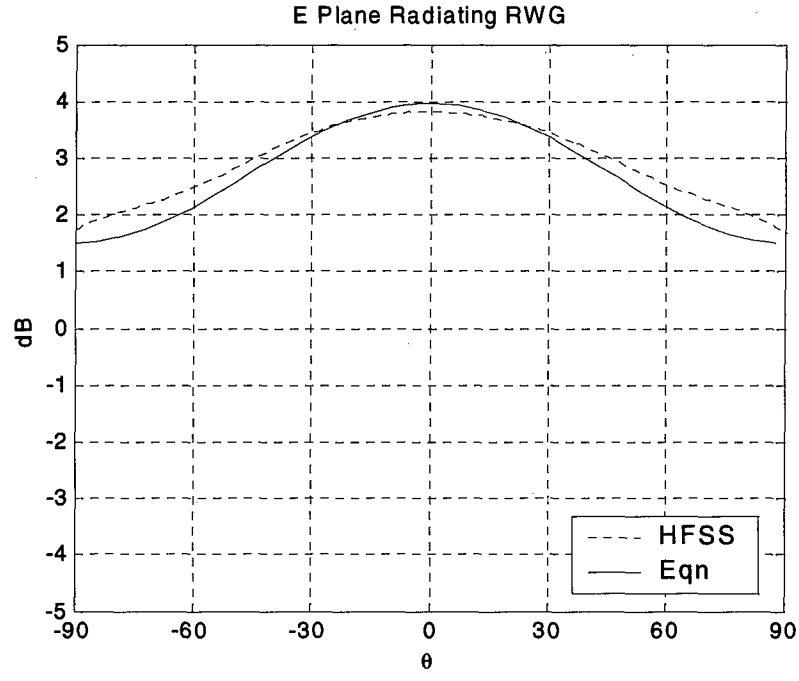

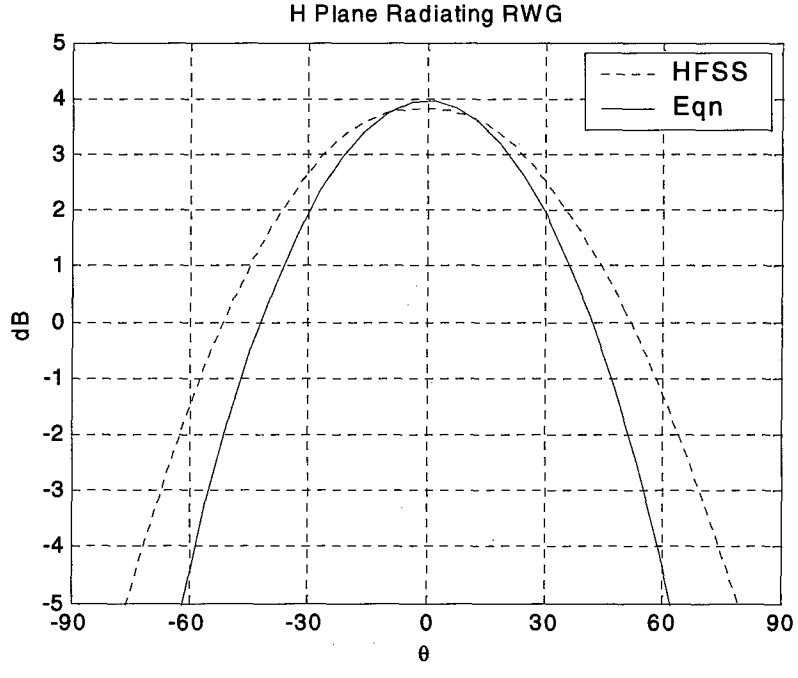

Figure 10. E- and H-plane RWG Radiation Pattern Comparison

The comparison between HFSS and the analytical solution are quite close. However, there are differences in the beamwidth in both the E- and H-planes. As mentioned in Chapter 2, the far-field pattern from the analytical equations does include the effect of diffraction at the edges of the waveguide. Furthermore, the effect of this diffraction is a desirable result as the element specifications call for a broad beamwidth. The results are sufficient to confirm the following:

a. the model and boundary conditions were correctly formulated within the simulated structure; and

b. HFSS can be used to predict the directivity of radiating RWG.

In Figure 10, E-plane beamwidth obtained from the results of both models exceeded the 120-degree beamwidth specification. The H-plane beamwidth (90 degrees for HFSS and 73 degrees from aperture theory) is less than the specification. However, a further decrease in width would put the TE10 cut-off frequency too close to the centre frequency. For example, a width decrease of 0.25 mm (10 mil) results in a beamwidth increase of only 1.5 degrees but a TE10 cut-off frequency increase to 18 GHz. Therefore, it is not theoretically possible to achieve the beamwidth specifications, in the H-plane, for a radiating aperture with a 20% pass band. Decreasing the width, as seen in Equation 2.10 will also decrease the maximum directivity. Thus, one can conclude that the height and width of the aperture are at the optimal value.

3.3. Laminated waveguide design

Once the dimensions of a RWG are known, it is then necessary to realise the same aperture in a LWG. The first physical properties to determine are via pitch and diameter. In the design guidelines from CRC, the via pitch is normally in the order of twice the via diameter. Logically, the smallest via diameter would then provide the greatest amount of flexibility in realising the walls and impedance matching networks.

Previous research has investigated the relationship between via pitch and insertion loss [13]. A minimum insertion loss could be obtained if the pitch size is 10% of the wavelength in the dielectric material. Thus, the pitch size, d, can be determined by:

$$d = 0.1\frac{2\pi}{k} = 0.846mm \text{ (33.3 mil)} \qquad (3.4)$$

This results in a via diameter of 0.423 mm (16.7 mil). The closest drill bit for the milling machine at CRC has a diameter of 0.406mm (16 mil). Therefore a 0.406 mm diameter via with a pitch of 0.812 mm (32 mil) was selected for the original designs of the LWG.

Table 4. Insertion Loss for 0.406 mm via ϕ and various pitches

Via Pitch (mm)	3.66 (<λ/4)	1.83 (<λ/8)	0.914 (<λ/16)	0.813 (<λ/32)	RWG (Cu)	RWG (PEC)
|S21|	0.834	0.936	0.95	0.95	0.957	0.961
Insertion loss (dB)	1.58	0.57	0.44	0.44	0.38	0.35
α (Np/m)	7.49	2.70	2.09	2.09	1.80	1.66

Using the same analysis technique as previous technical papers [13] [21], HFSS can determine the transmission characteristic of LWG with various via pitch configurations. These are compared to the solid RWG modelled with both Perfect Electric Conductor (PEC) and copper walls in Table 4. For all of the simulations, the physical parameters (width= 5.13 mm, height=3.40 mm, length=24.27 mm) and the dielectric properties of the material filling the waveguides are identical. The simulations were all conducted at the same frequency (20.7 GHz).

As there was some debate whether or not a 0.406 mm bit could be used with a 3.40 mm thick substrate, the same calculations were done for the optimum pitch with a 0.508 mm via as shown in Table 5.

Table 5. Insertion Loss 0.508 mm ϕ via

Via Pitch (mm)	0.813 (<λ/32)
|S21|	0.952
Insertion loss (dB)	0.43
α (Np/m)	2.04

A further comparison can be made between the LWG and RWG to verify the behaviour of the LWG. As described in Chapter 2, it is possible to predict various characteristics of the TE10 mode in a solid wall rectangular waveguide through analytical expressions. The field behaviour was also modelled with HFSS for both the solid wall and via-walled (LWG) waveguides. These results, detailed in Table 6, demonstrate that an optimum via spacing in a LWG has the same characteristics as a solid wall waveguide (RWG). Furthermore, the close agreement with the analytical results further validates both the HFSS predictions and the hypothesis that the characteristics of a LWG could be approximated analytically by a RWG.

Table 6. RWG and LWG Characteristics Simulation vs Calculation

	Z_{PI} (Ω)	β (rad/m)	α (Np/m)
RWG (Analytical)	316.87+j1.36	422.12	1.81
RWG (HFSS)	316.49+j1.37	422.59	1.80
LWG (HFSS)	316.57+j1.29	422.52	2.04

3.3.1. Attenuation comparison

Given a LWG with the minimum pitch, the insertion loss is very close to that of a solid wall copper waveguide. As shown in Chapter 2, it is also possible to determine the losses from the conductor and dielectric (Equations 2.6 – 2.8) of a RWG. One of the stated reasons for using LWG as a transmission line is its property of being less lossy than that of a planar transmission line. Using the quasi-static equations to determine the losses, it is possible to demonstrate that the

LWG, with the dimensions given, would have less loss than that of both the microstrip line and stripline.

The dielectric loss for a TEM wave in both the stripline and microstrip transmission lines is given by [12]:

$$\alpha_d = \frac{k \tan \delta}{2} \tag{3.5}$$

Attenuation, for a microstrip line, due to the conductor loss can be approximated by [12]:

$$\alpha_c = \frac{\sqrt{\omega\mu / 2\sigma}}{Z_0 W} \tag{3.6}$$

where W is the strip width.

The stripline conductor attenuation can be found from [12]

$$\alpha_c = \frac{2.7\times10^{-3}\sqrt{\omega\mu / 2\sigma}}{30\pi(h-t)} Z_o A \tag{3.7}$$

where

$$A = 1 + \frac{2W}{h-t} + \frac{1}{\pi}\frac{h+t}{h-t}\ln\left(\frac{2h-t}{t}\right)$$

with h=dielectric thickness and t=strip thickness.

The values of h and W can be found with a commercial transmission line calculator, assuming TEM propagation for the case where the desired microstrip and stripline impedance $Z_o = 50\Omega$. The calculated attenuation for the three types of transmission lines is summarised in Table 7. Although the RWG dimensions are selected for maximum beamwidth and not minimum attenuation, the approximate calculations show that the RWG can have lower losses than microstrip and very slightly less loss than that of stripline.

Table 7. Attenuation Comparison

Transmission Line	α (Np/m)
RWG (5.13 x 3.40 mm)	1.805
Microstrip (W=0.643 mm, h=0.254 mm)	2.098
Stripline (W=0.373 mm, h=0.630 mm, t=17.5 μm)	1.811

It is also possible to compare the losses of the LWG with RWG and the above planar transmission lines using a full wave solver (HFSS). This is necessary as the frequency is high enough that the quasi-static approximation of the analytical expression may not be valid at 20 GHz. These results are summarised in Table 8.

Table 8. RWG and LWG Characteristics Simulation vs Calculation

Transmission Line	LWG $d = 0.813$ mm $\phi = 0.406$ mm	LWG $d = 0.813$ mm $\phi = 0.508$ mm	Microstrip	Stripline
Insertion Loss (dB)	0.44	0.43	0.31	0.48

The above analysis is significant. Where it is necessary to connect the antenna to the other integrated circuitry, the LWG portion of the antenna makes an efficient microwave transmission line. At 20.7 GHz, the LWG is less lossy than a stripline transmission line.

3.4. Coaxial-to-probe transition design

The design of the coaxial probe transition was completed by first modelling the transition in a CLTE filled RWG (Figure 11). This is necessary to decrease the number of tetrahedra in the FEM solution and increase the speed of the simulations. The model consists of a RWG with two wave ports: one for the coaxial (port 1) and one on the radiating end (port 2) of the RWG. To further increase the speed of the simulations, all of the RWG walls are simulated as solid PEC.

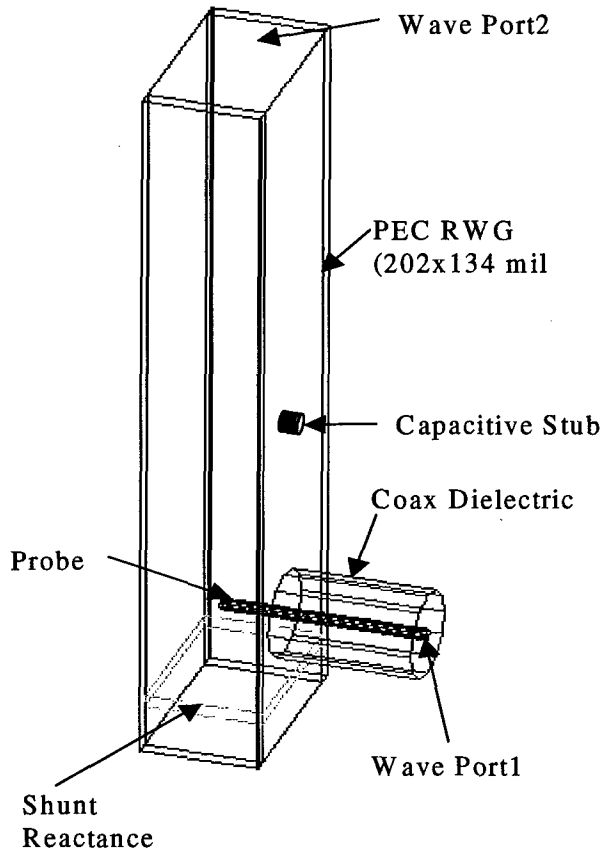

Figure 11. PEC Model (All dimensions can be found in the appendix)

The methodology for designing the LWG to coaxial probe transition is similar to that suggested for RWG probe transition given in [29]. For RWG, a broadband coaxial feed can be realised by using an offset probe and an electrically large aperture in the waveguide. The transition can be matched to the coaxial line adjusting the probe penetration depth and the shunt reactance, which is formed by the short-circuited back wall of the waveguide. The process, as completed with HFSS, is detailed below.

For the first simulation, the probe is placed $\lambda/4$ from the back wall, in the centre of the RWG with a probe penetration of $3/4b$. To improve the bandwidth, the probe is then moved off the centre and the probe length changed until the minimum S11 is achieved with the largest bandwidth. The back wall (a shunt reactance) is then moved to further improve the match. The final tuning is accomplished with a capacitive stub. As can be seen in Figure 13, a wideband coaxial to RWG transition can be achieved over almost the entire useable bandwidth (note there are two cut-off frequencies for TE10 and TE01 at 17GHz and 25.5 GHz respectively). Although the above process appears simple, in practice it took a large number of simulations to achieve a good result.

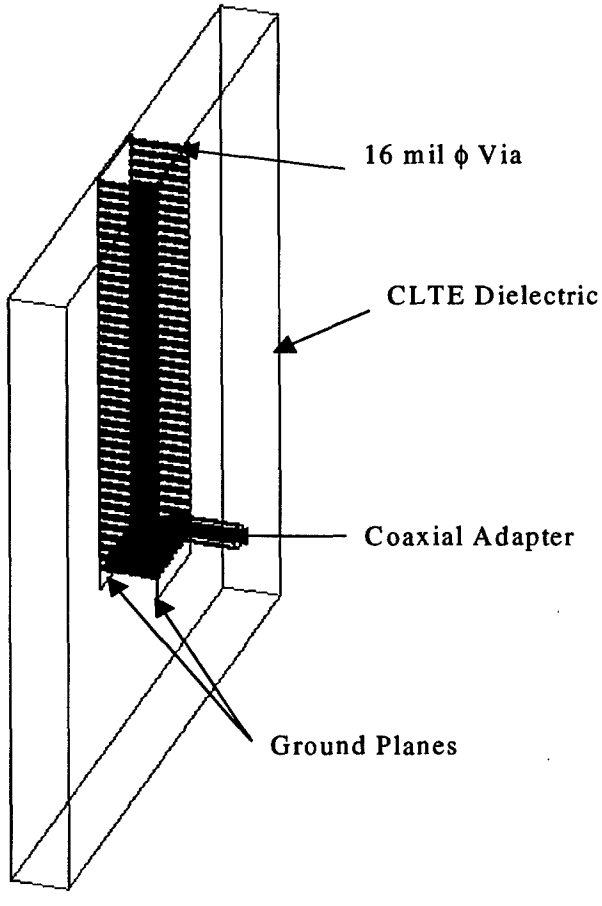

Figure 12. Coaxial-to-LWG Transition

Given the PEC model, it is necessary to convert the RWG to a LWG. The solid walls are replaced with PEC 0.406 mm ϕ vias with a 0.813 mm pitch as seen in Figure 12. As with the

PEC model, wave ports are located on the radiating edge and on the face of the coaxial adapter. Such a model generates a large number of tetrahedra in HFSS due to the vias and takes significant time to solve. The results are compared in Figure 13.

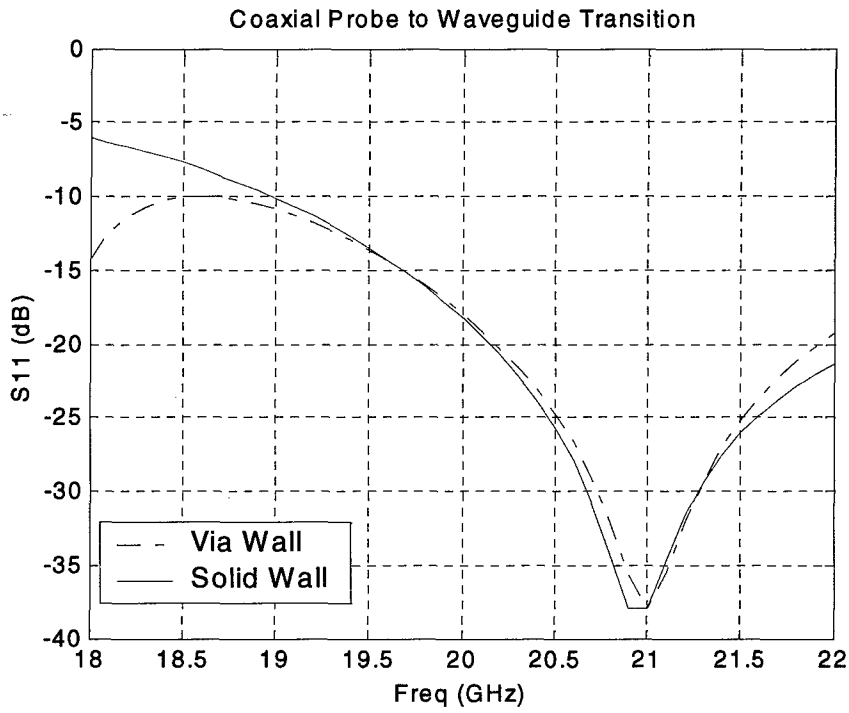

Figure 13. Coaxial Probe to Waveguide Transition

As can be seen from Figure 13, there is very little difference between the match achieved with solid wall RWG and a LWG. The matches are nearly identical. This further confirms that the fields and impedances of a LWG are very close to that of a RWG. It also provides evidence that matching techniques that are valid for a RWG can also be used in a LWG.

The next step in the transition design is to develop a model that can be built and tested. This model, shown in Figure 14, consists of the LWG with coaxial probe transitions at each end. Fabrication and modelling such a prototype are required to measure the effectiveness of the transition. This prototype allows for the estimation of the transition S-parameters that can be confirmed by measurements. As is it probable that other circuit types could be developed using laminated waveguide, a broadband transition may be essential for future work.

As the antenna specifications only call for a 1 GHz bandwidth, the capacitive stub, shown in Figure 11, is not required. Furthermore, simulating the entire pass band (17-25 GHz) requires a significant amount of computational time, therefore only the pass band of interest is simulated. The resultant S-parameters, by HFSS, are given below in Figure 15.

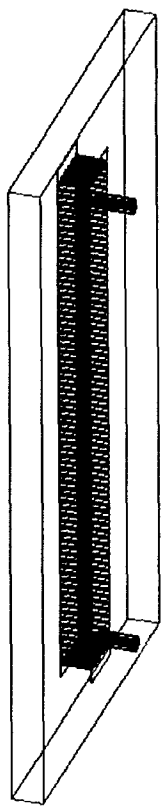

Figure 14. Coaxial-to-LWG Transition

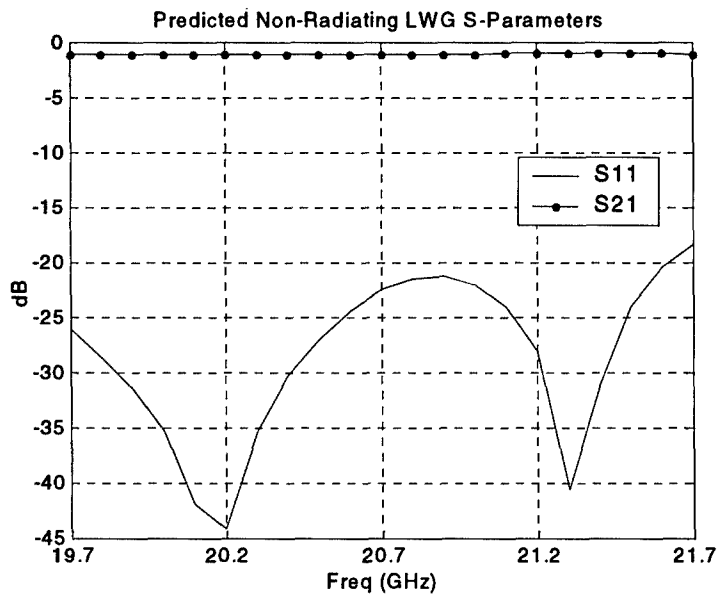

Figure 15. Non-Radiating LWG S-Parameters

The above results are very promising. Over the band of interest, the return loss is less than –20 dB with an insertion loss greater than –1.1 dB. The HFSS model clearly demonstrates that a broadband low loss coaxial transition can be designed using techniques applicable to RWG. Now that a design exists to excite the LWG with a coaxial line, the next step is to design the impedance network to match the aperture to the LWG.

3.5. Aperture impedance matching

In the previous simulations, the RWG and LWG have rectangular wave ports placed on the radiating aperture. This results in the aperture being a perfectly matched load necessary for the design of the transition. However, the LWG is to radiate into free space. Once the rectangular wave ports are removed, there is an impedance mismatch between the LWG and the aperture load. By replacing the coaxial probe with a rectangular wave port, HFSS can then be used to design the necessary matching components to match the aperture load to the LWG transmission line.

Before attempting the simulations required for matching the LWG aperture, matching techniques were first performed using a PEC RWG. The simulated model is similar to that of Figure 11 except that the RWG radiated into an air box and a rectangular wave port replaced the coaxial probe. Once the aperture impedance is calculated by HFSS, the load can be transformed with Equation 2.23 by moving a distance from the aperture where normalised input admittance is given by $\overline{Y_{in}} = 1 - j\overline{B}$.

At that point, a shunt susceptance in the form of a capacitive post is added. A capacitive post was selected as an initial tuning element as it could be easily realised in the LWG in the form of a blind via. By varying the length and thickness of the post, the aperture can be matched to the LWG. Although an excellent match can be designed (S11 < -30 dB) at the centre frequency, the bandwidth does not reach the desired 5% (1 GHz) as seen in Figure 16.

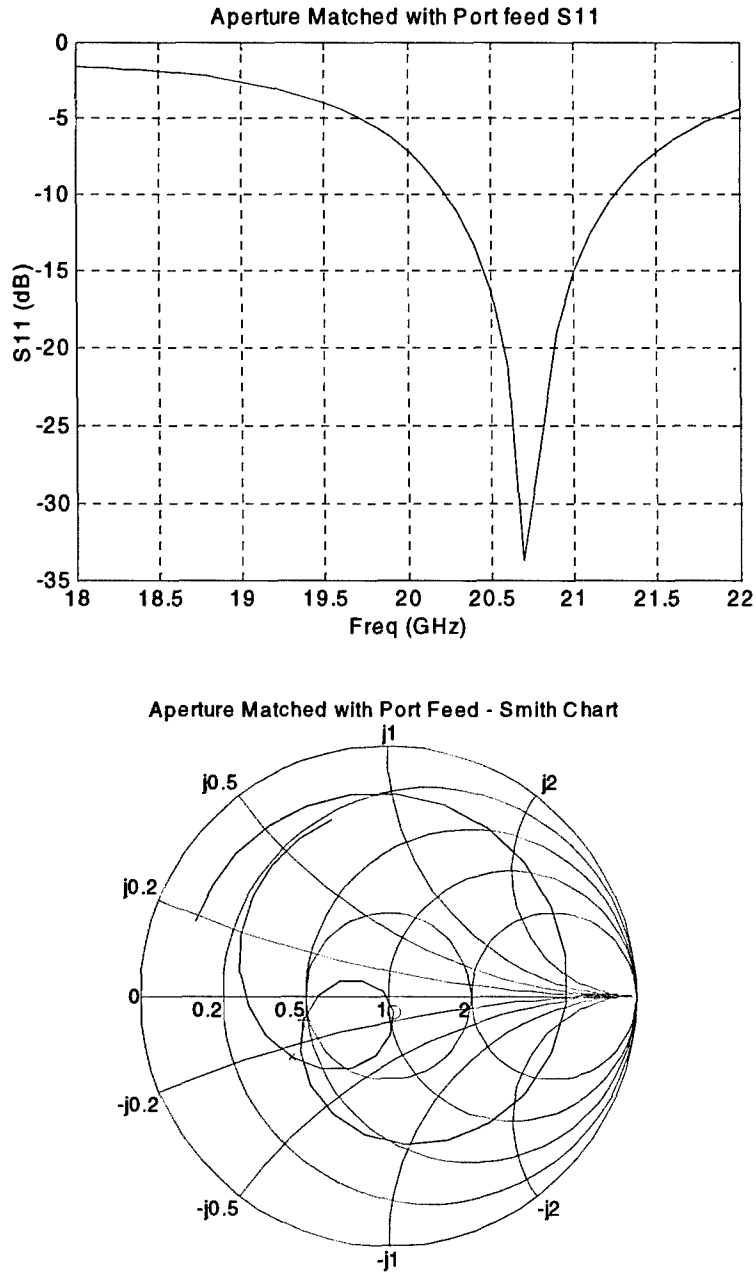

Figure 16. PEC Radiating Waveguide Input Impedance

The Smith Chart in Figure 16 reveals that the match is primarily capacitive. Making the load more inductive can increase the bandwidth. An inductance, in the form of a diaphragm, was added at λ/2 from the LWG aperture. The inductive diaphragm consists of two vias, same length and diameter as the vias that form the LWG walls, which reduce the width of the LWG forming a thin narrow window inside the LWG. When excited by TE10, the vias behaves as an inductive

diaphragm in a RWG. Thus the final aperture matching consists of a capacitive stub and an inductive diaphragm with the bandwidth results at Figure 17.

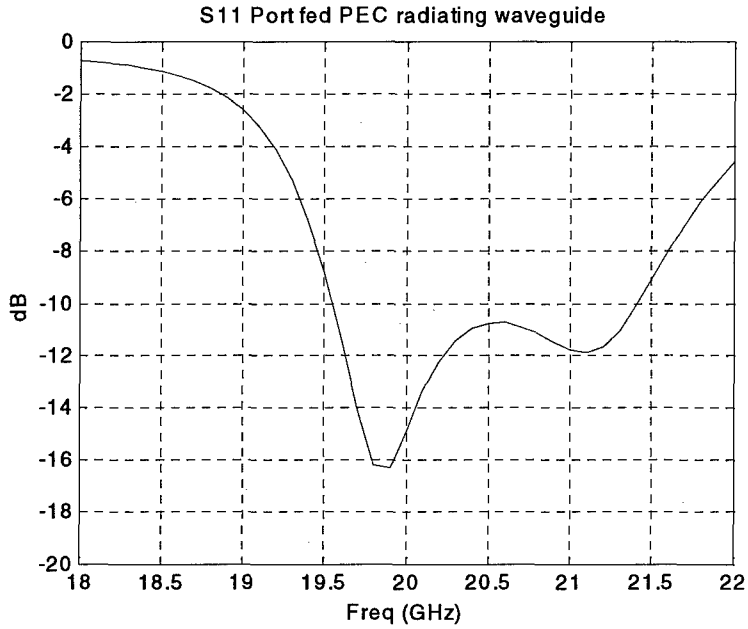

Figure 17. Input Impedance of the PEC Radiating Waveguide with Inductive Diaphragm

The above simulations demonstrate some significant points. First of all, achieving a wide band aperture match with reactive elements is not as simple as the theory would have one believe. Achieving the narrow band match with a capacitive stub/post is a commonly used method for tuning rectangular horns, so it is a logical decision to attempt the same thing with a radiating RWG. Capacitive posts are relative easy to design, and might be possible to implement with a small screw to allow for post-fabrication tuning. The final point is that the bandwidth can be increased with the inductive diaphragm, which resulted in an increase in the minimum reflection coefficient. This result is predicted by the Bode-Fano criteria.

Given the above aperture matching technique for a CLTE filled RWG, the next step is to implement the match in a LWG. As the outer edge of the LWG consists of two round vias, the aperture impedance and matching components are different than the PEC model. However, the matching technique is still valid.

HFSS was first used to determine the impedance at the port. Given the distance to the load and the propagation constant inside the waveguide, the aperture impedance was calculated to be Z_L=335.80 – j425.82. This resulted in |S11| = 0.51 at the centre frequency. As described in Chapter 2, the load has a non-zero real part, thus a matching network can also be realised.

Using the same technique for achieving an initial narrow band match as above, a capacitive stub was placed at the minimum distance from the load (aperture) such that the normalised admittance Y_L= 1-jB_L. By adjusting the thickness and length of the stub, as shown in the HFSS model of Figure 18, the S11 can be reduced thus matching the aperture to the LWG. It is important to note that a capacitive stub is not entirely reactive and has a small resistive component. However, adjustments to stub length and thickness resulted in the match shown in Figure 19. A symmetric boundary condition was used for the inner wall to reduce the complexity of the simulation.

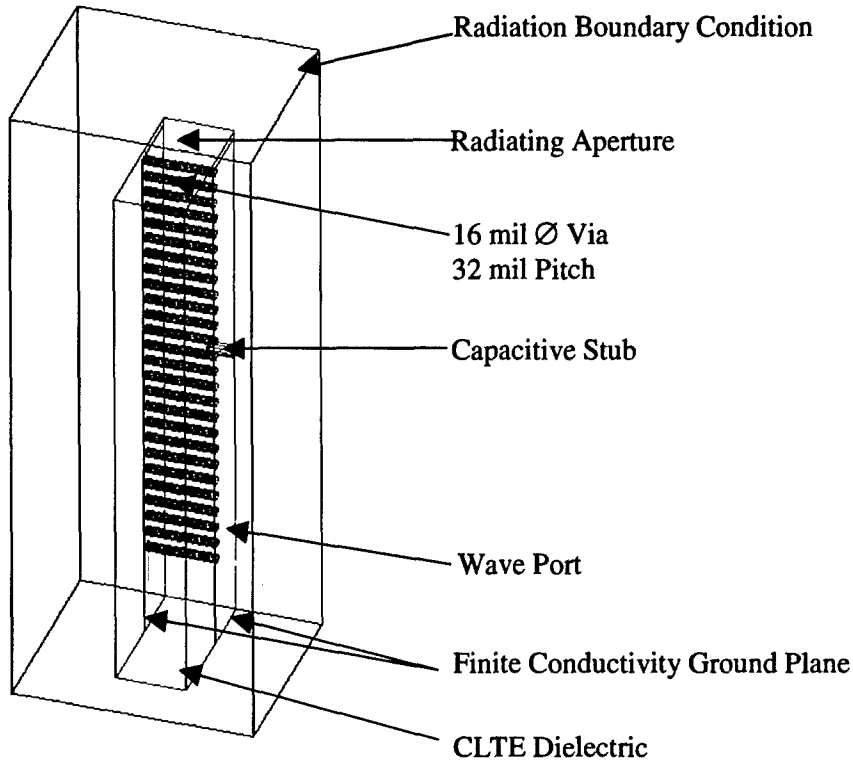

Figure 18. Aperture Match HFSS Model

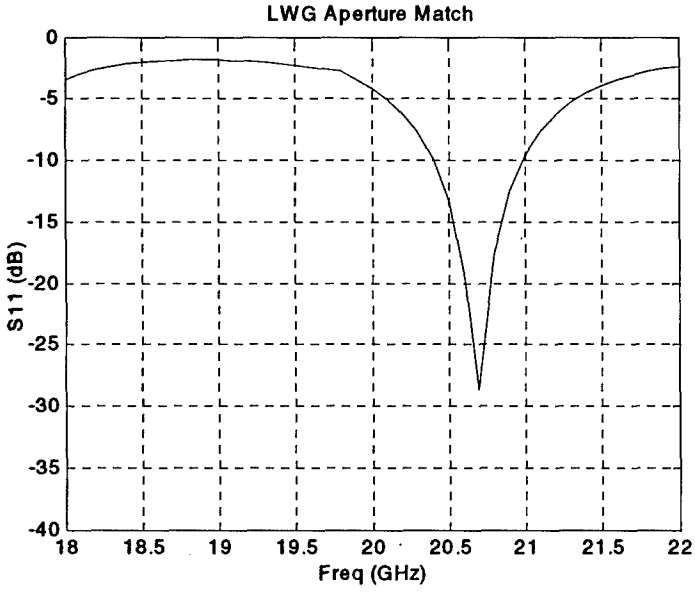

Figure 19. LWG Aperture Bandwidth

As with the initial aperture match with the RWG, the capacitive stub resulted in a narrowband match. An inductive diaphragm could be used to increases the bandwidth but the effect of the coaxial transition on the aperture was not known. Therefore, it was prudent to complete the final tuning and broad banding after integrating both the aperture matching and coaxial transition designs. The final model was then the combination of the two designs.

3.6. Integrated LWG design

The final step in the design modelling stage is to integrate the aperture-matching model with the coaxial transition model. Although the original design and subsequent models were developed using 0.406 mm ∅ vias, the 3.40 mm substrate was too thick for that via configuration. However, thick substrates could be drilled with a 0.508 mm ∅ bit, so the final models are designed for the larger via diameter.

Two versions of the LWG were designed, with one being a longer version of the other as shown in Figure 20. An elongated LWG is necessary for potential testing as an array element. For the element spacing, $\lambda_o/2$, there is insufficient room for the coaxial adapters. As the aperture matching and probe transition circuits were designed independently, it is possible to lengthen the LWG without changes to the design. The two models, the short and long radiating LWG, are depicted below.

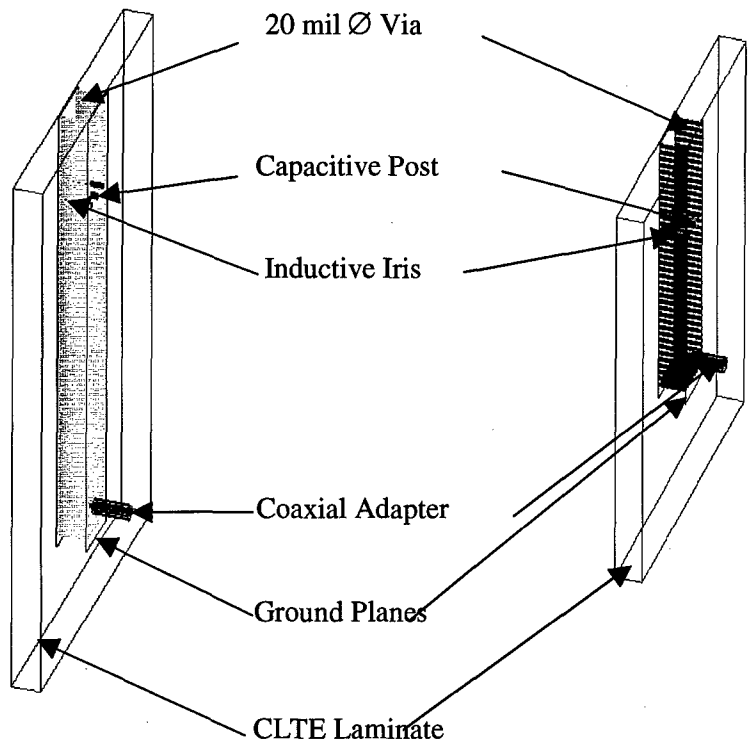

Figure 20. Long and Short Radiating LWG

Following the hypothesis that the LWG aperture field could be approximated by a radiating RWG, it is possible to calculate the directivity analytically as defined in Chapter 2. These results can be used to validate the simulations performed by HFSS for both the maximum directivity and the E- and H-plane radiation patterns. The maximum directivity results are summarised in Table 9. The maximum directivity results predicted by HFSS for the RWG and LWG are extremely close to the analytical results.

Table 9. Directivity Comparison

	D_o (eqn. 2.18)	RWG (HFSS)	LWG (HFSS)
Directivity	2.49	2.41	2.43

The SWR results and far-field patterns for both the HFSS modelled results of the radiating LWG are given in Figure 21 and Figure 22. Figure 23 details a comparison of the LWG radiation pattern from HFSS with that predicted by the analytical expressions (2.19) and (2.20) for a radiating RWG.

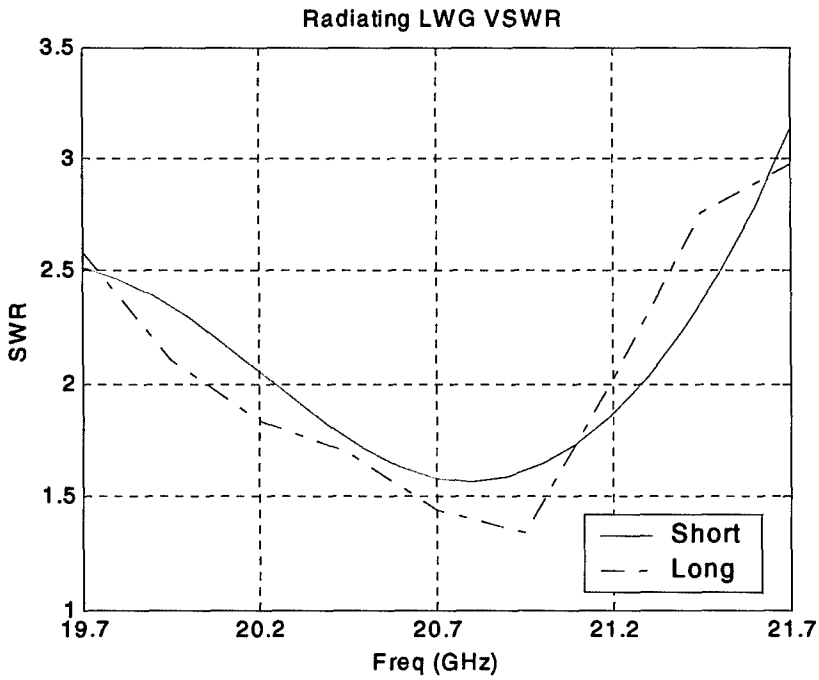

Figure 21. Radiating LWG SWR

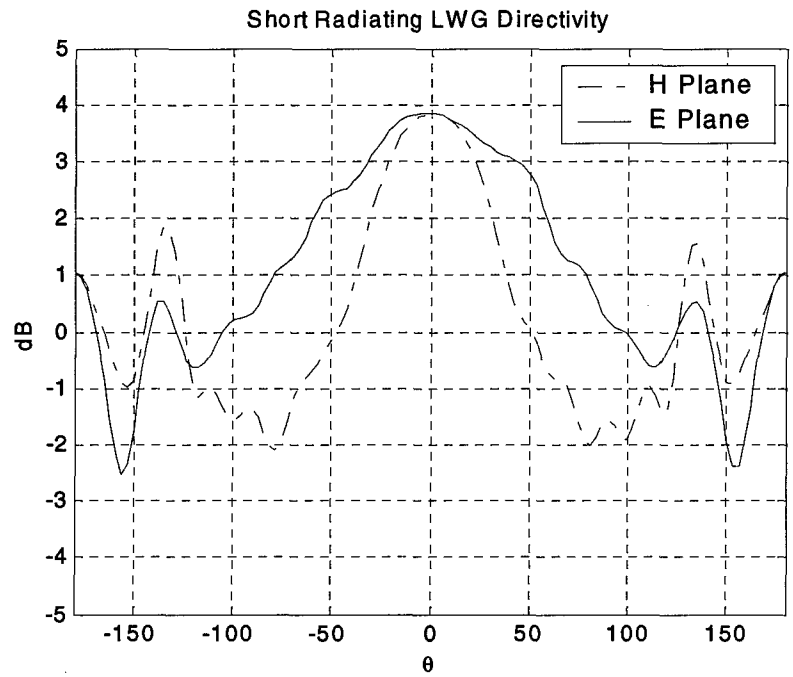

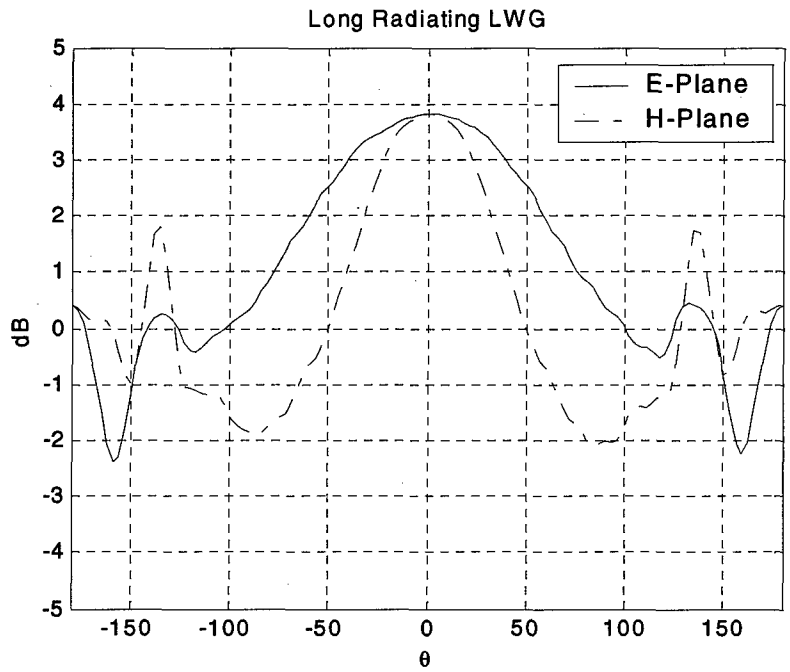

Figure 22. Short and Long Radiating LWG Directivity

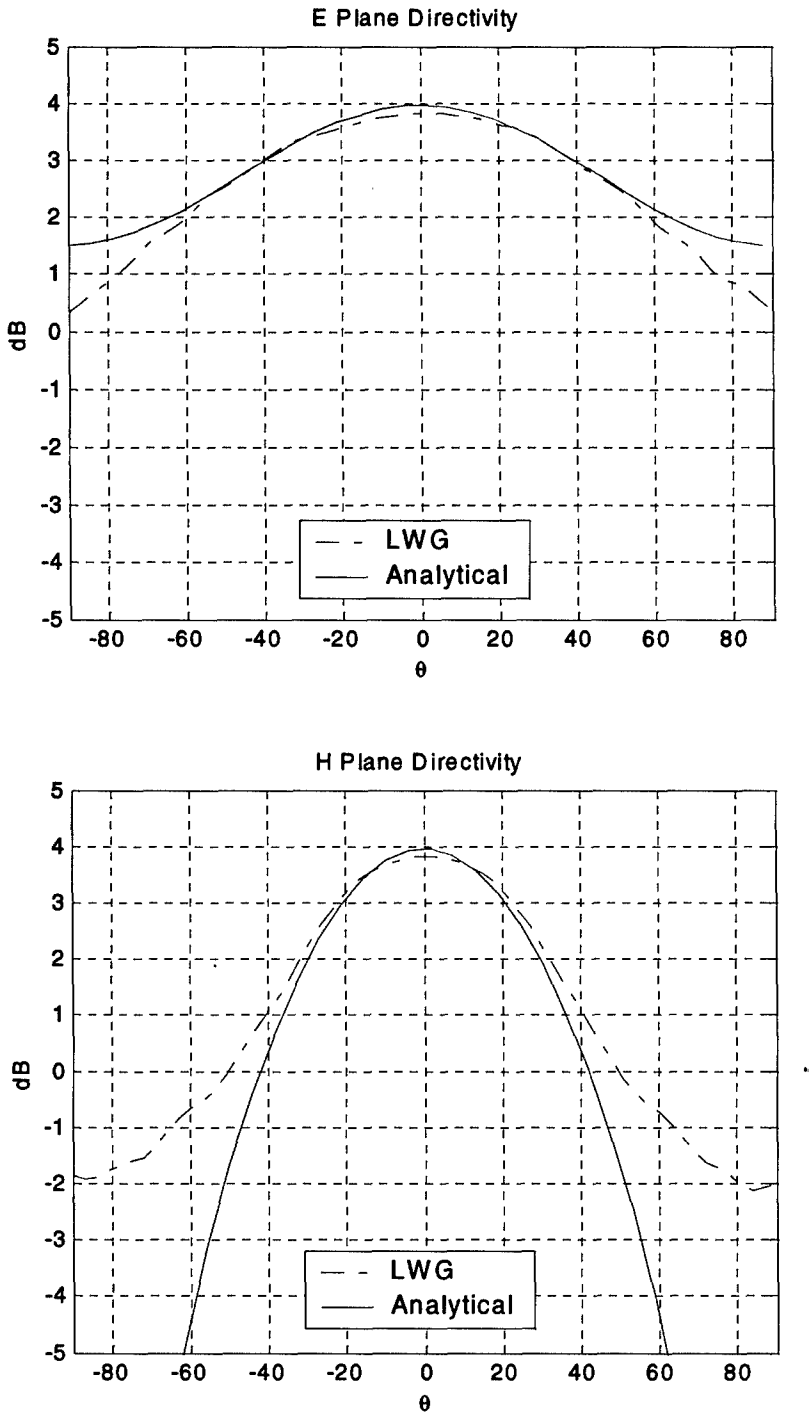

Figure 23. E- and H-Plane Long LWG Comparison

As can be seen from Figure 3.16, the desired bandwidth was obtained for both elements. In Figure 23, the HFSS ADP of the LWG strongly correlates with that of a radiating RWG within

the main lobe's 3 dB beamwidth. The beamwidths of the LWG (Figure 22) is very broad being 78° in the H-plane and 162 ° in the E-plane. As an array element, the LWG could be used for scanning ± 39° from the bore sight with a maximum single element directivity of 3.85 dB. The designed element also has sufficient bandwidth (20.2 to 21.2 GHz) for operation in the AEHF band as seen in Figure 21. Although a slightly broader beamwidth in the H-plane is desired for the AEHF project, this could only be accomplished by decreasing the aperture size at the expense of reducing both the bandwidth and maximum directivity of the antenna.

The ADPs of both the long and short elements have significant side lobes at +/-135 degrees. These side lobes were not present in the analytical rectangular aperture result or the HFSS result for a radiating RWG. There is, however, a significant difference between these models and the LWG models that may account for the side lobes. The LWG models are fabricated within a finite width block of dielectric substrate. It is suspected that the additional side lobes are caused by diffraction at the edges of the substrate.

3.7. Radiation pattern improvement by RF chokes.

Figure 22 reveals one of the principle areas of concern with a radiating LWG in that there is a significant amount of back radiation from a single element. When the elements are combined into an array the back radiation may result in interference with the circuitry feeding the antenna. The back radiation can be reduced with a beam shaping device known as an RF choke [35].

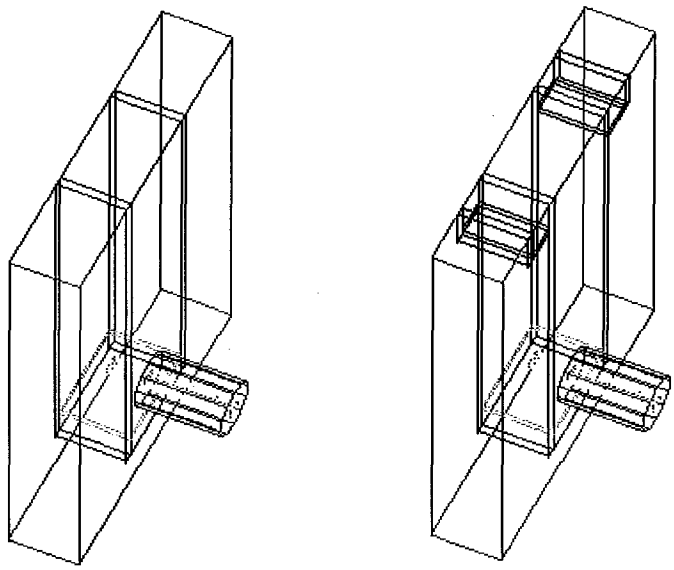

RWG RWG with RF Choke

Figure 24. RF Choke Configuration

An RF choke is a short-circuited stub located on the outside edge of the radiating aperture as can be seen in Figure 24. The fields that diffract around the aperture edge, heading toward the back of the antenna, are attenuated by the choke thus reducing the back radiation. Although such devices are used with cylindrical horns, RF chokes can also be used with rectangular apertures (horns and RWG).

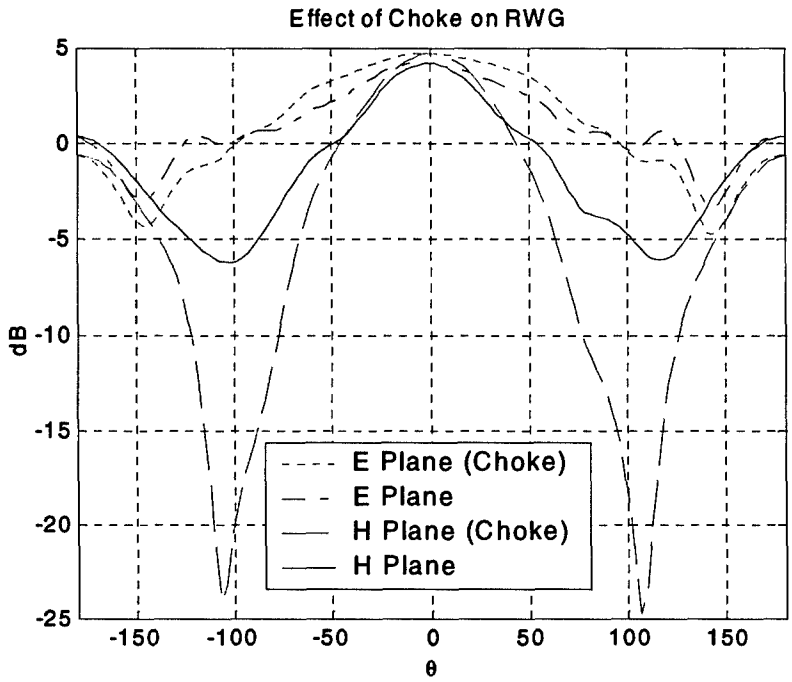

Figure 25. HFSS Simulated ADP of RWG with/without RF Choke

The results shown in Figure 25 demonstrate the effect of a RF choke on the ADP of a radiating RWG. HFSS was used to determine the effect of placing an RF choke in the H-plane of the RWG. The directivity at +/- 180° was reduced by 1 dB for both the E- and H-planes with about ½ dB increase in the main lobe maximum directivity. Thus, as with the cylindrical horn, an RF choke could also be used to sharpen the beam of a radiating RWG and reduce the back radiation. Chokes could also be placed in the E-plane; however, this would increase the thickness of the substrate. Nevertheless, the greatest impact of the choke was near +/- 135-degree of the H-plane. This is close to the location of the large side lobes noted in the LWG radiation patterns in Figure 22. Thus, such a choke may be more useful for reducing the effect of diffraction from the edges of the substrate than for reducing the back radiation levels.

Obviously, the RF choke has a desirable affect on the ADP, however it increases the size of the antenna. Given the current aperture dimensions, the addition of an H-plane choke will increase the width of the antenna. This will increase in the minimum spacing of elements in an array. Whether or not the increased complexity in fabricating LWG with chokes is worth the moderate advantages gained in the ADP would require additional research and is considered to be beyond the scope of this project.

3.8. Summary

The end result of the analytical and HFSS analysis in this chapter was two-fold. First of all, the original hypothesis that a LWG could be closely approximated by a RWG appears to be quite plausible. This allowed for the basic dimension of the LWG antenna aperture to be determined from the analytical expressions for a RWG. Given the aperture dimensions, HFSS was used to determine a sufficient via pitch and diameter to realise the vertical walls of the LWG. Once the basic LWG parameters were known, various HFSS models were then used to design the impedance matching networks for the coaxial transition and aperture. Once integrated, these models formed the specifications for the fabrication of the various prototypes. In the next chapter, the measured results, antenna gain patterns (AGP) and S-parameters, from a variety of LWG prototypes are compared to the models designed in this chapter.

4. ANALYSIS OF LWG PROTOTYPES

Using the designs from both the radiating and non-radiating LWG models developed in the preceding chapters, several prototypes were fabricated and tested by CRC. The first prototypes discussed are the non-radiating LWG circuits used to verify the performance of the LWG as a microwave transmission line and illustrate the effectiveness of the coaxial transition in the K-band. Measured results from the radiating LWG prototypes are then analysed to demonstrate the performance of the radiating LWG as an antenna and reveal the effects of various fabrication techniques on the matching and radiation pattern. The measured results are also compared to the various analytical and FEM based models.

4.1. Fabrication of prototypes

A number of prototypes were fabricated by CRC to test the radiating and non-radiating waveguides. The first prototypes are constructed with only two layers of CLTE laminate thus greatly simplifying the fabrication. The total substrate consists of one thick layer of 3.175 mm and one thin layer of 0.254 mm of substrate with the bonding material to realise a final 3.48 mm (137.4 mil) thick laminated substrate. All of the vias were drilled after laminating the layers together. Although this does not exactly replicate the LTCC process, it simplified the fabrication process at CRC and allowed for manufacturing/testing of the prototypes to be completed within a reasonable time.

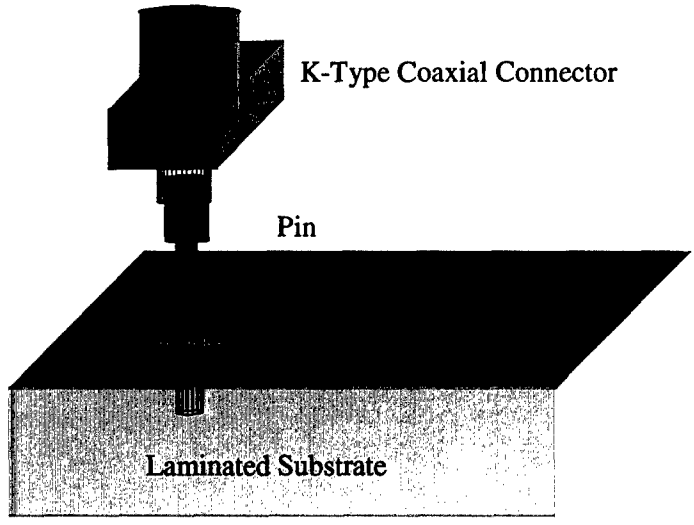

Figure 26. 1 LWG Transition Fabrications

The non-radiating waveguide, modelled in Figure 14, consists of the LWG with two coaxial feeds. This prototype is necessary to verify the performance of the coaxial-to-LWG transition. After lamination and drilling, all of the holes, except the probe hole, were plated to form the vias. A pin was inserted for the probe and then the K-type connector was placed over the pin. The connector was then bolted to the laminated substrate to reduce the possibility of

changing the transition characteristics with excess solder. This created the coaxial-to-LWG transition as depicted in Figure 25.

Five single element prototypes were fabricated using this technique. The first two prototypes were the non-radiating waveguides as shown in Figure 27. Two versions, one being longer than the other, were fabricated. This allowed for an estimate of the losses of both the LWG and the connectors, which are detailed in section 4.3. All of the non-radiating LWG K-type connectors were bolted to the substrate.

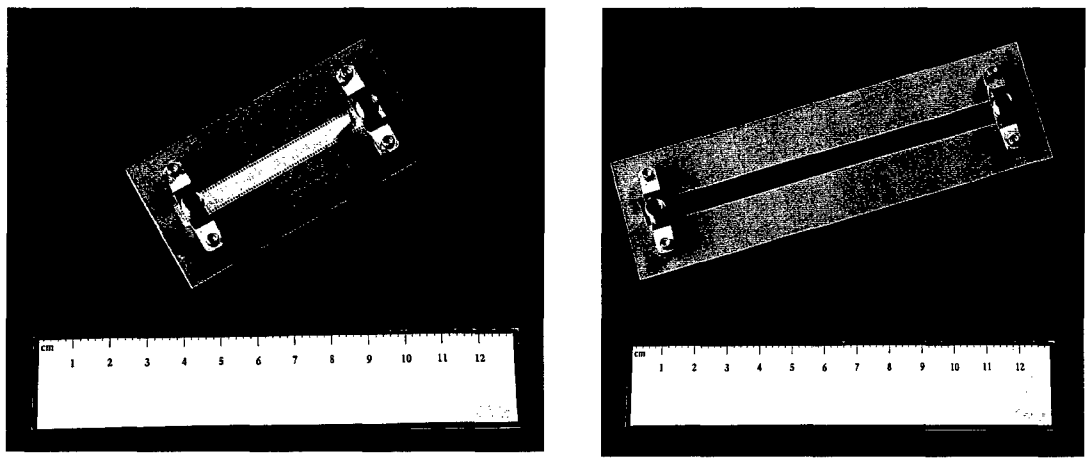

Figure 27. Non Radiating LWG Prototypes

The short and long radiating waveguides were also fabricated. However, two different techniques were used to attach the connectors of the long radiating LWG. Prototypes, type A and type C, are long and short radiating LWG respectively with the K-type connector bolted to the substrate. The other prototype, type B, is a long radiating LWG with the connector soldered to upper metal surface of the LWG. Although it would have been prudent to fabricate and test the non-radiating waveguides before construction of the radiating variety, it was more efficient for CRC to produce all of the prototypes at the same time. All of the radiating LWG prototypes, including the array, are shown in Figure 28. A more detailed diagram of the radiating prototype, showing the various elements, is given in Figure 29.

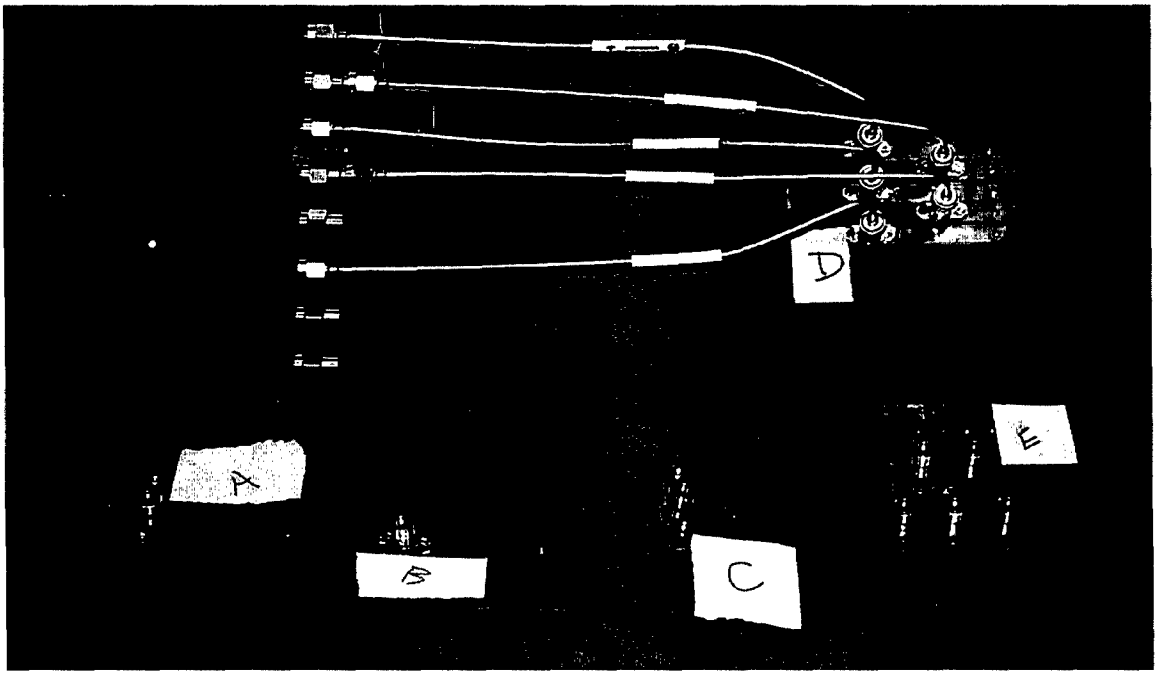

Figure 28. Radiating LWG Antenna Prototypes

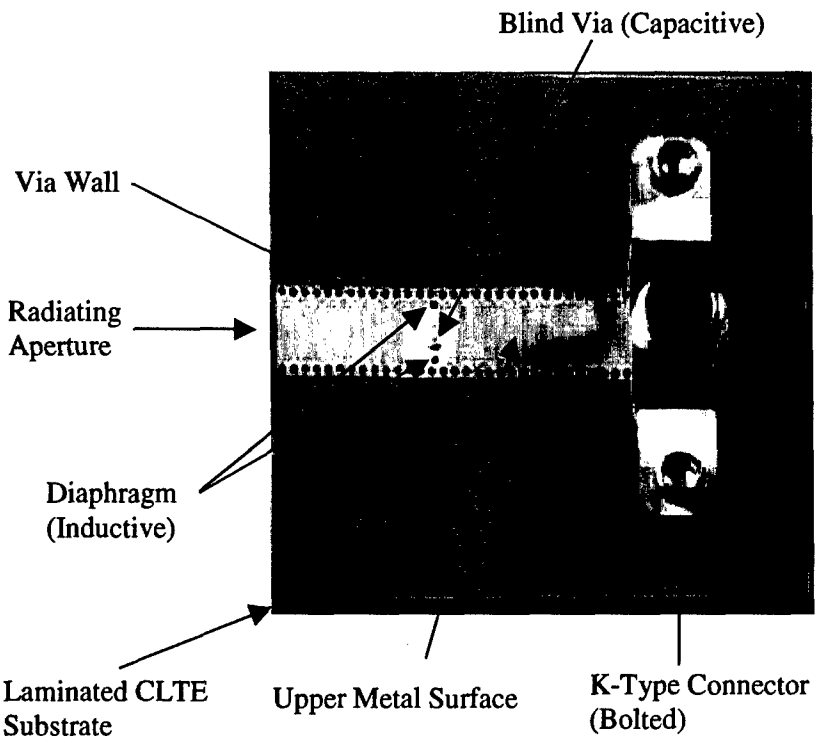

Figure 29. Detailed Radiating LWG Prototype (Viewed from the top)

4.2. Measured results

All of the measurements were conducted at CRC. This was done for two principle reasons. First and foremost, the facilities to test circuits in the K-band are not available at RMC. Secondly, using an independent agency to complete the testing ensures that an external non-biased party verifies the results. Copies of the actual measurements (raw data) are available in Appendix C.

4.2.1. S-parameters

The S-parameters measured from the first four prototypes are given in the Table 10 and in Figure 30 through Figure 35. These results are compared to the HFSS simulations where available. Due to the size of the longer non-radiating LWG, it is not possible to predict the results with HFSS, so only measured results are provided. Furthermore, the HFSS simulations presented in the previous chapter were completed for a 3.40 mm thick dielectric. All of the HFSS results presented below are for a 3.48 mm thick dielectric, thus allowing an accurate comparison with the manufactured prototypes. The analysis of the results and comparison to the desired specifications are given in the following section.

Table 10. Measured S-parameters (3.48 mm substrate)

	Bandwidth (SWR = 2)	S11 (20.7 GHz)	S21 (20.7 GHz)
Short Waveguide	>7 GHz	-28.61 dB	-1.35 dB
Long Waveguide	>7 GHz	-32.08 dB	-2.42 dB
Short Radiating LWG	0.99 GHz	-17.72 dB	
Long Radiating LWG	1.03 GHz	-22.28 dB	

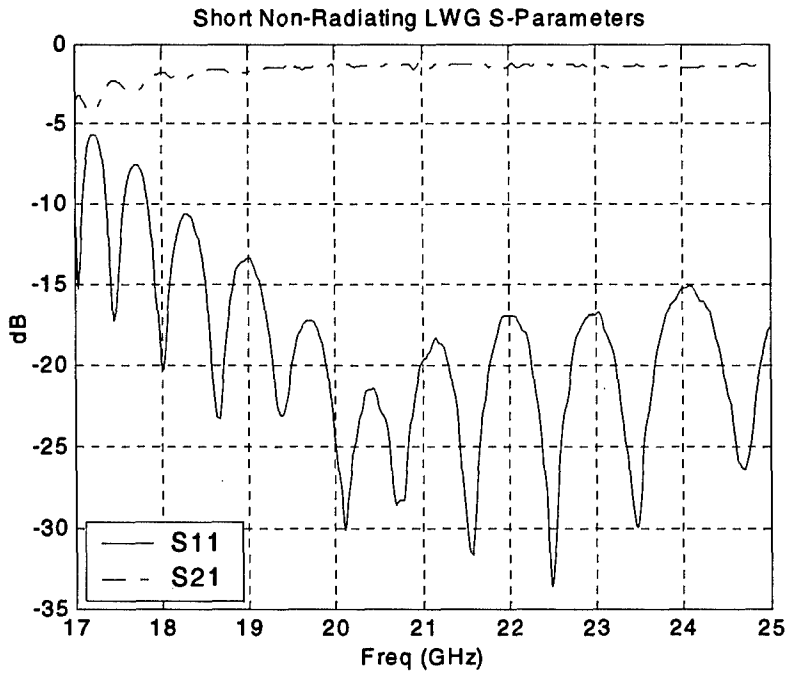

Figure 30. Short Non-Radiating LWG Measured S-Parameters

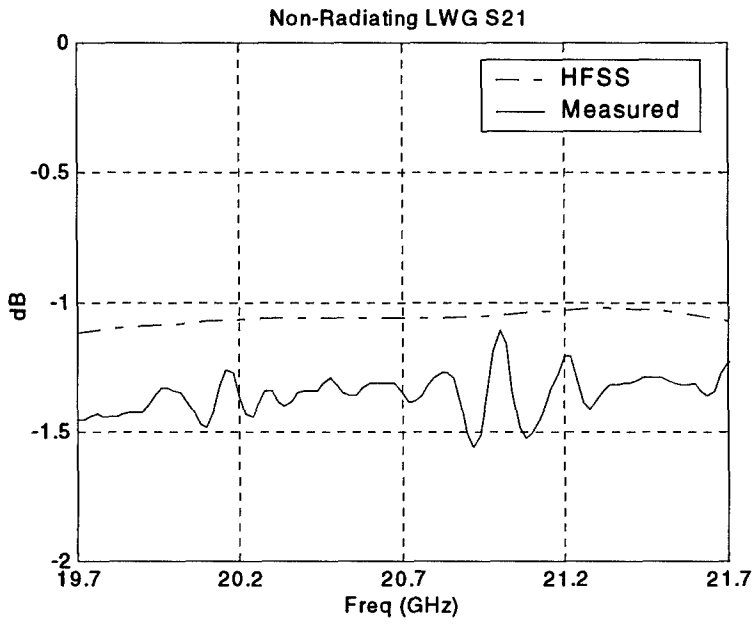

Figure 31. Short Non-Radiating LWG Insertion Loss Comparison

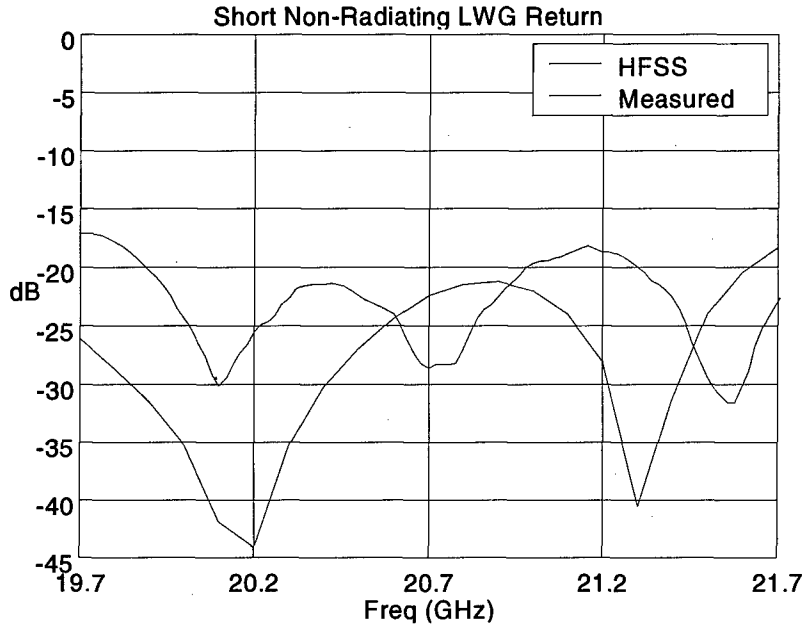

Figure 32. Short Non-Radiating LWG Return Loss Comparison

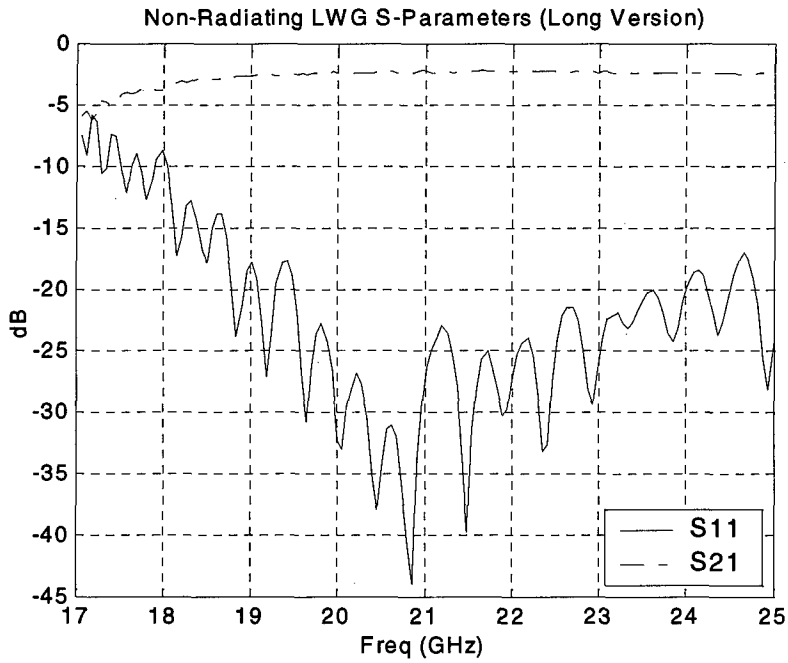

Figure 33. Long Non-Radiating LWG Measured S-parameter

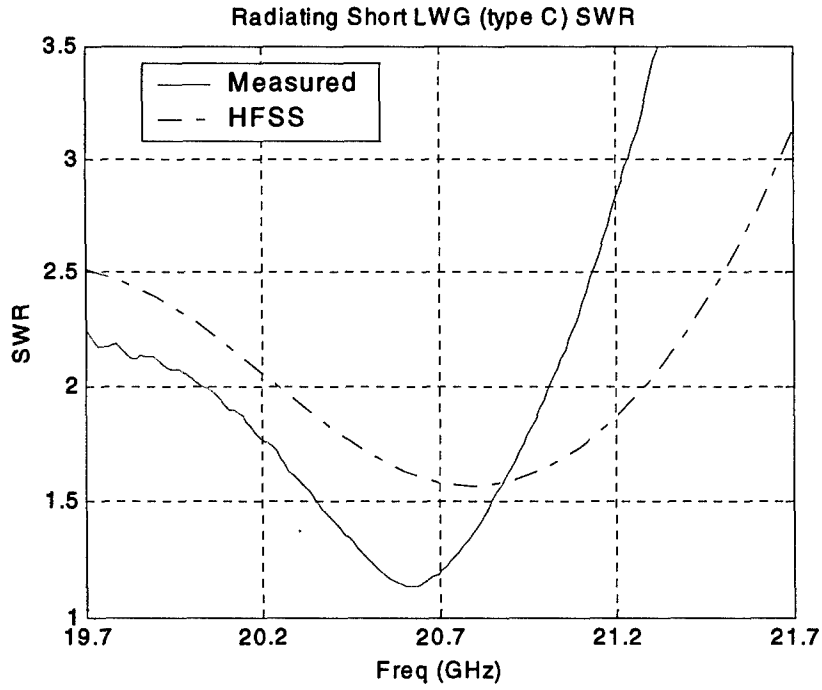

Figure 34. Short Radiating LWG SWR Comparison

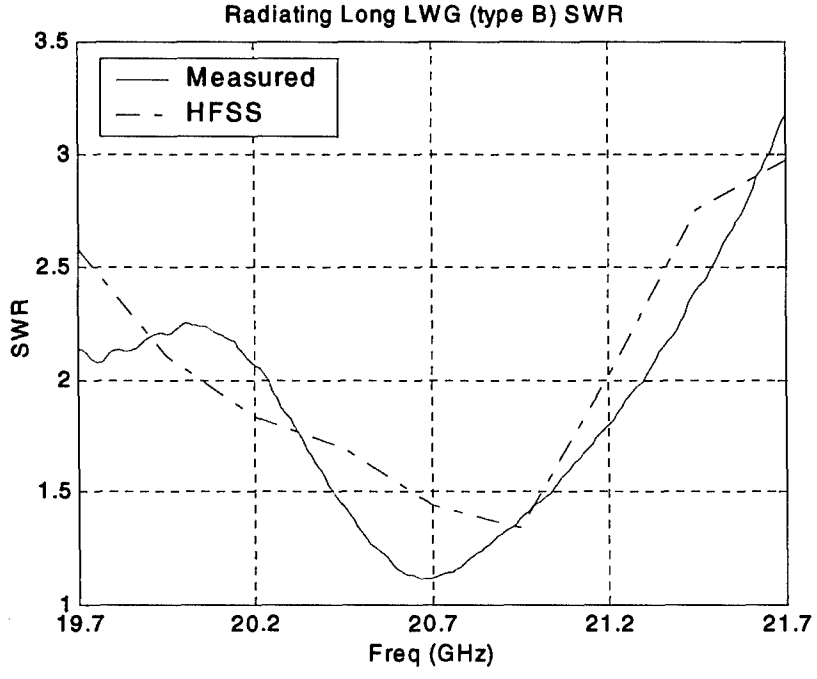

Figure 35. Long Radiating LWG SWR Comparison

4.3. Analysis of single elements

The following sections provide the analysis of the behaviour of the single elements. These elements include the two non-radiating LWG elements and the two radiating LWG antenna prototypes. This analysis compares the measured results with those of the applicable models. These results demonstrate the performance of the coaxial probe fed LWG as a low loss transmission line and as a radiating element.

4.3.1. Non-radiating LWG

Both the simulations and measured results indicated that the coaxial transition is broadband. The non-radiating LWG prototypes have a bandwidth that exceeded 7 GHz or 35% of the centre frequency. This proves that the broadband matching techniques [29] for RWG are also applicable for LWG design. Although the HFSS predictions for return loss do not correlate 100% with the measured results, the results clearly demonstrate that it is possible to use HFSS to impedance match the broadband LWG transition.

Although the measured insertion loss was slightly greater than the predicted HFSS model, the simulated model was within 0.5 dB. A number of explanations are provided for the slight differences. First of all, the K-type connector used was not entirely replicated in the HFSS model. In the HFSS model, the connector was simply an extension of the coaxial transmission line. This was done to reduce the complexity and size of the model. There are also a number of possible effects resulting from the imperfections of the fabricated prototype, as it is impossible to exactly replicate the simulated model. This results in predicted losses normally being less than the measured losses. Finally, there is a tolerance inherent to the actual measurements.

The measured insertion losses of both LWG prototypes are quite low. Given the insertion losses from the two non-radiating LWG prototypes, it is possible to estimate the attenuation constant, α. Assuming that the losses from the coaxial transitions (CL) are the same and that both prototypes have the same attenuation constant, the following derivation is valid:

$$\begin{aligned} CL + \alpha l_{L1} &= S21_{L1} \\ CL + \alpha l_{L2} &= S21_{L2} \\ \alpha &= \frac{S21_{L2} - S21_{L1}}{l_{L2} - l_{L1}} \end{aligned} \qquad (4.1)$$

where l_{L2} and l_{L1} are the probe to probe lengths of the long and short LWG and CL the total coaxial transition losses.

This results in $\alpha = 2.182$ Np/m and CL = 0.314 dB at the centre frequency. It is also important to note that CL includes losses from both coaxial transitions, so the actual loss due to one coaxial transition will be half the value. The analytical calculations of attenuation for a RWG, from Equations (2.6) – (2.8), result is 1.80 Np/m. Although a RWG or other transmission line was not fabricated for direct comparison to the LWG prototypes, the measured losses are only slightly higher than the predicted result for a RWG. The HFSS calculation for attenuation of a LWG, based on losses in Table 5, is 2.04 Np/m. This provides a sufficient degree of confidence in the above calculations (4.1). Therefore one can conclude that there is very little loss due to leakage between the vias and most of the losses are from the conductor and dielectric (ohmic). This confirms that the via pitch was sufficiently small to minimise leakage. The average loss for each coaxial transition is half of the total coaxial transition loss or 0.157 dB.

Given these results, the LWG is a very effective transmission line in the K-band and the lower portion of the AEHF band. The coaxial transition had a relatively wide bandwidth, especially considering the cut-off frequencies, and reasonably low losses at the transition. As a

K-band microwave transmission, measured losses of 2.182 Np/m for the CLTE substrate are quite low.

This also demonstrates that the pin connection technique, shown in Figure 26, works reasonably well. The pin allows for the coaxial adapter to be directly mounted on the LWG, forming both the electrical connections for the coaxial adapter and the blind via probe. Such a technique, combined with the transition design, allows for an effective low loss coaxial transition to excite the LWG in the dominant mode.

4.3.2. Radiating LWG

As can be seen from the measured results (Figure 34 and Figure 35), a bandwidth of 1 GHz was achieved for both the short and long radiating LWG elements. This proves that the capacitive stub and inductive diaphragm, as designed with HFSS, can be effectively used to match the LWG aperture to the LWG transmission line. However, the desired pass band is between 20.2 and 21.2 GHz, which was not accomplished with the radiating elements. The short radiating LWG pass band is between 20.03 and 21.01 GHz, shifted down 0.2 GHz from the designed pass band. The long radiating LWG pass band is between 20.07 and 21.10 GHz, very close to the upper limit specification.

There is a difference between the predicted (HFSS) and measured results as shown in Figure 34 and Figure 35. This is most likely due to the fabrication tolerances. Prior to fabrication various simulations were done to estimate the effect of varying the probe and capacitive stub length as this had the greatest manufacturing tolerance (1- 2 mil). The results of this study, in appendix A, demonstrate that a 50 μm (2 mil) difference in probe and/or stub length has a significant impact on the aperture match.

In the original design, the capacitive stub and probe length were designed to be an integer number of dielectric and bonding material layers. This was done, as it is not possible to have via through a partial layer of tape with the LTCC fabrication process. Vias must penetrate the entire layer. This is true for any process where the layers are drilled before lamination. However, the first prototypes were fabricated by laminating the layers before drilling in order to simplify the manufacturing. This resulted in the additional tolerance in via length.

4.3.3. Antenna gain – measured results at 20.7 GHz

The far-field AGP of the three LWG prototypes (A-C) were measured by CRC using an anechoic far-field chamber. Although pattern measurements were made from 19.7 to 21.7 GHz, only the results and subsequent analysis for the centre frequency are detailed below with the other measured data available at DRDC. The following results contain the co-polarised and cross-polarised AGP for each of the radiating prototypes as well as a comparison between the model (HFSS) and the measured values for prototypes B and C.

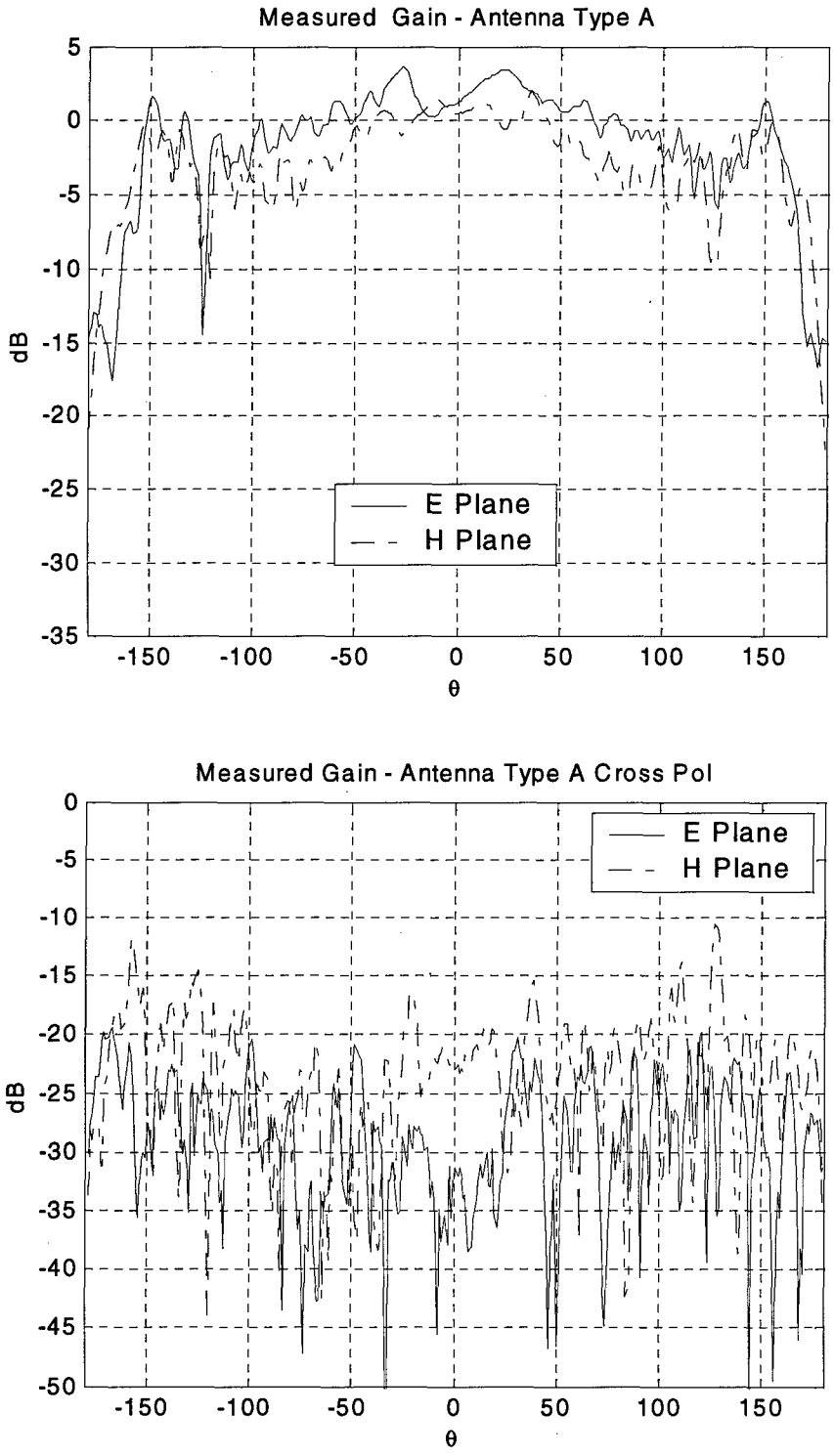

Figure 36. Co- and Cross-Polarisation Radiation Patterns of Long Radiating LWG (bolted connector)

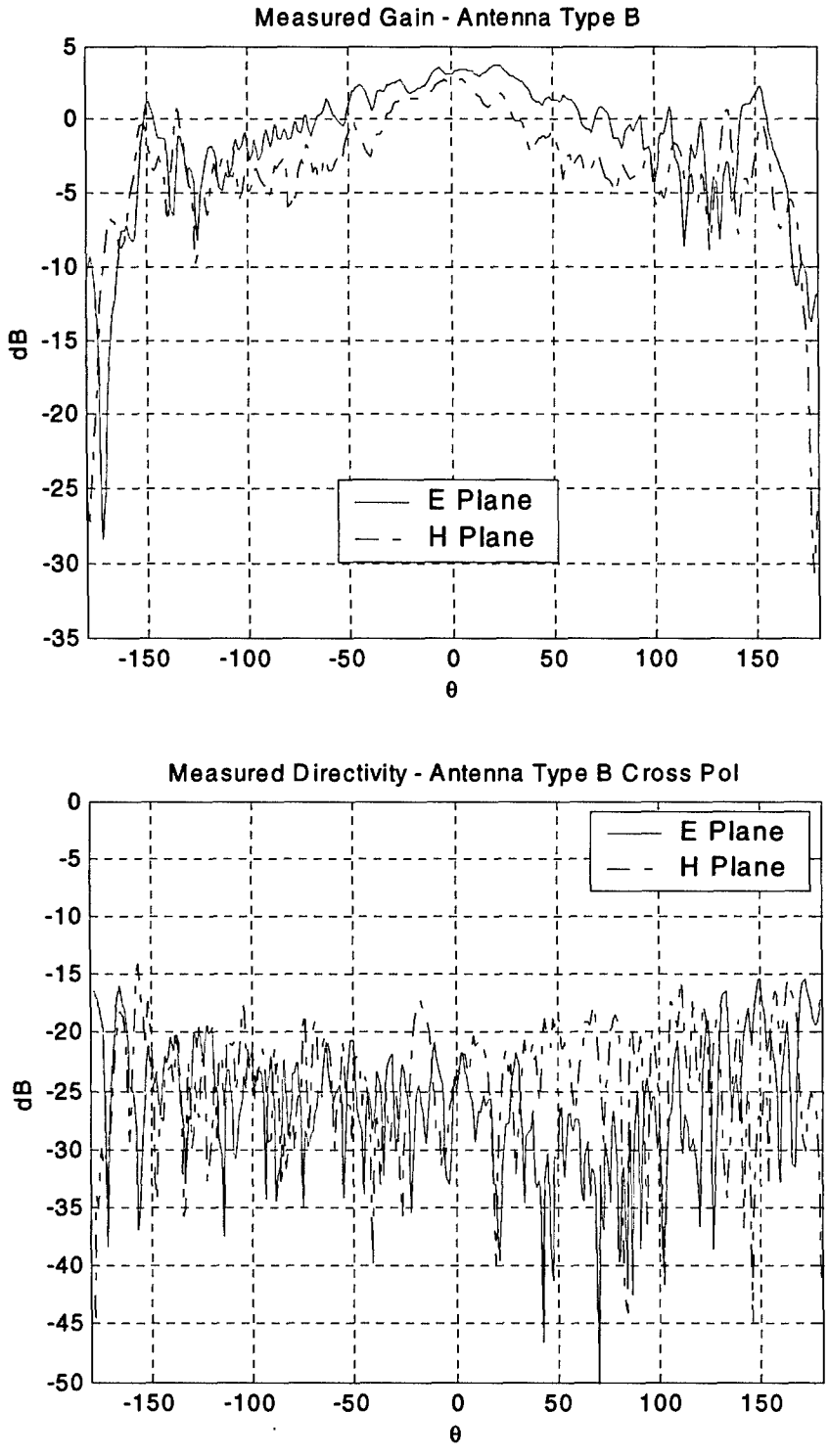

Figure 37. Co- and Cross-Polarisation Radiation Patterns of Long Radiating (soldered connector)

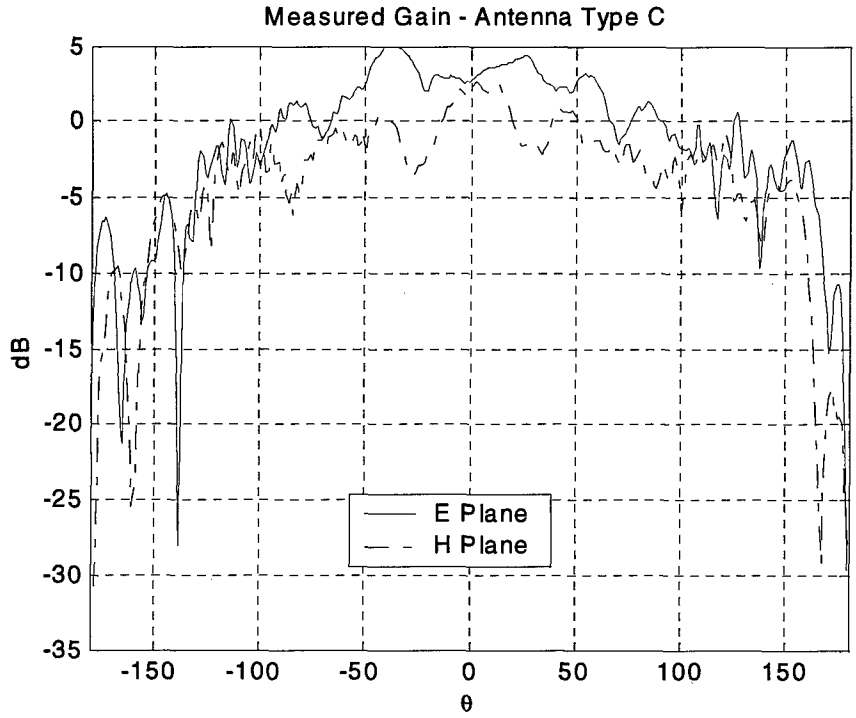

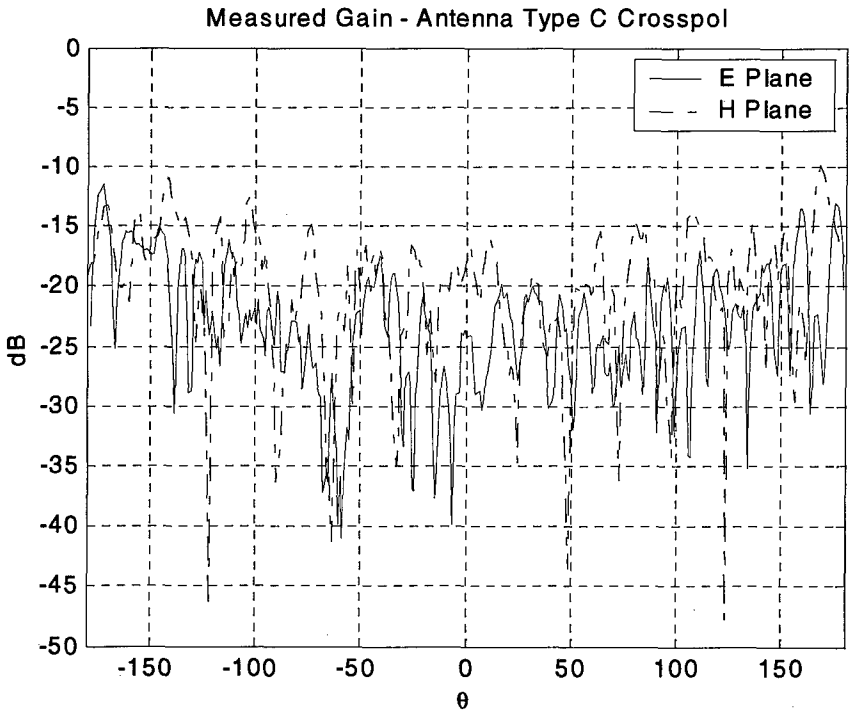

Figure 38. Co- and Cross-Polarisation Radiation Patterns of Short Radiating LWG (bolted connector)

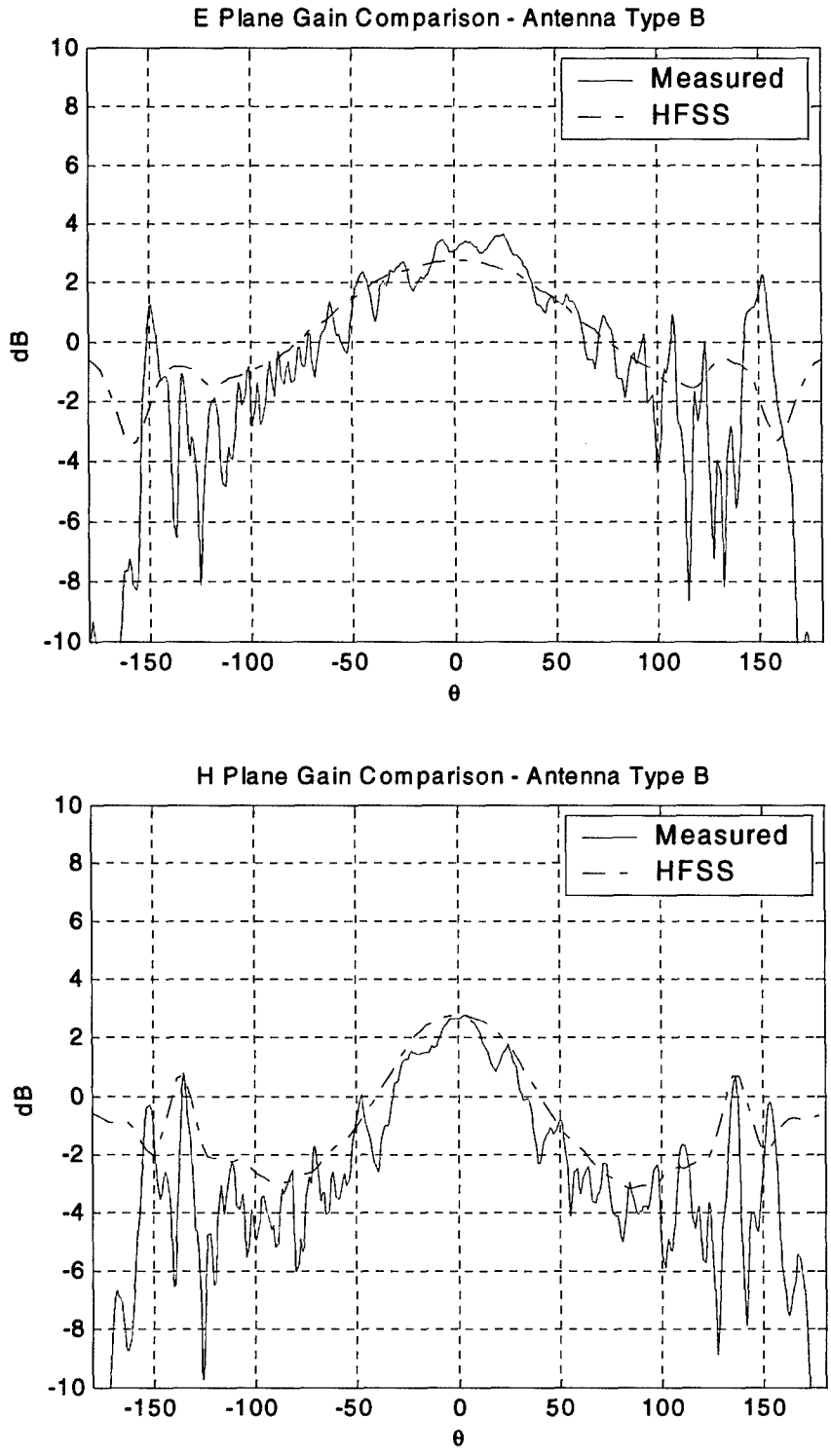

Figure 39. E- and H-Plane Radiation Patterns of Long Radiating LWG (soldered connector)

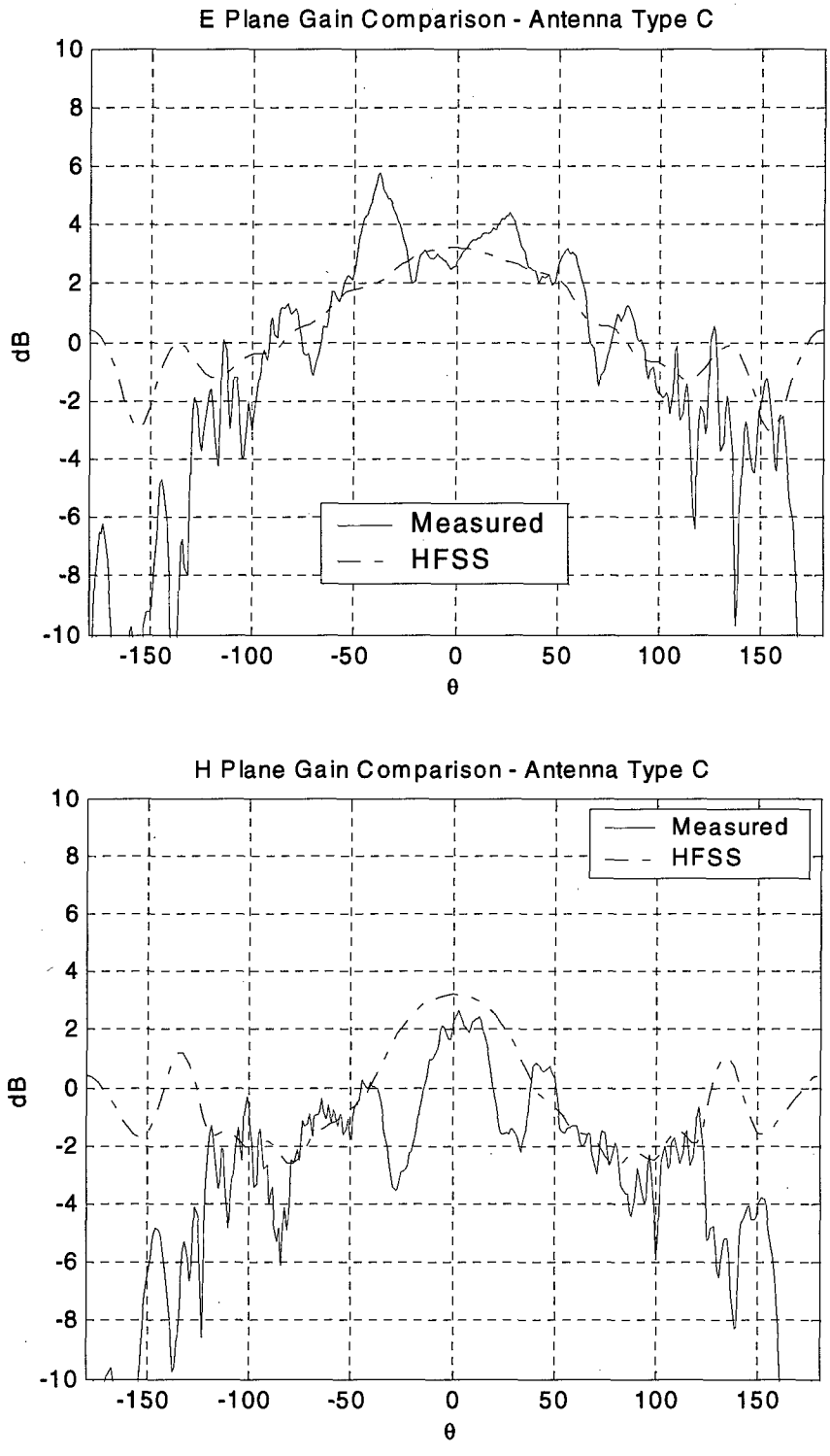

Figure 40. E- and H-Plane Radiation Patterns of Short Radiating LWG (bolted connector

4.3.4. Radiation pattern analysis

After a review of Figure 36 to Figure 40, it is clear that the best results were from the long radiating LWG with the soldered connector (antenna type B). As can be seen in Figure 39, the AGP correlates in both planes closely to the expected result. The measured maximum gain was nearly identical to the prediction. Both the E and H-plane patterns had a broad beamwidth. The measured cross-polarisation levels were reasonably low being 15-20 dB down from the co-polarisation levels. A summary of the prototype B antenna performance is summarised in Table 11.

Table 11. Antenna Type B Measured Results (20.7 GHz)

	Gain (dB)	HPBW (degrees)
E-plane	3.65	122
H-plane	2.76	64

Of particular interest is that the maximum E- and H-plane gains, Figure 37, at the bore sight ($\theta=\phi=0$ degrees) are not the same, as one would expect. Based on the standard set-up for the anechoic far-field measurement system at CRC, the measured gains for the E- and H-plane at $\theta=0$ must be equal (to within the accuracy of the measurement system). The only difference between the two measurements is that both the antenna under test and calibrated system antenna have been rotated 90 degrees. Therefore any discrepancy between the two measured gains ($\theta=0$) must be the result of tolerances and/or set-up of the antenna measurement system.

However, during the antenna measurements, CRC staff noted that the radiating face of the LWG was not orthogonal to the upper and lower planes of the dielectric slab. This could result in the maximum directivity to be shifted from the bore sight ($\theta=\phi=0$ degrees). Given the complexities of measuring AGP at 20 GHz, the measurement tolerances are the most likely cause of the discrepancy.

The AGP for antenna types A and C are different from the expected results. Although the lengths of the antennas were different, both had the coaxial adapter bolted to the substrate. To understand why the patterns are so different, it is first necessary to compare the results of antennas A and B.

The impedance matches of the two long radiating LWG are nearly identical as can be seen in the Figure 41. However, the AGP for both antennas are considerably different with the gain pattern for antenna type A being quite distorted from the expected result. As the two antennas are identical in design, except for the configuration of the adapter, the most logical conclusion is that there is leakage from the adapter. This is further supported as the short radiating LWG (antenna type C) is distorted as well. On probable effect is RF leakage is occurring between the connector and ground plane due to a poor electrical connection at the adapter. This may have allowed radiation from an air gap between the upper ground plane and the K-type connector, thus significantly altering the AGP of the antennas. When the connector is soldered to the LWG, the pattern more closely resembles the expected result.

There is an additional problem that can result from bolting the connector to the substrate. Apart from resulting a potentially poor electrical connection, the stress caused by the bolts can deform and even delaminate the substrate. This could cause fractures in the vias allowing radiation to leak from the wall and further degrade the antenna performance.

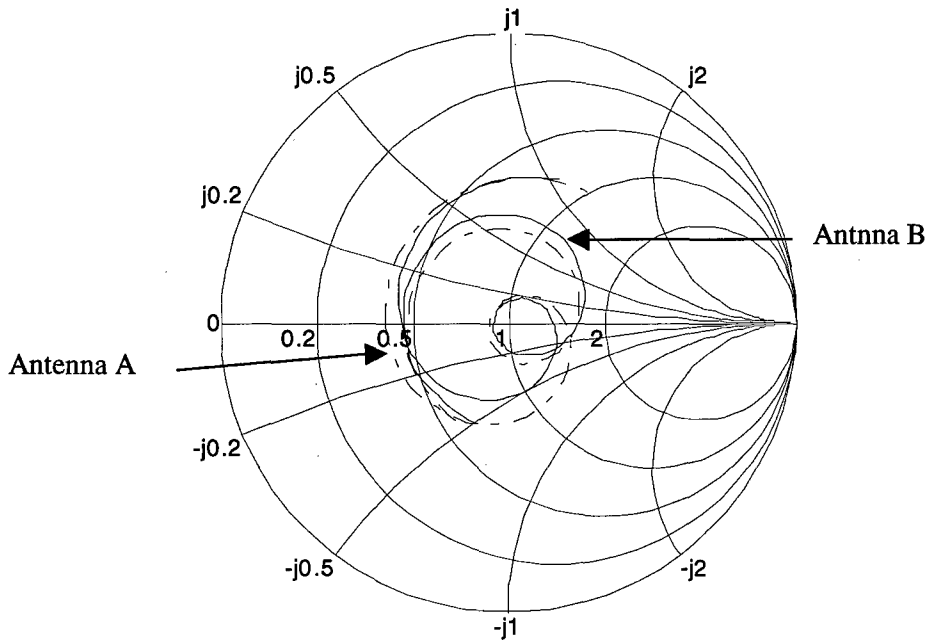

Figure 41. Smith Chart Input Impedance Comparison of Antenna A and B

One other difference was noted between the prototypes and the design. The PCB fabrication process used to laminate the layers of dielectric did not result in a uniform final substrate thickness. Measurements by DRDC indicated that the substrates of antenna types A through C varied in thickness by 25-50 μm. Such thickness variations in the substrate, especially where blind vias are located, impact the impedance match of the radiating LWG antennas (see appendix A).

Although there was some unexpected variation in the performance of the three single element prototypes, one prototype met the expected results. The measured AGP of prototype B closely correlated with the results of the HFSS model. This antenna had a broad beam width in both planes, and achieved the required 1 GHz bandwidth. The measured maximum H-plane gain was essentially identical to that predicted by the HFSS LWG model.

During the initial design of the LWG antenna, there was some concern due to the relatively high level of radiation in the backward direction and the relatively high side lobe levels (+/- 135 degrees). The measured prototype B did not suffer from the same level in the backward direction (Gain < -25 dB), however there were relatively high (1 dB) side lobe levels. To determine the cause of the side lobe levels, additional models were run with the same LWG configuration with differing widths of dielectric substrate. These simulations, Appendix B, indicate that the level and intensity of the side lobes varies with substrate width. Therefore, it is suspect that the side lobes are most likely caused from diffraction at the edges of the substrate. Such effects, as demonstrated in Chapter 3, may be reduced by the use of RF chokes.

4.4. Array analysis

When the radiation pattern for an antenna element has been determined, the radiation pattern of an array of these elements can be determined by the theorems described in Chapter 2. It has been demonstrated that the antenna directivity pattern of a radiating LWG can be approximated by a RWG. Therefore, a first approximation of the antenna directivity pattern of an array of radiating LWG elements can be determined using Equations 2.13-2.17 for an array of radiating RWG apertures.

The analytical approach has some limitations. As with the differences between analytical expressions and HFSS simulation results in Figure 23, the effects of diffraction from the edges of the elements is not taken into account in the analytical expressions. Furthermore, any affects on the field resulting from mutual coupling between the elements are also ignored by the analytical expressions. Therefore, the pattern multiplication is only valid if the mutual coupling and diffraction are negligible. However, the analytical method can provide an estimate of the maximum directivity and some insight into the array's directivity pattern.

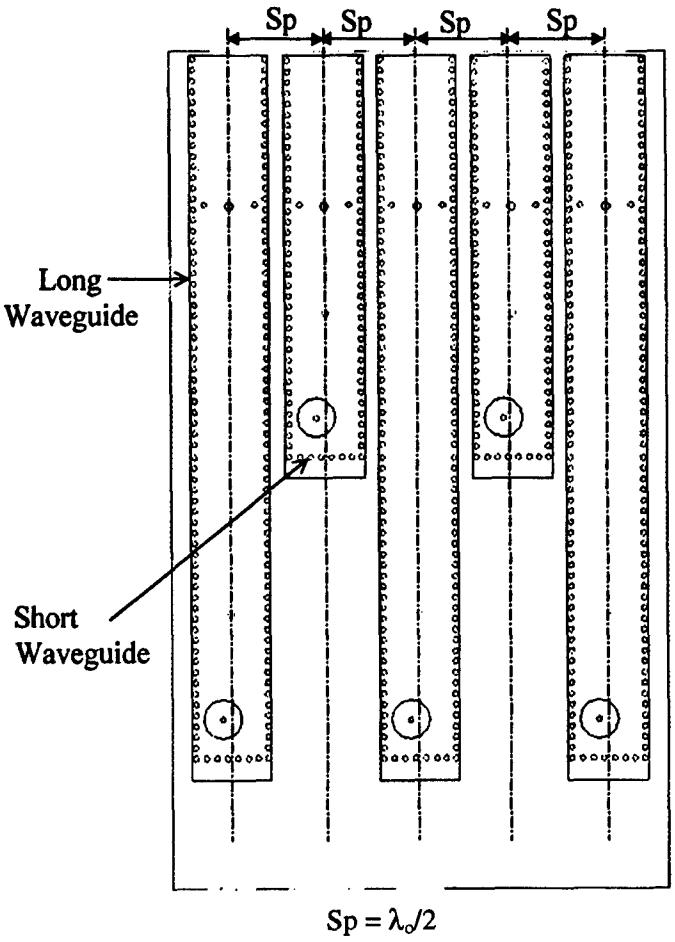

Figure 42. Five Element LWG Array Configuration

A simple array can be realised by placing the LWG elements parallel to each other with a centre-to-centre spacing of $\lambda_o/2$ within the same substrate. Spacing closer than this is not realisable due to the width of the LWG apertures and thickness of the walls (vias). This results in a linear array in the x-axis with the maximum radiation intensity of each element in the z direction. The array factor (AF) of this array geometry is given in Equation 2.28. The array is shown in the Figure 42.

In order to stagger the coaxial connectors, both short and long LWG antenna elements were necessary. However, the total attenuation of the long element is greater than the short element. For the same input power, the excitation coefficient of the array elements will be different. The effect of the non-uniform amplitudes can be predicted by the expressions derived for the array directivity. The difference between uniform amplitude and attenuated amplitude is shown in Figures 4.23 and 4.24. Utilising non-uniform amplitudes in arrays can have beneficial effects as in the reduction of side lobes with an array with binomial excitation coefficients but with a reduction in gain as seen in Figure 4.25. The difference between the lengths of the two elements also results in a phase difference between the aperture fields of the short and long LWG elements.

The design of the longer element was implemented by simply adding $(3/2)\lambda_g$ of length between the coaxial adapter and the aperture matching components. This was done to minimise the effect of the length change on the impedance matching circuits and to provide the minimum length required for the coaxial adapter staggering. As it is not possible to implement exact length changes due to the via pitch and diameter requirements, this resulted in a phase difference between the long and short elements.

The length, taken between the probe and the substrate end, of the long and short elements is 50.89mm and 28.19mm respectively. This length difference of $1.528\lambda_g$ results in a phase difference of 3.056π radians. Such a phase differential must be taken account for in the excitation of the elements in order to ensure the maximum directivity at the desired angle.

4.4.1. Analytical array results

Given the equations for the element radiation pattern and array factors detailed in Chapter 2, it is possible to study the ideal behaviour of the five-element array depicted in Figure 4.22. It is important to note that the following results are from uniform phase and/or progressive phase excitation of the apertures. The first effect of using non-identical elements to be studied is that of non-uniform amplitude distribution across the array.

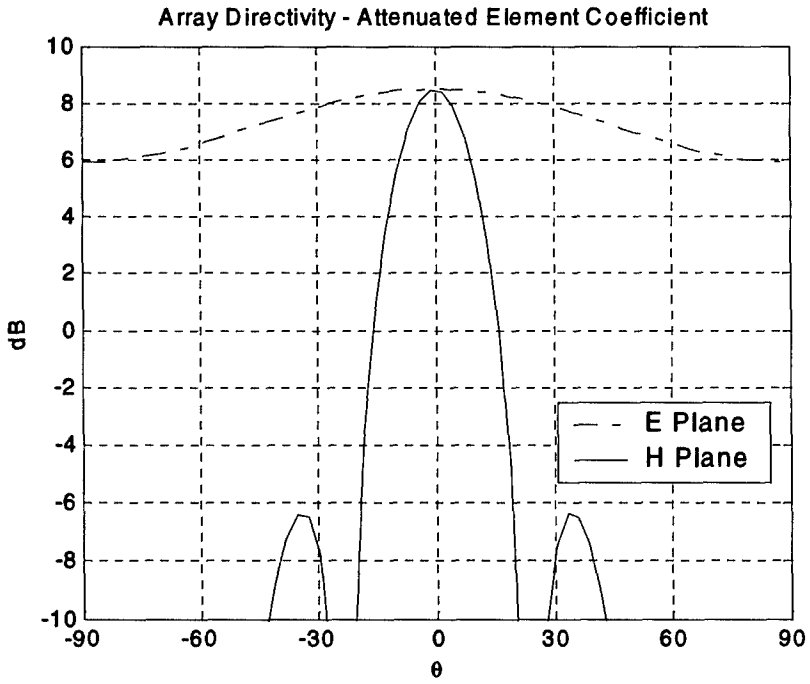

Figure 43. Five Element Array ADP (with Attenuation).

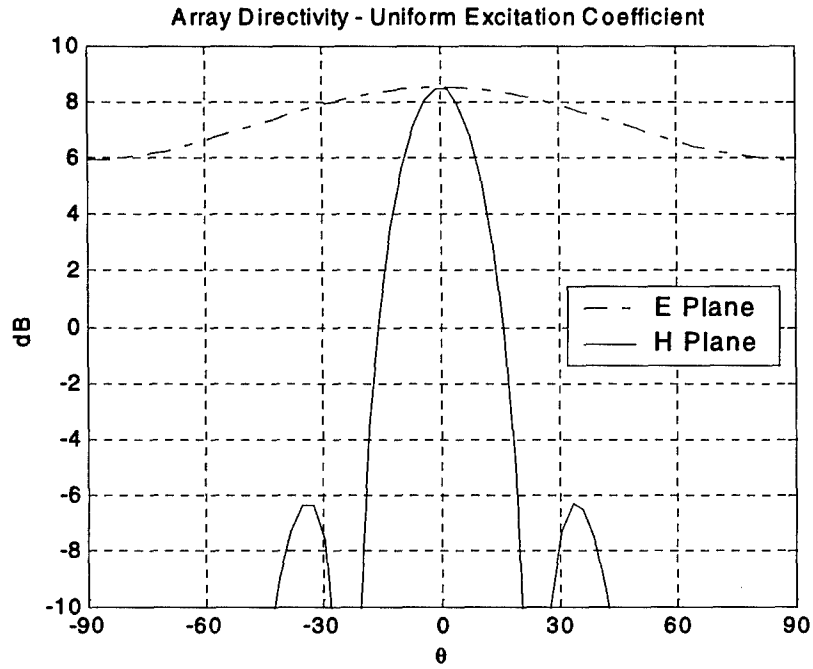

Figure 44. Five Element Array with no Attenuation

The two Figures, Figure 43 and Figure 44, detail the results of a five-element array of radiating rectangular apertures. Figure 43 depicts the effect of non-uniform excitation. The excitation coefficient of the array is given by

$$I_m = e^{-\alpha l} \tag{4.2}$$

where l is the length of the element and α the attenuation constant for the LWG (Equation 4.1). Such a configuration results in a maximum directivity of 8.48 dB.

Figure 44 is that for uniform excitation coefficients. This results in a maximum directivity of 8.51 dB, and an almost identical ADP. Therefore, the effect of non-uniform amplitude between the elements can be considered to be negligible.

As can be seen from the Figures, the array factor has resulted in additional side lobes in the H-plane (≈+/- 30°). These side lobes can be eliminated if the excitation coefficient follows a binomial distribution [30]. Multiplying the non-uniform excitation coefficient by the coefficients of a 5-element binomial array [30] yields the ADP of Figure 45. The maximum directivity is reduced to 7.1 dB, but the side lobes are eliminated.

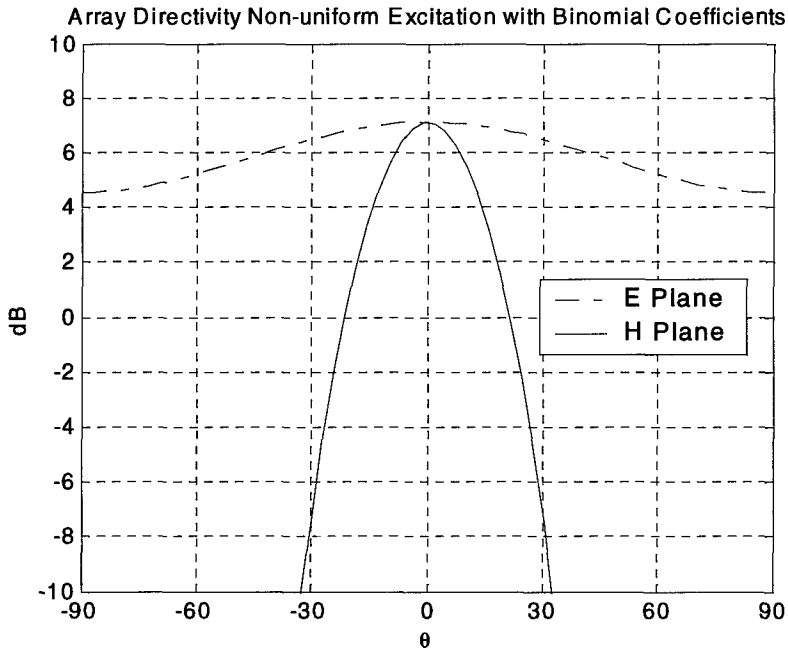

Figure 45. Five Element Array with Binomial Excitation

It is also possible to electronically scan with the array depicted in Figure 42. To direct the beam in the direction of θ_o, the required phase shift between the elements is given by [31]

$$\beta_x = -kd_x \sin\theta_o \cos\phi_o \tag{4.3}$$

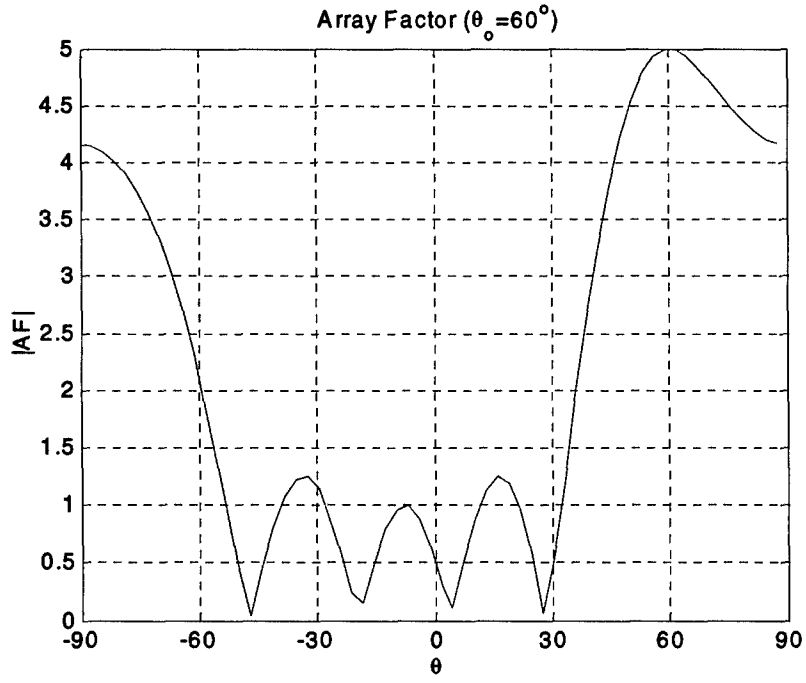

Figure 46. Array Factor (θ_0=60°)

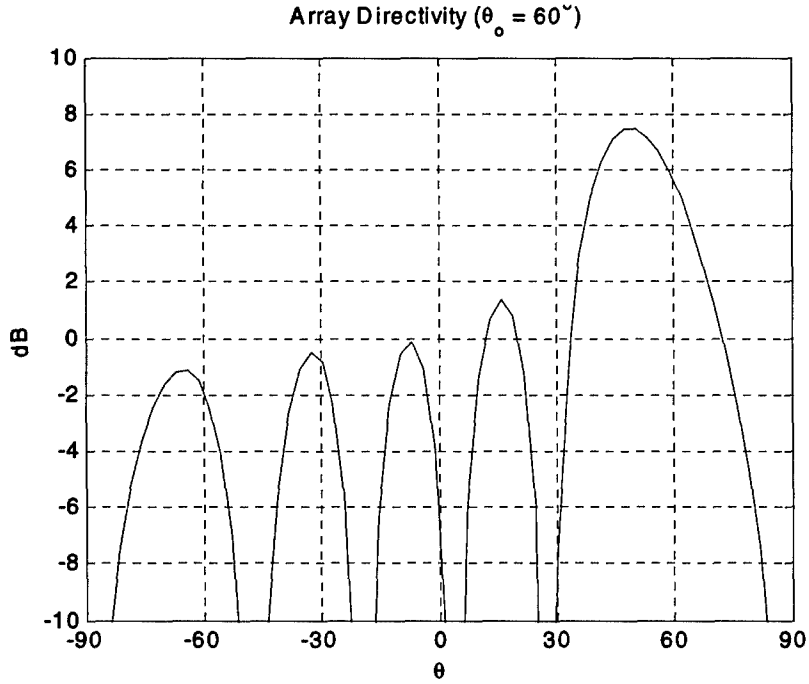

Figure 47. Array Directivity (θ_0=60°)

As the array has elements along the x-axis, the array can only be effectively scanned along this axis, which is in the H-plane (ϕ=0). The result of the array factor and the array directivity, where the beam is steered at θ_o=60°, are shown in Figure 46 and Figure 47 respectively. Figure 46 is a plot of the absolute value of the array factor (Equation 2.28) whereas Figure 47 depicts the directivity in dB, resulting from the multiplication of the element ADP and the array factor utilising the numerical integration technique detailed in Section 2.6.

As can be seen from the previous figures, the five-element array can be scanned to 60° from the bore sight with a gain of 6 dB at 60°. Such a configuration does result in a number of additional side lobes. The side lobe levels are relatively high and are the result of the array factor seen in Figure 46. These can be reduced with binomial excitation, but at the expense of the maximum gain at the desired scan angle as seen in the Figure 48. Even with the binomial excitation, the side lobe level at -60° is still relatively high.

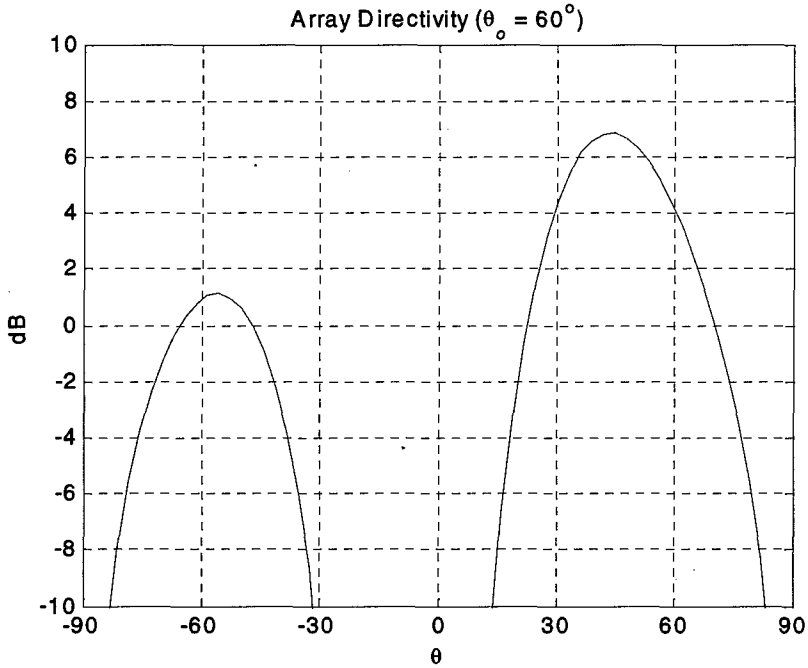

Figure 48. Array Directivity with Binomial Excitation and Scan (θ_0=60°)

4.4.2. HFSS array results

Simulating an array of five LWG elements is not a trivial problem. Although it may be possible to simulate five separate elements within one substrate, the numbers of tetrahedra required will be impracticably large. In fact, a single long radiating LWG takes a substantial amount of time to simulate. As it has been reasonably established that a radiating RWG can approximate the far-field radiation pattern of a single LWG element, the same can be done for an array. There will be differences between the mutual coupling between elements that alter the far-field pattern, but such analysis should be more accurate than that performed analytically. It provides an estimate of the mutual coupling and some insight into the electromagnetic

interference issues, which result from the array and between the elements. With the LWG, the mutual coupling between the elements could be greater due to the leakage between the vias.

The array was simulated by replacing the via walls with solid walls. To account for the diffraction at the edges of the elements, a round edge with the same diameter as the via is used on all of the vertical walls at the radiating edge of the model. Elements are spaced $\lambda_o/2$ and are each fed by a separate coaxial line. This results in a 5-port device. Port calibration lines must be used in HFSS to ensure uniformity of phase at each port. The model is depicted in Figure 49.

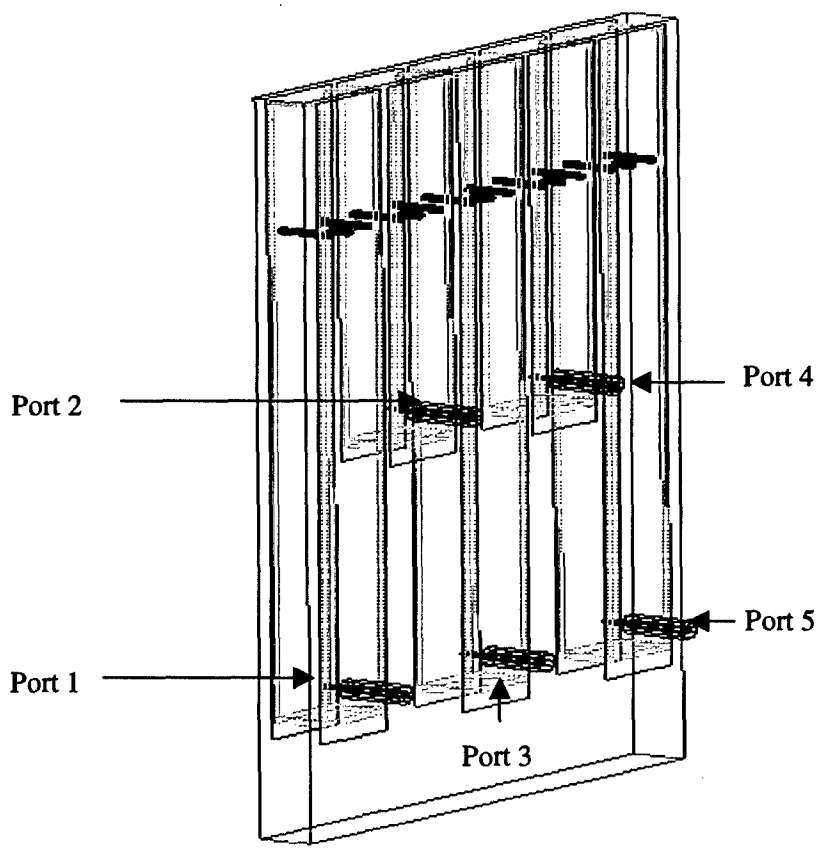

Figure 49. HFSS Array Model

Another complicating factor is the differing phase change imparted by the lengths of the long and short radiating elements. Although the difference in amplitude has a minimal effect on the pattern, demonstrated in the analytical analysis, a non-progressive phase difference between the elements has a substantial effect on the directivity. The E-fields at the apertures must be in phase in order to achieve the maximum directivity. A progressive phase shift, Bx, between elements is also necessary for scanning the array.

The first HFSS results detailed in Figure 50 and Figure 51 are for the far-field pattern of the 5-element array. All of the coaxial ports are excited with the same amplitude with a phase difference to account for the element length differential. Adjusting only the amplitude coefficient to ensure uniform amplitude had a negligible effect on the ADP as predicted by the analytical result.

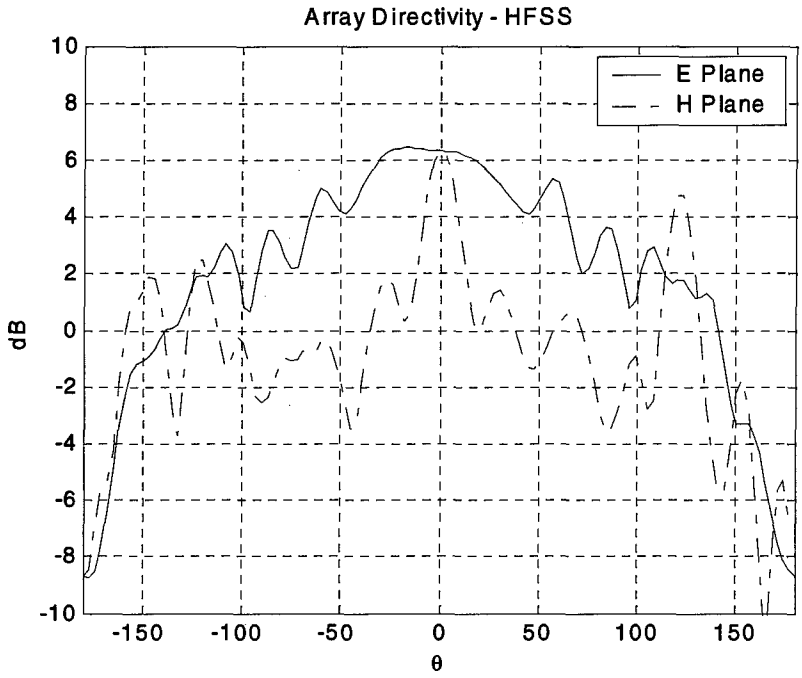

Figure 50. HFSS ADP 5-Element Array

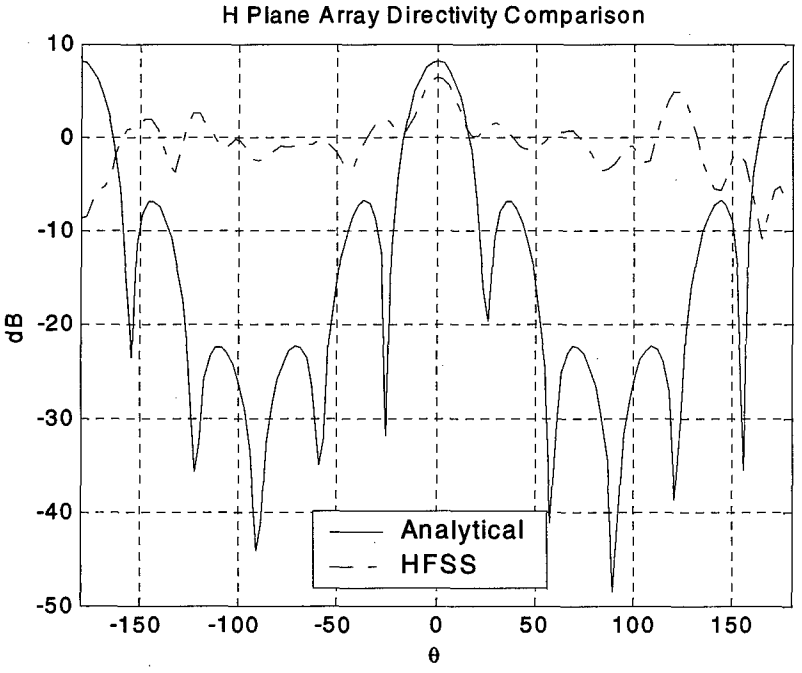

Figure 51. HFSS and Analytical H-Plane Directivity Comparison

When the phase of the short elements is changed to ensure uniform phase at all of the apertures, the ADP is close to that predicted analytically. However there are some noticeable differences as demonstrated in the H-plane comparison of Figure 51. Although there is a correlation between the locations of the lobes, there is a difference in the amplitudes of the main and side lobes. The maximum directivity predicted by HFSS is 1.75 dB lower with the side lobes about 9 dB greater than the analytical result. This is most likely due to the effect of mutual coupling between the elements. The mutual coupling could have increased the intensity in the side lobes, which resulted in a decrease of the main lobe maximum intensity.

The amount of coupling between the array elements can also be estimated by HFSS. Numbering the coaxial adapters from right to left, Figure 52 details the S-parameters relative to the centre element (#3). This provides an estimate of the power that will be coupled from each port to the centre port. Although the coupling from the outer most elements to the centre element can be considered negligible (<-30dB or 0.1% of the power), there is some coupling from the adjacent elements. One would expect even greater coupling from an array of LWG elements due to the leakage through the wall, which does not exist in the solid wall case of the array in Figure 42. The measured mutual coupling, relative to the centre element, is provided in the next section.

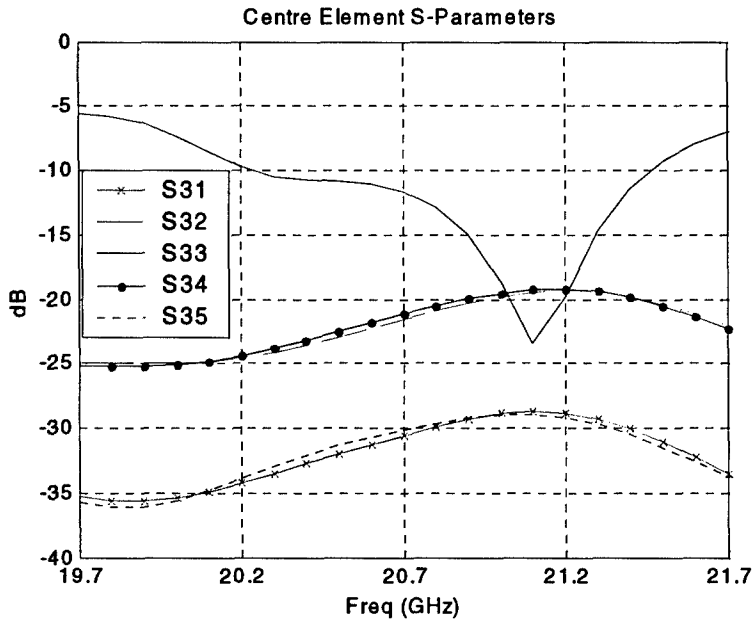

Figure 52. Centre Element S-Parameters HFSS

4.4.3. Measured array results

Measurement of the array was completed in two parts. The first portion involves the measurement of return loss and the E- and H-plane radiation patterns for each separate element. This is similar to the method used for antennas A through C, however all element ports, with the exception of the port for the element under test, ports were terminated with matched loads.

Due to the manufacturing process used at CRC, it was easier to fabricate an array of elements during the fabrication of the individual elements. However, the goal of the project was to fabricate single element prototypes only, so the analysis of an array can be considered as a

natural extension of this research. For this reason, the array was fabricated before detailed simulations with HFSS were performed. Although fabrication before detailed modelling is not a recommended method, the results from the array are available and merit some investigation. As described in the previous section, it was not possible to model a five LWG element array, so the LWG elements were approximated by equivalent RWG elements.

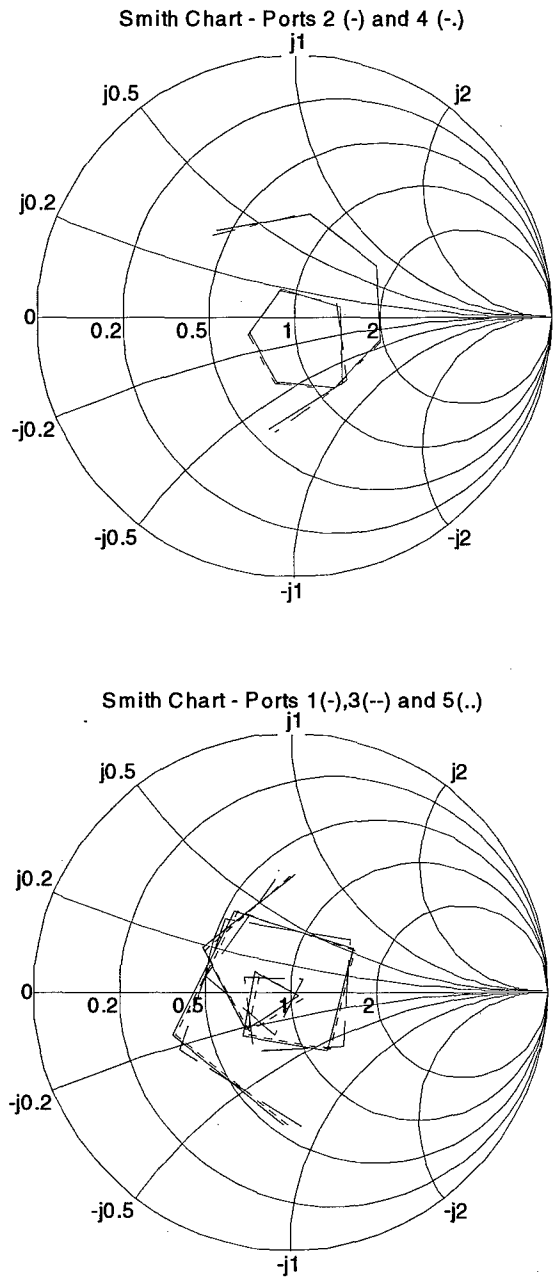

Figure 53. HFSS LWG Array Element Input Impedance

Simulated analysis for each of the element, in the smith charts of Figure 53, indicates that the return loss for similar elements should be the same. Thus one expects the return loss for elements 1,3 and 5 to be similar as well as the return loss for elements 2 and 4 provided that all of the elements are fabricated in the same way.

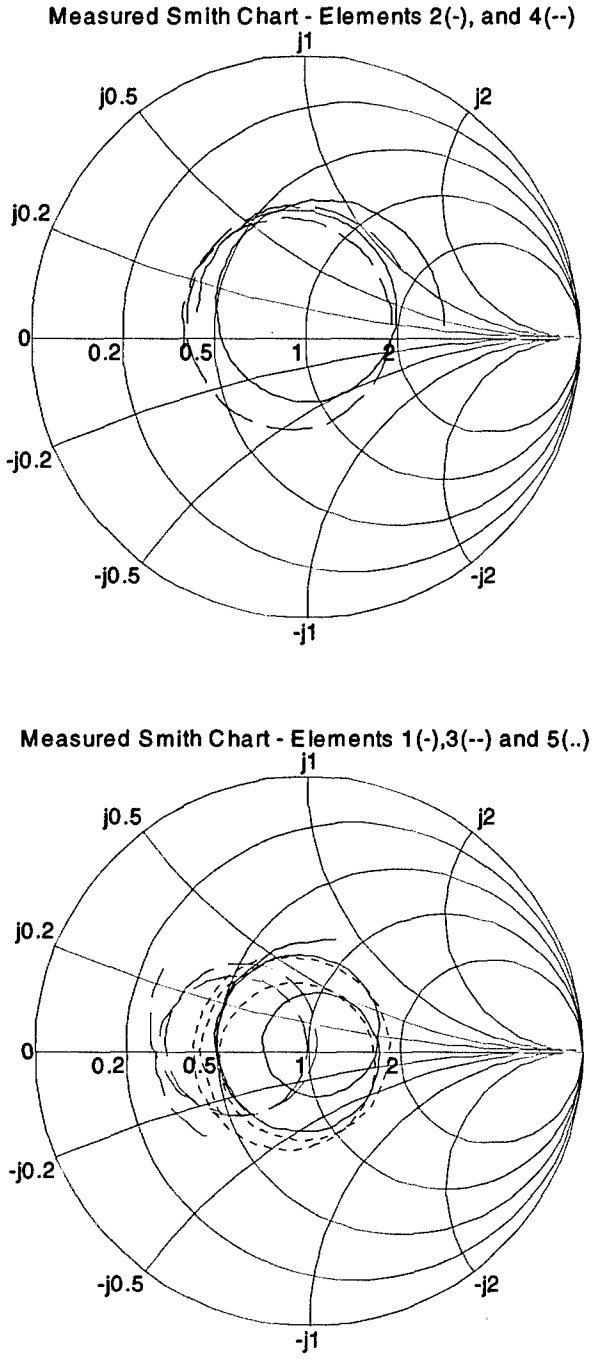

Figure 54. Measured LWG Array Element Input Impedance

As can bee seen from Figure 54, the S11 for elements 2 and 4 are reasonably close to each other but differ from the expected results. Element 3 differs significantly from both the expected results and from elements 1 and 5. The results are also significantly different from the antenna type C. Thus, it is suspected that there is a problem in the fabrication of the centre element.

The results from element 5 also differ from element 1, indicating that the element is not as well matched as expected. The element 5 results differ significantly from that of antenna types A and B as well. Given the predictions for identical elements, the most likely conclusion is that the final fabrication of elements 1,3 and 5 differ and that something had gone awry with the coaxial connector and/or capacitive post soldering during the final assembly of the array. These inconsistencies in fabrication have also affected the far-field radiation patterns as can be seen in the Figure 55 and Figure 57.

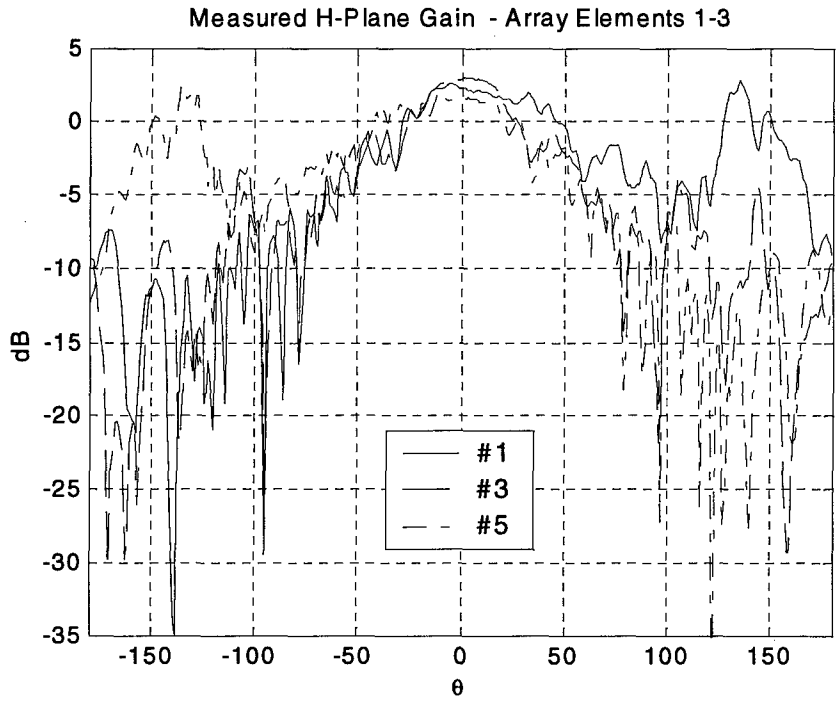

Figure 55. Measured H-plane Gain – Long LWG Array Elements

The input impedance and far-field patterns for the short radiating LWG array elements (#2, #4) do not correlate well with the expected results. Furthermore, as a single element, antenna type C, the results were significantly different from expectations. From the analytical results, if the distribution at the aperture is purely TE10, then the far-field pattern must correlate with the expected results.

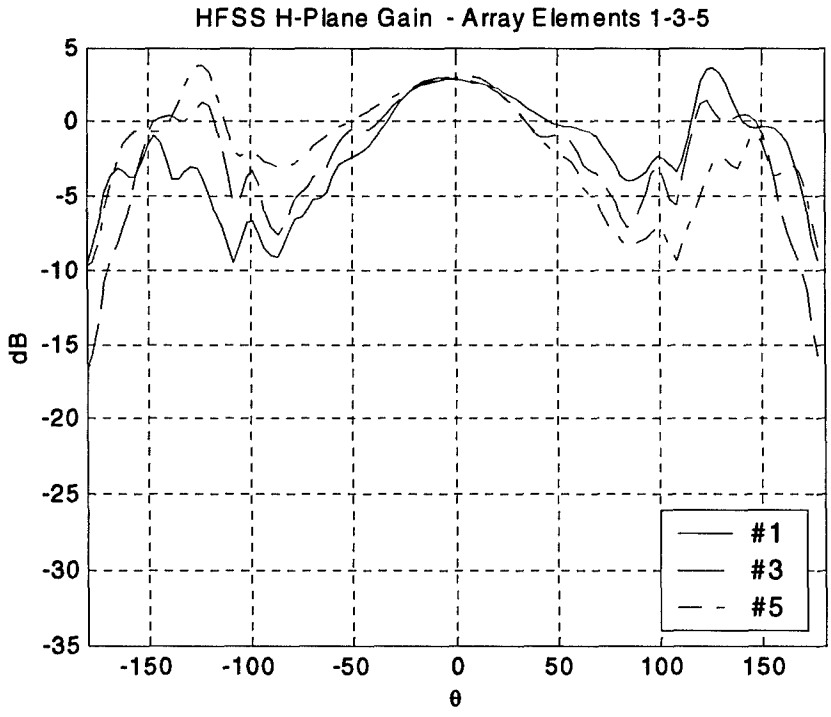

Figure 56. H-plane AGP Long LWG Array Elements (1,3,5) - HFSS

There are two plausible causes for the poorer performance of the shorter elements. The first, and least likely, is that a poor electrical connection between the coaxial adapter and LWG surface has resulted in RF leakage that has corrupted the far–field radiation pattern. However, as the longer element's AGP correlate with the expected results and have the exact same connector configuration, this is less likely the cause. However, the difference may be the results of the distance between the coaxial transition and the aperture.

As can be seen in Figure 22, the ADP of the short LWG has a slight ripple, which is not evident in the long LWG ADP. This is likely caused by modes, in addition to TE10, occurring (or existing) at the aperture. Since the aperture matching components are at the same distance from the aperture in both the long and short LWG elements, these additional modes must be from the coaxial-to-LWG transition. In the longer elements, these modes are sufficiently attenuated so they do not disturb the aperture distribution from TE10. However, with the short elements, these modes have suffered less attenuation and still have sufficient amplitude to corrupt the desired aperture field distribution and far-field pattern.

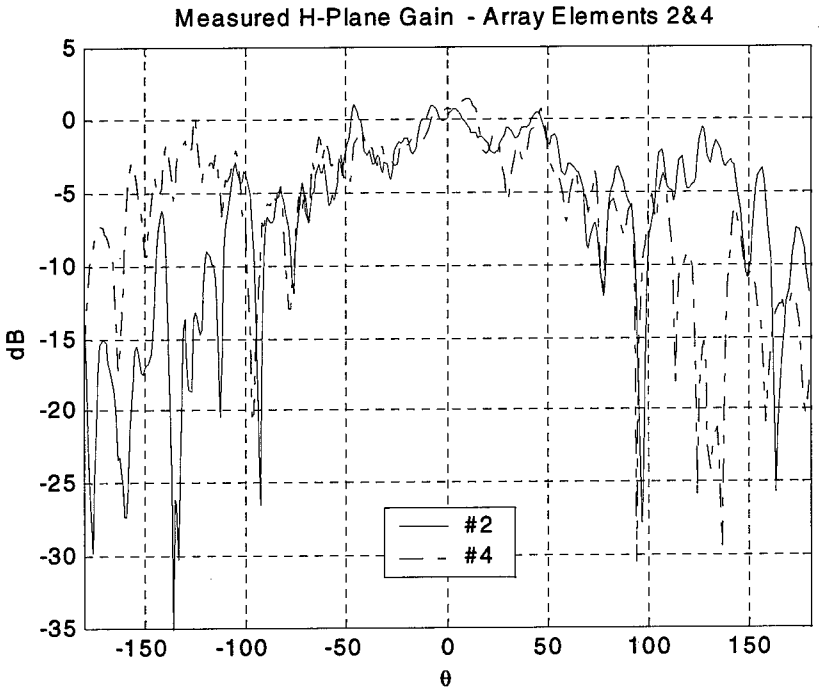

Figure 57. H-plane AGP Short LWG Array Elements- Measurement

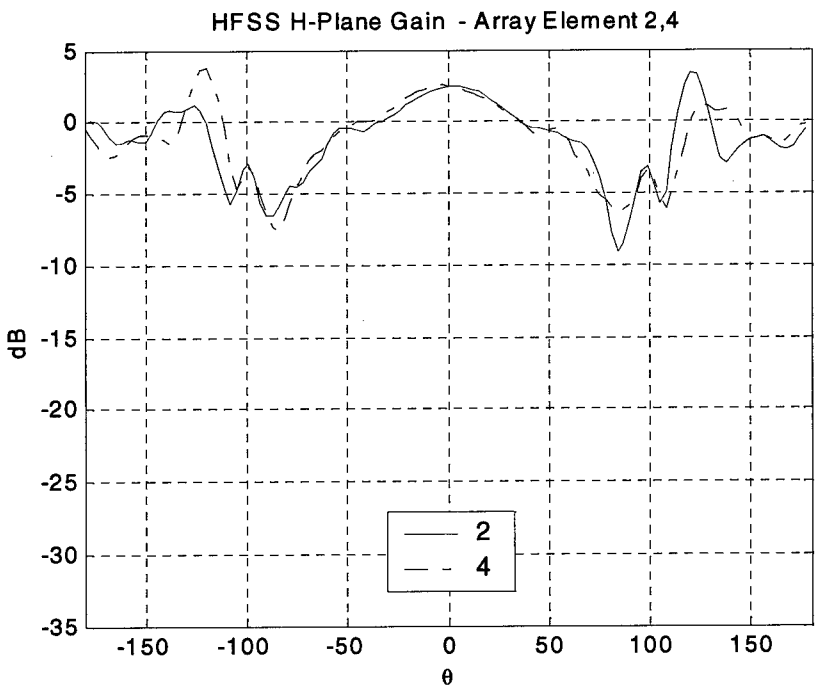

Figure 58. H-plane AGP Long LWG Array Elements (2,4) - HFSS

As the shorter element's AGP differs significantly for the H-Plane at the centre frequency, the entire array will not generate the desired result. This is evident in the Figure 59 comparing the HFSS prediction with the measured result. Given the poor performance of the shorter elements, which comprise 2/5 of the array, further analysis of the array's radiation pattern results is not necessary, but the mutual coupling between elements does merit some discussion.

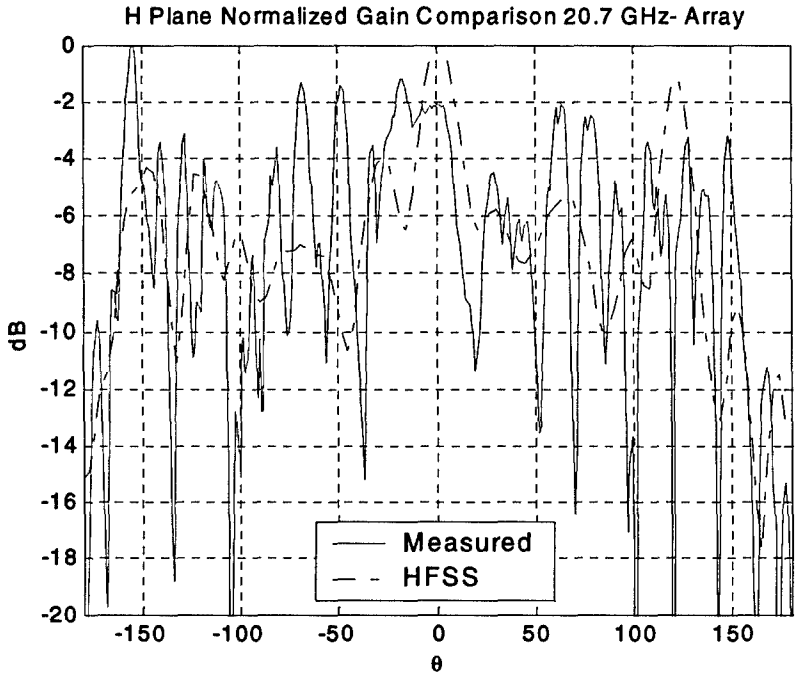

Figure 59. Array H-plane Comparison (20.7 GHz)

Figure 60 shows the measured amount of mutual coupling from all of the other elements to the centre element for direct comparison to the solid walled RWG array mutual coupling in Figure 52. The mutual coupling between the LWG elements is quite low and is in the same order as that predicted for the solid walled RWG elements. At the centre frequency, the mutual coupling from adjacent elements is about –24 dB. The coupling between the adjacent elements and the centre element (S32 and S34) is nearly identical, which is not surprising considering that S22 and S44 (Figure 54) are very close. Even though the centre element is not well matched, at the two resonance frequencies where the maximum power is transferred to the element, the coupling is still less than –22 dB (or less than 0.7% of the power). This is an insignificant amount of coupling and probably has not contributed to the poor far field pattern results for the entire array.

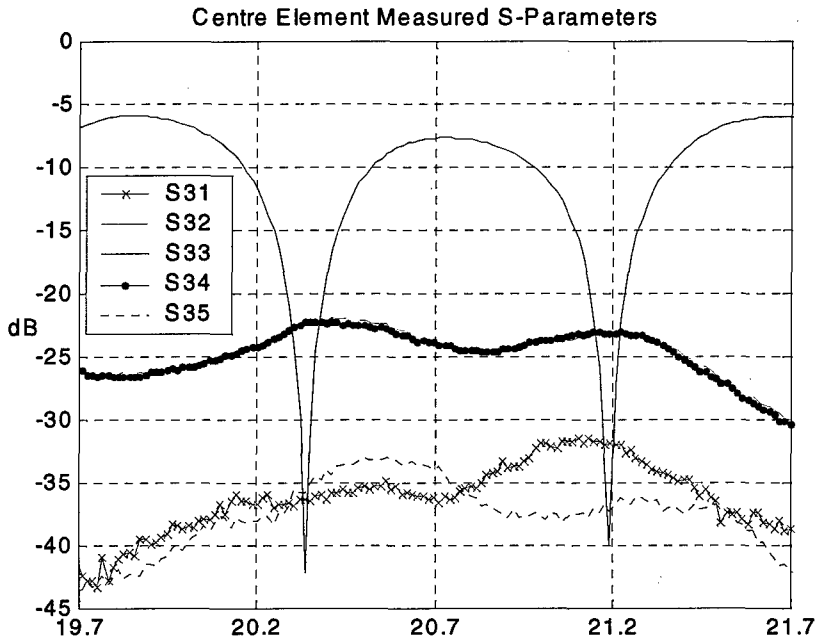

Figure 60: Centre Element Measured S-Parameters

For the outer most elements, the coupling to the centre element is extremely low being less than –30 dB (0.1% of the power). This provides some guidance to future LWG array design such that the element spacing, for 20.7 GHz, can be $\lambda_o/2$ with low mutual coupling between adjacent elements. One can also consider the low mutual coupling results as additional proof that there is very little leakage between the vias that could be coupled through adjacent LWG walls.

Further analysis of the individual elements also merits further discussion. From the smith chart for antenna element #1 in Figure 54, it is apparent that this element's input match is close to the expected result. Thus, with some confidence, one can presume that the coaxial probe and capacitive stub have been accurately fabricated. In this case, as can be seen in Figure 61 and Figure 62, there is good correlation between the expected far-field patterns and the measured results. This provides additional evidence that some of the prototypes, of the long LWG versions, had both far field radiation patterns and bandwidths that met the expected results.

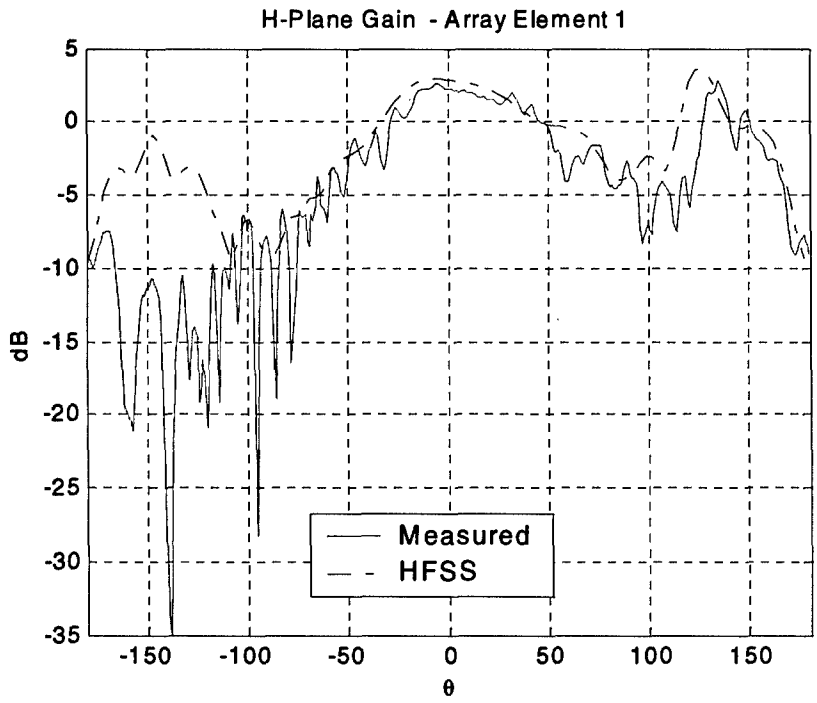

Figure 61. H-plane AGP Array Element 1

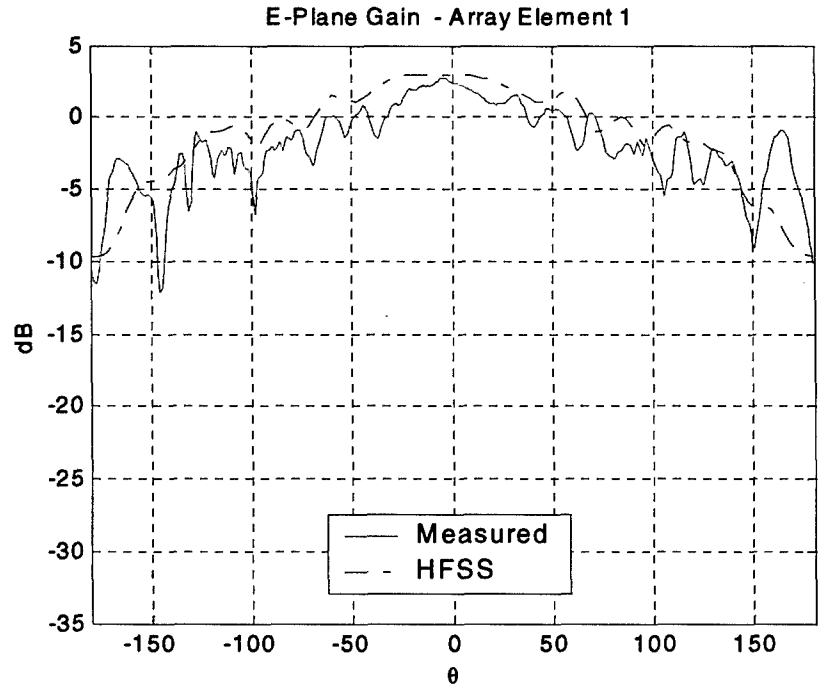

Figure 62. E-plane AGP Array Element 1

4.5. Summary

The measured S-parameters and AGP of the various radiating LWG prototypes demonstrate some key points and issues. As seen with the non-radiating prototypes, a good coaxial match and low loss transmission line can be realised with LWG in the K-band. Bolting the connector, over a pre-fabricated pin, directly to the substrate resulted in an effective feed mechanism for the LWG. The measurements for the radiating prototypes indicated some inconsistencies in both the matching and far field patterns. However, one version of the LWG, the long LWG element, performed as expected as a single antenna by itself and when integrated in an array. Nevertheless, the inconsistencies revealed some of the concern with respect LWG fabrication.

The quality of fabrication and soldering has a significant impact on both the measured matching and AGP results. Although the attempts to attach the connector to the radiating LWG in the various circuits was made with the outmost care and attention by CRC staff, consistency in the final assembly may be beyond the "human" capabilities. Furthermore, some experimentation with adding the connectors to the LWG was performed. This resulted in adapters being soldered to the substrate and then subsequently removed. As the size of the aperture in the upper ground plane is critical to the impedance match of the coaxial transition, any solder, which leaks into the aperture, will corrupt the transition.

As the non-radiating LWG circuits did not have the same problems with inconsistent matching, the problem may be more prevalent with the aperture matching components. The capacitive stub, used for matching the aperture, was added post-lamination by filling a pre-drilled hole with solder. As detailed in the appendix, variation of the depth of the stub will affect the aperture match. With certain array elements and with antenna type B, it was possible produce a working radiating LWG with the coaxial feed. However, the inability to replicate the process with multiple elements on the same substrate prevents fabrication of an array from being probable. If the reliability of the fabrication process can be resolved, then a viable array can be produced.

Some of the other inconsistencies in fabrication of the radiating LWG may have resulted in the varied performance between prototypes. There are two other areas of concern in the fabrication process. One of these is with the uniformity or lack or, in the thickness of the final laminated dielectric. Given the difficulties with forming the blind vias necessary for creating the correct length of capacitive stub, any variation in substrate thickness at the location of the stub, combined with the inaccuracies of drilling the correct depth, has an impact on the quality of the match as seen in the appendix. The other concern is with the quality of the cut at the end of the substrate. During the measurements, it was noticed that the substrate edge at the open end of the LWG substrate was not straight. This resulted in the aperture at the substrate edge not being orthogonal to the top/bottom of the substrate as desired. Such a taper at the aperture will affect both the aperture impedance and AGP.

These fabrication anomalies are specific to the process used to manufacture the LWG prototypes. Other laminated packaging techniques, such as LTCC, are more reliable in forming blind vias and will not suffer from the inaccuracies in drilling depth. However, these other techniques will most likely have other technical hitches to overcome.

5. CONCLUSION AND DISCUSSION

The analytical and design work described in the previous four chapters resulted in a number of functioning LWG prototypes. Before the designs detailed in Chapter 3 were submitted for fabrication, a number of important steps were taken to achieve the final design. To understand the behaviour of radiating apertures, it was first necessary to study the transmission line characteristic, such as losses and bandwidth, of a RWG. Then the relevant analytical expressions for the RWG and for radiation from rectangular apertures were studied to determine the best radiating RWG design to meet the specification. This resulted in the basic dimensions for the RWG. Once the dimensions were known, the RWG design was converted to that of a LWG.

Although it was hypothesised that the characteristics of a LWG and RWG were the same, a more robust model was developed using HFSS. This model was then used to determine the required via spacing and confirm that the RWG hypothesis was applicable. Confidence in the HFSS model was gained by comparing HFSS results for a LWG to those of analytical expressions for RWG. Given the dimension and via configuration, impedance matching networks had to be developed to match the aperture and the coaxial connector to the LWG. No previous work had been published on coaxial feed systems or aperture matching techniques for LWG antennas, so novel solutions had to be developed. Fortunately, previous work had been published on coaxial transitions for RWG [29], but such techniques had never been proven applicable to the relatively new LWG transmission line. The similar was true for the aperture-matching network. Capacitive stubs have been used to tune horn antennas, but no previous published work had proven that blind vias and diaphragms formed by vias could be used as capacitive and inductive circuit elements in a LWG.

The following sections discuss the results of the prototypes as a transmission line, single radiating element and as an array. As with any research, there is a great deal of follow-on work, also described in this chapter, necessary to bring the LWG antenna to its final goal: integration in an array for the AEHF project. Although the beginning of the chapter summarised the general achievements and design process, the final section of this chapter specifically outlines the project accomplishments and validity of the original RWG hypothesis.

5.1. Laminated waveguide

The non-radiating laminated waveguide prototypes, with the two coaxial transitions, had very good results. This demonstrates a number of important items. First of all, the broadband matching techniques used in a coaxial to RWG transition are also applicable for LWG. The non-radiating LWG circuits did not suffer from the same problems as the radiating LWG, which provides additional confidence in the assembly technique used to connect the adapter to the LWG. The results also validate the HFSS model used for designing the LWG to coaxial transition. Given this broadband transition, other circuits used in RWG, such as couplers and filters, can also be implemented in LWG.

Previous work has suggested that LWG is a less lossy transmission line than planar version in the EHF band. As there are now working LWG examples, a direct comparison of losses could be measured by fabricating similar lengths of microstrip and/or strip line circuits in the same CLTE laminate. However, such additional circuits for comparison may be more useful when the LWG is fashioned in the final desired material (LTCC).

These non-radiating LWG prototypes are significant accomplishments. They prove that a RWG can be implemented within a substrate using standard PCB fabrication techniques. The

excellent reflection and transmission co-efficient demonstrate the effectiveness of the LWG as a low-loss microwave transmission line. Furthermore, the measured results show that a coaxial adapter can be directly integrated with a LWG resulting in broadband (17-25 GHz) and very low loss (0.15 dB) coaxial transition. New LWG circuits, such as couplers and filters, can now be developed and fed directly with a simple coaxial adapter.

5.2. Radiating LWG – single element

The long radiating LWG (prototype B) performed quite close to the expected result. A bandwidth (SWR < 2) of 1.1 GHz (20.2 – 21.3 GHz) was achieved. This met the desired AEHF uplink specification. Both the E- and H-plane AGP were relatively broad (HPBW > 60 degrees) with a maximum gain in the order of 3 dB. The far field radiation patterns correlated closely to the expected results of the HFSS. The antenna had low cross-polarisation levels and very low backfire radiation levels. This prototype design resulted in an end fire antenna element that may be very useful for future use in an array in the AEHF band.

The performance of this LWG prototype demonstrated some of the primary goals of this project hypothesis. First of all, it is possible to implement a radiating RWG in a substrate using LWG. All of the impedance matching networks can be implemented using vias fabricated with standard PCB techniques. A simple capacitive stub and an inductive diaphragm can be used to match the aperture to the LWG over the desired bandwidth. As with the non-radiating prototypes, a broadband coaxial transition can be implemented with the coaxial connector directly on the LWG substrate. The design was accomplished through analytical and HFSS models utilising the design constraints of both the CRC model shop and a standard LTCC foundry.

The measured antenna properties (beamwidth, bandwidth and gain) correlated closely with those predicted by the HFSS model. This confirms that LWG antennas can be designed using modern EM design software such as HFSS. As the ADP of the analytical model and HFSS model were closely matched for the main lobe, the LWG radiating aperture can be designed using simple analytical expressions to achieve the desired far-field radiation pattern and directivity. Using such expressions greatly simplifies the design process. The analytical analysis of the aperture demonstrated that the optimum specifications for beamwidth of a single element could not be met with a radiating aperture on a CLTE substrate. The HFSS model and measured results confirmed that the beamwidth, in the H-plane, was less than the DRDC Ottawa specification. Essentially, the specified beamwidth cannot be met for a waveguide with a design constraint that the cut-off frequencies (TE 10 and TE 01) are at least 20% from the centre frequency.

The behaviour of the long radiating prototypes, and the correlation between the measurements, HFSS models and analytical results, provides substantial evidence with respect to the validity of the RWG hypothesis. This project has shown that the analytical results for ADP and transmission line characteristic (impedance and losses) correlate with the HFSS model. As the HFSS model results correlate with the measured results, one can state that the behaviour of a LWG can be closely approximated by a RWG. Therefore, the design techniques applicable to RWG, as proven with the coaxial probe to LWG design, should be applicable to LWG design.

None of the short radiating LWG prototypes were able to meet the expected performance characteristics. The short elements were poorly matched and did not correlate well with the predicted results. This may have been a result of the inconsistencies in the fabrication such as soldering of the coaxial transition, the capacitive stub, or a combination of both. The end result was a poorly matched antenna.

The AGP of the short radiating LWG elements were also distorted. This may have been the result of having the aperture too close to the coaxial transition. The effect of this was predicted by HFSS, as seen by a ripple in the ADP, but was not as severe as in the measurements.

This poor AGP could have also resulted from the soldering problems noted above. Nevertheless, the short version of the LWG did not result in a useful antenna.

5.3. LWG array

Although the array did not perform as expected, array element 1 functioned quite well. This element was well matched, as can be seen from the return loss plot in appendix C, with a bandwidth (SWR <2) of 20.1 – 21.4 that exceeded the requirement of the AEHF specifications. The H-plane results correlated very well with the expected HFSS results with the E-plane pattern being reasonably close to the HFSS result. This element was a long version of the LWG antenna. It was fabricated with same coaxial adapter configuration as antenna type B and provides further evidence as to the potential performance of a radiating LWG as an end-fire antenna.

The poor performance of the entire array can be attributed to the performance of the individual elements. Array element 1 was the only element that was well matched. As detailed in the Smith charts for elements 2-5 (Figure 54), the reflection coefficients were significantly different from the expect results. Therefore, a majority of the array elements were poorly matched. As described above, short radiating LWG (prototype C) suffered from a distorted AGP. Thus, the final array was comprised of 4 poorly matched elements and two of those elements had significant distortion with the far field patterns. This resulted in the array measurements being significantly different from the analytical and HFSS results

Analysis of the array was able to provide useful information for any follow-on LWG array designs. One of the more important lessons learned is that careful attention must be made to the length of the LWG elements in the array. In this project design, the element spacing of $\lambda o/2$ was too small for the K-type connectors and the coaxial connectors overlapped. For this reason, two elements of differing length were used to stagger the connectors. Unfortunately, the difference in element length should have been chosen to be $n\lambda_g$, where n is an integer, to ensure that the fields were in phase at the aperture. This would simplify the feed arrangement by removing the necessity for a 180-degree phase shift. As shown in the analytical array analysis, this extra length has very little effect on the array directivity since the LWG losses are small.

Obviously, there was a significant problem with the inconsistency of the matching with the various elements. Although the exact cause is not known, the most likely cause of the mismatch is due to the fabrication of the capacitive stub or coaxial connector. As the coaxial transition is broadband, it is more resilient to fabrication tolerances. The aperture-matching network is narrowband will therefore suffer greater affects from deviations in fabrications as noted in Appendix A. This leads one to suspect that there may be a problem with the fabrication of the capacitive stub. One potential solution is to replace the stub in future prototypes with a small screw or bolt. This would allow for fine-tuning of the elements after fabrication. Once the element is tuned, the bolt can then be soldered in place to ensure long-term performance. The other solution may be to determine a more accurate way of implementing a blind via in the substrate or by fabricating a prototype with LTCC. Nevertheless, the process used with CLTE was somewhat inconsistent and must be rectified in order to produce a working array.

5.4. Future work

As is true for most research, the work is never entirely complete. Although the initial study of determining if a radiating RWG could be implemented within a substrate in the form of LWG is complete, there is much more that should be investigated. In support of this, a variety of items recommended for further investigation are provided in the following sub-sections.

5.4.1. Multi-layer fabrication

To simplify the fabrication process and remove sources of potential error, the first prototypes were fabricated by laminating two layers of substrate. This was done to reduce the possibility of lateral displacement of the post-fired layers. The original design submitted consisted of multiple layers of 0.254 mm substrate with the vias formed before laminating the layers together. However, the CRC model shop was not certain if the lateral displacement between layers would be less than 50 μm (1-2 mil). Such a lateral displacement could have resulted in connectivity problems within the via stacks.

To remove this source of error, layers were laminated first and then drilled to form the vias. Unfortunately, this resulted in a substrate that was too thick for drilling to the originally specified via diameter. This also created an additional source of error in the blind via depth for probe and capacitive post fabrication. Nevertheless, the technique resulted in a functioning LWG. Given the promising results for the long version of the radiating LWG, additional circuits should be fabricated using multiple layers of thin substrate to better replicate the laminated packaging technique process of LTCC.

5.4.2. Fabrication with LTCC

The next recommended step is to fabricate the circuits in LTCC with a low loss material (943 tape). This will demonstrate whether a radiating LWG can be effectively mass-produced in the original material specifications. However, as the material properties and fabrication guidelines are different, some additional design work is required. The initial part of this "design work" is provided in the following section.

5.4.3. Design conversion for LTCC

The previous prototypes have demonstrated that it is possible to implement a radiating RWG in LWG. These prototypes have also validated the analytical expressions used in designing the LWG. The final design step is to provide the framework and basic specification to implement a radiating LWG in LTCC according to available design rules from National Semiconductor [36].

Three basic expressions govern the LWG design. Equations 3.2 and 3.3 provide the RWG dimensions as a function of cut-off frequency for the first two modes. The final expression, Equation 3.4, provides the via pitch required to minimise the losses between the vias. Given these expressions, and the material properties of LTCC (Table 12) at the desired frequency, it is possible to provide the framework for a future design (Table 13) and predict the main lobe far-field radiation pattern (Figure 63).

Table 12. Material Properties for LTCC (943 Tape)

Dielectric Constant (ε_r)	7.5
Loss Tangent	0.001
Fired Thickness	111.8 μm (4.4 mil)

Table 13. LWG Dimensions for LTCC (943 Tape)

a	3.3 mm
b	2.1 mm (19 layers)
d	0.53 mm (20.8 mil)

Table 14: LTCC Design Guidelines

Via ∅ (mm/mil)	0.43/17	0.22/8.7	0.18/6.9	0.13/5.2	0.09/3.5
Via Pitch (mm/mil)	1.29/51	0.66/26.1	0.53/20.7	0.39/15.6	0.27/10.5
Vias Stack Limit (layers)	22				

As in the design with CLTE laminate, the LTCC LWG thickness is implemented by a finite number of tape layers. A desired thickness of 2.2 mm, calculated by Equation 3.3, can be implemented with 19 – 20 layers of tape. 19 layers should be selected, as this will result a lower thickness (b) that increases the H-plane beamwidth.

Comparing the design with the LTCC fabrication limits in Table 14, the LTCC LWG is best implemented with the 0.18 mm via. It is also important to note the limit on stacked vias (22) and the catch pad size (round or square of 0.66 mm). As the design guidelines (via diameter and pitch) and material properties are different from the CLTE prototypes fabricated by CRC, the impedance matching circuitry for the LTCC circuit will be different. HFSS could be used to design the aperture and transition matching networks for the LTCC LWG.

Using the analytical expressions (Equations 2.17 and 2.18), it is also possible to predict the antenna directivity of the LTCC LWG. Implementation of the above design should result in a single element with a maximum directivity of 4.07 dB and a beamwidth (H-plane) of 74.5 degrees. The main lobe pattern is provided in Figure 63.

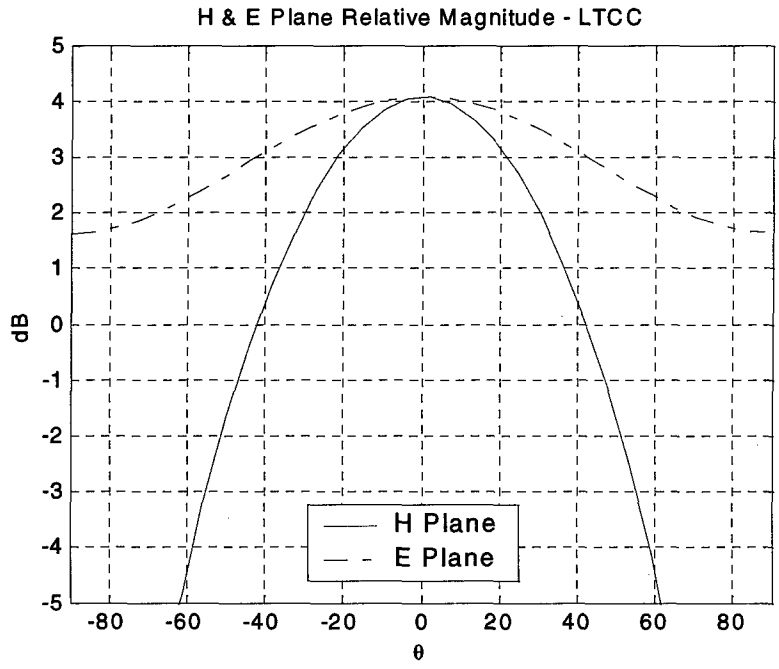

Figure 63. LTCC LWG Antenna Directivity Pattern

5.4.4. Planar transmission line feed

If the LWG antenna is to be integrated into the same substrate as the other RF components, then a planar transmission line feed system may be desirable. A planar transmission line, such as stripline, microstrip or CPW, would allow for the antenna to be directly connected to the other RF components within the same substrate. Although it is possible to accomplish this with coaxial connectors, a planar transmission feed system would reduce the space required for the circuit card. Previous research has suggested [37] that a microstrip to probe transition may result in an effective feeding system for a LWG. Some preliminary research on a narrowband stripline to LWG probe transition was conducted for this project, but was abandoned for the broadband coaxial transition. Nevertheless, it may be possible to implement a stripline to probe fed LWG transition.

5.4.5. LWG array

Once the above steps are completed and an effective single element can be reliably reproduced in LTCC, the entire array could be fashioned. The element spacing limitations may be avoided through the use of either a planar transmission line or changing the coaxial adapter type. The LTCC packaging method, which allows blind vias, may be able to effectively replicate numerous elements. Nevertheless, a functional array can only be fabricated once a method to consistently reproduce the individual elements is developed.

5.5. Project accomplishments

The research of this project has demonstrated two substantial accomplishments. First of all, it is possible to implement a broadband coaxial transition for LWG as proven with the two fabricated LWG prototypes. Such a design allows for the coaxial adapter to be connected directly to the substrate using only a pin to form the electrical connection between the adapter and the LWG. Once placed over the pin, the connector can be either bolted to the substrate or soldered to the LWG. This provides a simple yet highly effective method to connect a coaxial transmission line to the low-loss LWG microwave transmission line.

The other significant accomplishment was the use of LWG to implement a radiating RWG within a substrate. This project proved that the AEHF bandwidth specifications could be met with a radiating LWG. The impedance matching network was comprised of vias that formed the necessary reactive elements to match the aperture to the LWG. As an antenna, the LWG had a broad beamwidth, reasonable gain, low cross-polarisation and backfire radiation levels. Although the beamwidth in one plane, the H-plane, did not meet the specification, such a specification cannot be met with a rectangular aperture while maintaining sufficient bandwidth between the cut-off frequencies.

Nevertheless, the long radiating LWG (prototype B) demonstrated excellent promise as a potential array element for the AEHF band. Although the array did not function as predicted, the long radiating LWG element proved that an end fire radiating antenna could be realised in a laminated substrate. This research provided the necessary analytical models and prototypes to demonstrate that a brick architecture array fashioned with radiating LWG antennas is entirely feasible in the AEHF band.

6. REFERENCES

1. Balanis, C., "*Antenna Theory*", 2nd Ed., John Wiley & Sons, New York, 1982, pg.1.

2. Garg, R., Bhartia, P., Bahl, I.,and Ittipiboon, A., "*Microstrip Antenna Design Handbook*", Artech House, Boston, 2001, pp. 753-756.

3. Balanis, C., "*Antenna Theory*", 2nd Ed., John Wiley & Sons, New York, 1982, pg. 249

4. Mailloux, R. "*Phased Array Antenna Handbook*", Artech House, Boston, 1994, p. 311.

5. http://sensor.northgrum.com/esss/ltcc/LowTemperatureCofiredCeramics(LTCC).pdf

6. Garg, R., Bhartia, P., Bahl, I.,and Ittipiboon, A., "*Microstrip Antenna Design Handbook*", Artech House, Boston, 2001, pg. 399.

7. Gupta, K.C., Garg, R. Bahl, I., and Bharitia,P., "*Microstrip_Lines_and_Slotlines*", 2nd ed., Artech House, Boston, 1996, p.294.

8. Yngvesson, K., et al., "*The Tapered Slot Antenna – A New Integrated Element for Millimeter-Wave Applications*," IEEE Transactions on Microwave Theory and techniques, vol. MTT-37, 1989, pp 365-374.

9. Balanis, C., "*Antenna Theory*", 2nd Ed., John Wiley & Sons, New York, 1982, pp. 575-643.

10. Deal, W., Kaneda N., Sor, J. Qian Y, Itoh, T., "*A new Quasi-Yagi Antenna for Planar Active Antenna Arrays*", IEEE trans on MTT., vol. 48., no. 6, June 2000, pp. 910-918

11. Balanis, C., "*Antenna Theory*", 2nd Ed., John Wiley & Sons, New York, 1982, pp. 651-682.

12. Pozar ,D., "*Microwave Engineering*", 2nd Ed., John Wiley & Sons INC., New York, 1998, pp. 104-176.

13. Uchimura, H.,Takenoshita, T., and Fujii, M., "*Development of a Laminated Waveguide*," IEEE Transactions on Microwave Theory and Techniques, December 1998,vol. 46, no. 12, pp. 2438-2443.

14. Sherman, J., "*Application Note: Introduction to Impedance Definitions*", ANSOFT: September 9, 1998. pp. 1-14.

15. Collin,R., *Foundations for Microwave Engineering*, 2nd Ed., IEEE Press, New York, 2001, pp. 71-219.

16. Pozar, D., "*Microwave Engineering*", 2nd Ed., John Wiley & Sons INC., New York, 1998, pg. 16.

17. Cheng, D., "*Field and Wave Electromagnetics*", 2nd Ed., Addison-Wesley, New York, 1989, pp. 524-530.

18. Pozar, D., "*Microwave Engineering*", 2nd Ed., John Wiley & Sons INC., New York, 1998, pg. 56-65.

19. Sherman, J., "*Application Note: Introduction to Impedance Definitions*", ANSOFT: September 9, 1998. pp. 11.

20. Hirokawa, J., Ando, M., "*Single-layer Feed Waveguide Consisting of Posts for Plane TEM Wave Excitation in Parallel Plates*," IEEE Trans. Antennas Propagation., vol. 46, no. 5, May 1998, pp. 625-630.

21. Bray, J. and Roy, L., "*Laminated Waveguide Couplers in LTCC Technology*," ANTEM 2000 – Symposium on Antenna Technology and Applied Electromagnetics, August 2000, pp. 527-530.

22. Balanis, C., "*Antenna Theory*", 2nd Ed., John Wiley & Sons, New York, 1982, pp. 116-132.

23. Collin, R., "*Antennas and Radiowave Propagation*", McGraw-Hill, New York, 1985, pg. 188.

24. Balanis, C., "*Antenna Theory*", 2nd Ed., John Wiley & Sons, New York, 1982 pp. 28-98.

25. Pozar, D., "*Microwave Engineering*", 2nd Ed., John Wiley & Sons INC., New York, 1998, pp. 251-296.

26. Collin,R., "*Foundations for Microwave Engineering*", 2nd Ed., IEEE Press, New York, 2001, pp 303-360.

27. Cheng, D., "*Field and Wave Electromagnetics*", 2nd Ed., Addison-Wesley, New York, 1989, pg. 451.

28. Marcuvitz, N., "*Waveguide Handbook*", vol. 10, MIT Radiation Lab Series, McGraw-Hill Co., 1951.

29. Keam, R., Williamson, A., "*Broadband design of coaxial line/rectangular waveguide probe transition*", IEE Proceedings Microwave, Antennas and Propagation, Vol 141, No.1, Feb. 1994, pp.53-58.

30. Balanis, C., "*Antenna Theory*", 2nd Ed., John Wiley & Sons, New York, 1982, pg 251.

31. Balanis, C., "*Antenna Theory*", 2nd Ed., John Wiley & Sons, New York, 1982, pg. 289-311.

32. Terret, C. "*Propagation Libre et Guidee des Ondes Electromagnetiques*", University De Rennes, pg.43.

33. Cheng, D., "*Field and Wave Electromagnetics*", 2nd Ed., Addison-Wesley, New York, 1989, pg. 557.

34. www.ansoft.com

35. Kraus, J., Marhefka, R. "*Antennas*" 3rd Ed. McGraw-Hill, New York, 2001, pp. 309-340

36. *"Design Rules For Physical Layout of Low Temperature Co-Fired Ceramic Modules"*, National Semiconductor Corporation, Revision 8.1,2000.

37. Uehimura, H., Takenoshita, T "A Ceramic Planar 77GHz Antenna Array", Microwave Symposium Digest, 1999 IEEE MTT-S International , Vol 2 , 1999, pp. 453 –456.

7. APPENDICES

7.1. Appendix A - Effect of tolerances on return loss

The original fabrication plan was to emulate the LTCC process and fabricate the vias prior to lamination. With this technique, the via length would be fixed by the number of layers. However, forming the desired LWG thickness with as few layers as possible greatly simplified the fabrication processes. The vias were then drilled after laminating the substrate. This resulted in an additional tolerance (+/- 50.8 μm or 2 mil) for the length of the capacitive post and the coaxial probe due to the accuracy limits of the milling machine. The overall effect on the bandwidth of the circuit was not known, however, previous simulations had noted that changing the length of post by one thin layer (0.254 mm) of substrate had an affect on the match. Just prior to fabrication, a number of simulations were performed to predict the effect of via depth tolerance on the blind vias (probe and capacitive post).

Four groups of simulations with HFSS were completed. The first group, detailed in Figure 64 and Figure 65, show the effect of varying both the length of the probe and post by the maximum tolerance (+/- 50.8 μm or 2 mil) on the long and short radiating waveguides respectively. The second group of simulations, Figure 66 and Figure 67, illustrate the effect of probe thickness on the match. These latter simulations were required, as there was some concern over the manufacturing of the probe and possible variation of the diameter of the probe used to connect the coaxial adapter to the LWG.

The effect on the probe and post length variation is significant. As can be seen from above, a difference of only 50.8 um on either circuit element will change the impedance match. However, this change is not always adverse, and in some cases improved the match. The effect to probe diameter variation was not as significant as long as there was no gap between the probe and dielectric material as seen in Figure 67. This effect is less likely due to the extremely tight tolerance in drill diameter as opposed to the tolerance in drilling depth.

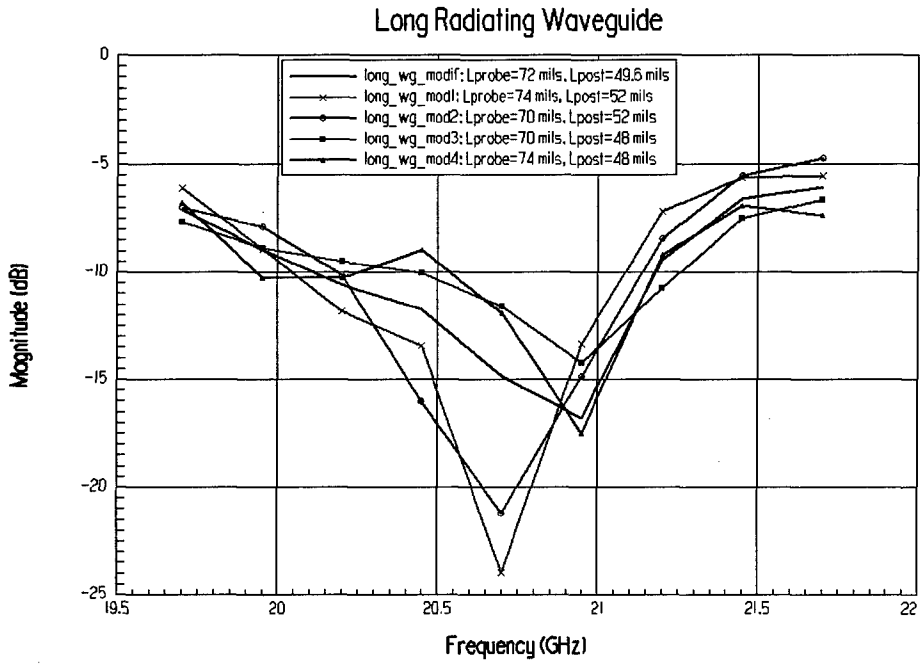

Figure 64. Variation of Probe and Post – Long Antenna

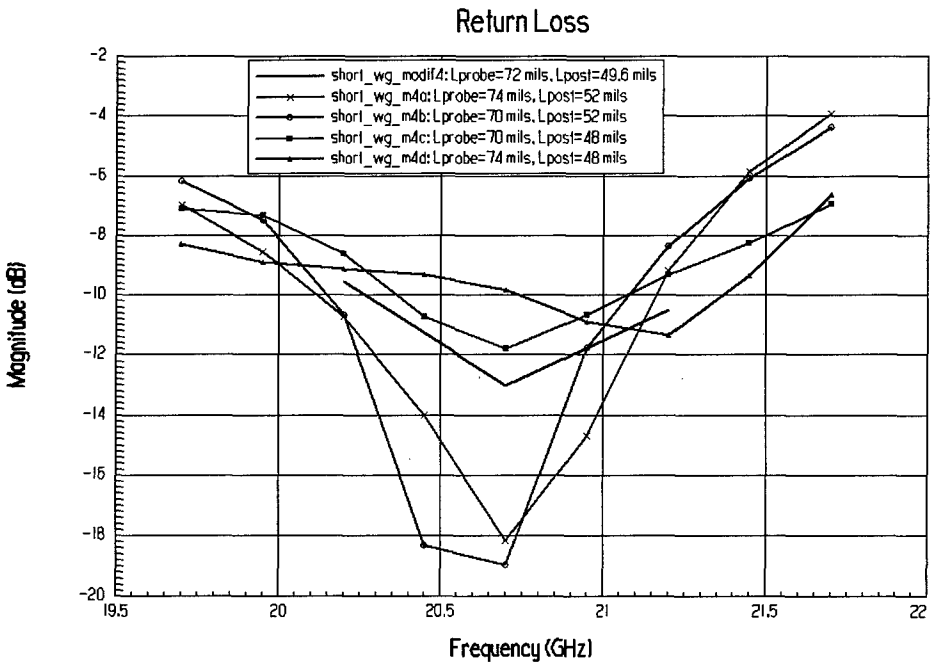

Figure 65. Variation of Probe and Post – Short Antenna

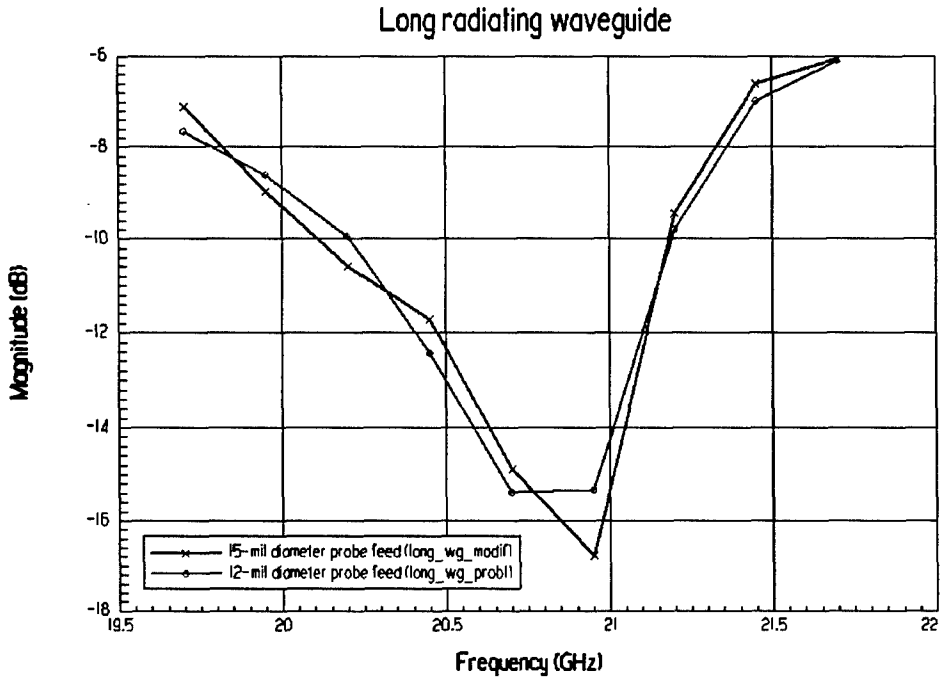

Figure 66. Variation of Probe Diameter – Long Antenna

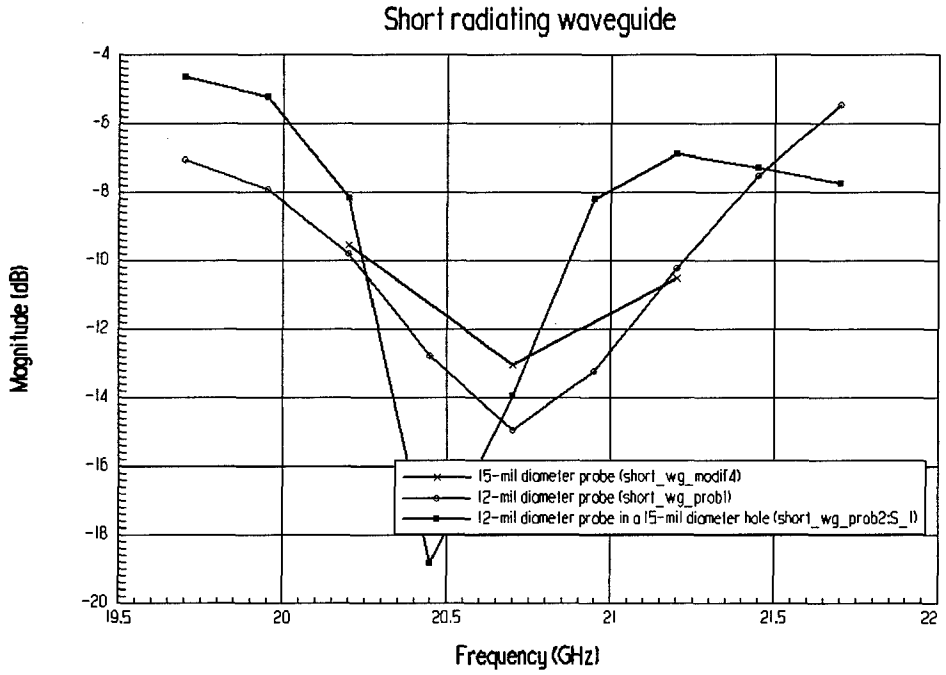

Figure 67. Variation of Probe Diameter – Long Antenna

7.2. Appendix B - Effect of substrate width on radiation pattern

The one significant difference between the far field radiation pattern of a rectangular aperture and a radiating LWG is that of side lobes. Evident in Figure 22 of Chapter 3, the ADP for both the short and long radiating LWG versions had significant side lobes at +/- 135 degrees in both the E- and H-plane plots. These side lobes are also not apparent in an HFSS simulation of a radiating RWG in Figure 68.

Figure 68 is the HFSS ADP, taken from Figure 10, of a dielectric filled RWG radiating into free space. The RWG is not embedded in a block of dielectric. As can be seen in the resultant ADP, there are no side lobes.

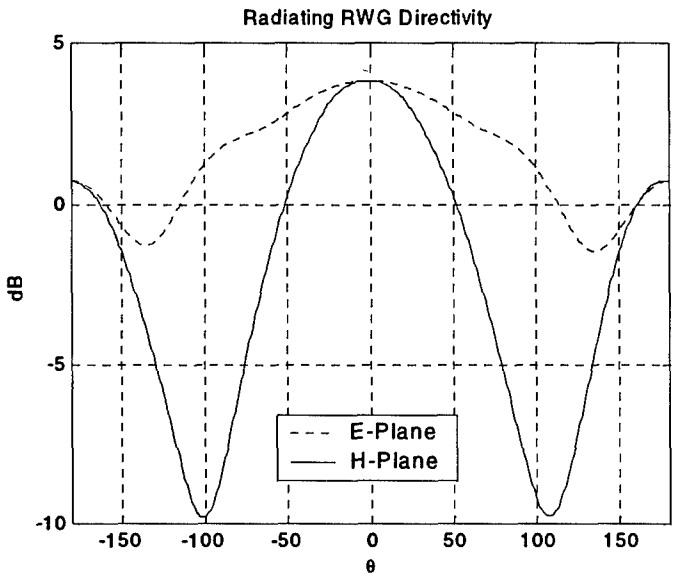

Figure 68. Radiating Rectangular Waveguide (Dielectric Filled) Directivity

When the same RWG is placed in the centre of a block of dielectric in which the substrate thickness is the same as the RWG but the dielectric width is greater than the RWG, HFSS predicts the occurrence of side lobes. As can be seen in Figure 69 and Figure 70, there is a relationship between the side lobe and the size of the substrate (thick narrow = 1", thick short = 1.5", thick wide = 3"). Although it appears that the maximum intensity changes with substrate size, it is important to note that the plot for the E- and H-plane for the RWG in the narrow substrate is a directivity plot, whereas the others are for gain (gain < directivity as the antenna is not 100% efficient).

Given the three Figures, the only difference between the HFSS models was the lack of a substrate (Figure 68) and width of substrate (Figure 69 and Figure 70); therefore it is obvious that the side lobes are caused by the additional substrate outside of the RWG. It is also reasonable to assume that the side lobes are the result of diffraction at the substrate edge, which would account for the side lobe location changing with substrate width in the H-plane. In the E-plane, increasing the substrate width has both a positive effect in reducing the

backfire radiation and side lobe levels. In the H-plane, increasing the substrate thickness reduces the backfire radiation, but at the expense of increasing the side lobe level.

In the LWG design, a substrate width of 1.5" was selected which corresponds to the green RWG case. Given the results from the RWG models, it is suspected that the side lobes evident in the measured radiating LWG (prototype B) are the result of diffraction from the substrate edge.

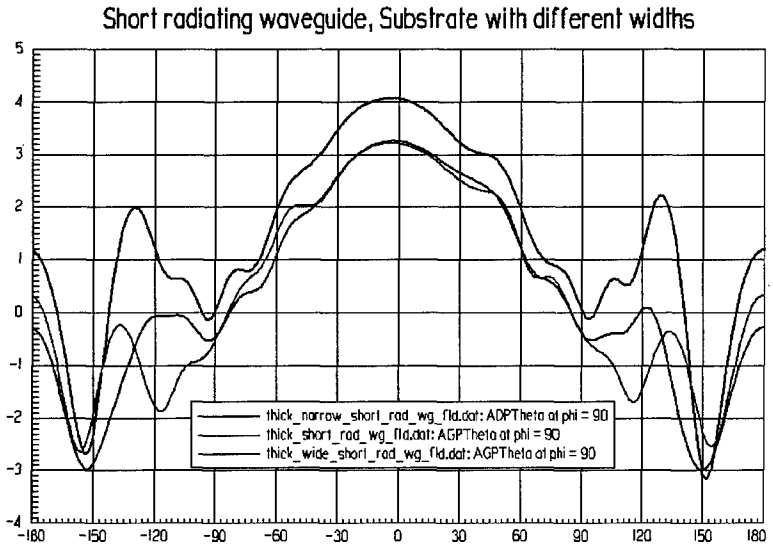

Figure 69. Effect of Substrate Width on E-Plane Radiation Pattern

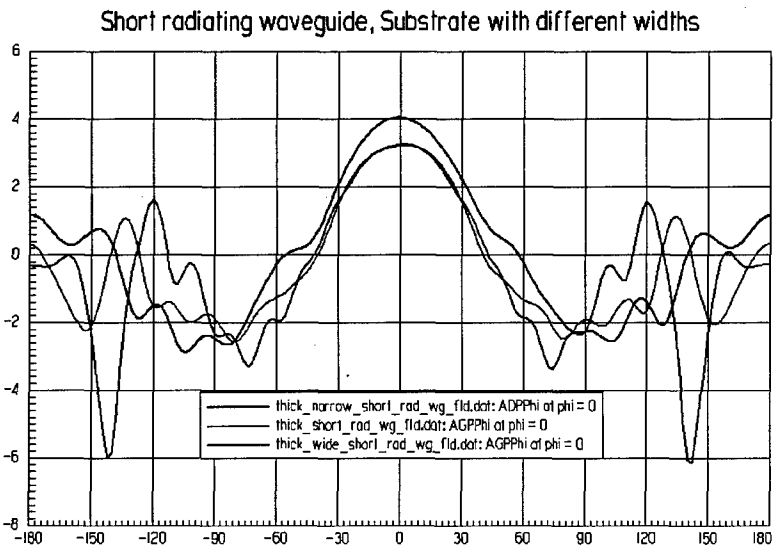

Figure 70. Effect of Substrate Width on H-Plane Radiation Pattern

7.3. Appendix C - Measured data

The following graphs contain the raw measurement data provided to DRDC-Ottawa by CRC for the various prototypes designed for this project. The graph labels correspond to the prototypes in Figure 27 and Figure 28.

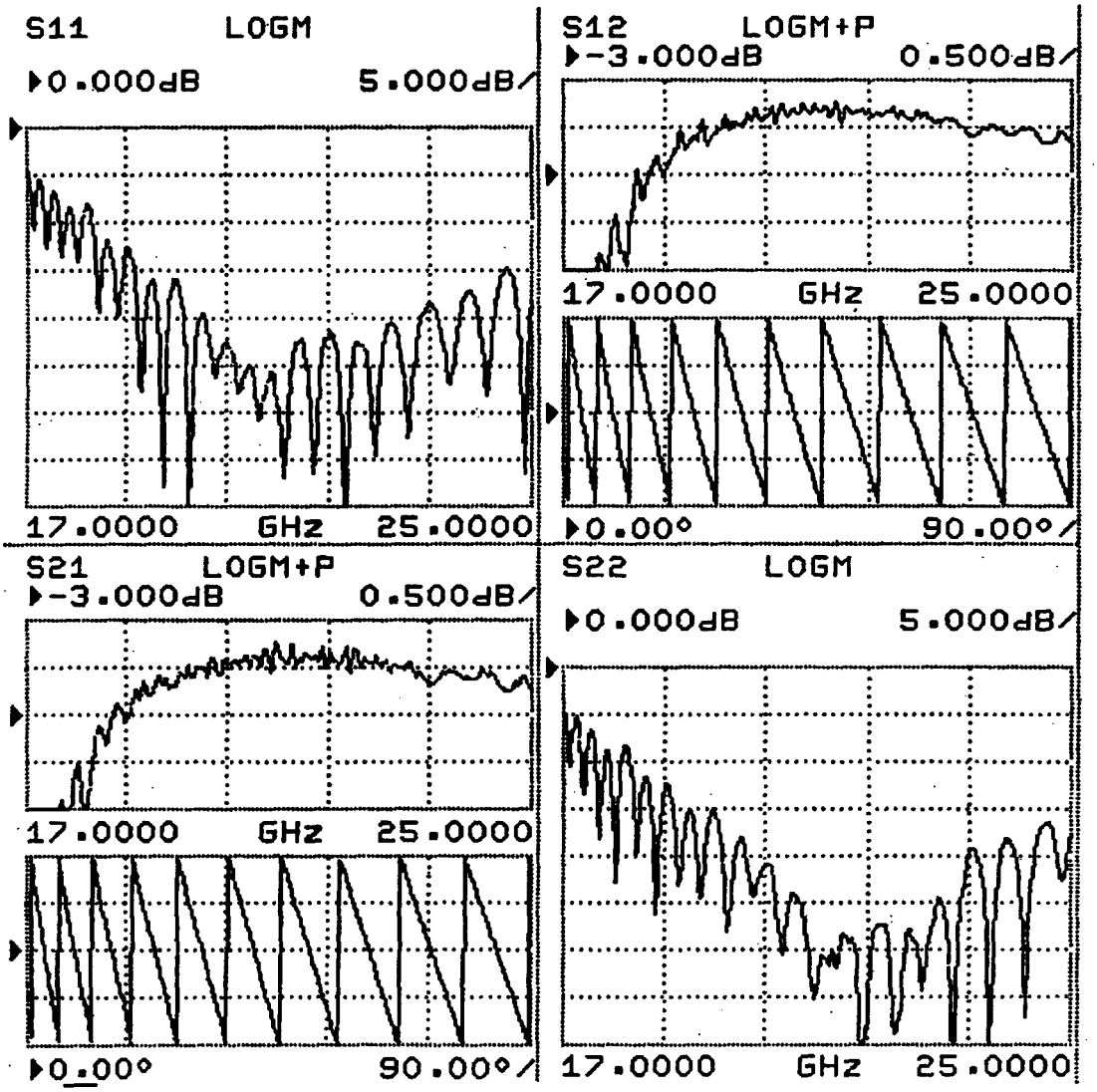

Figure 71. Long non-radiating LWG S-parameters

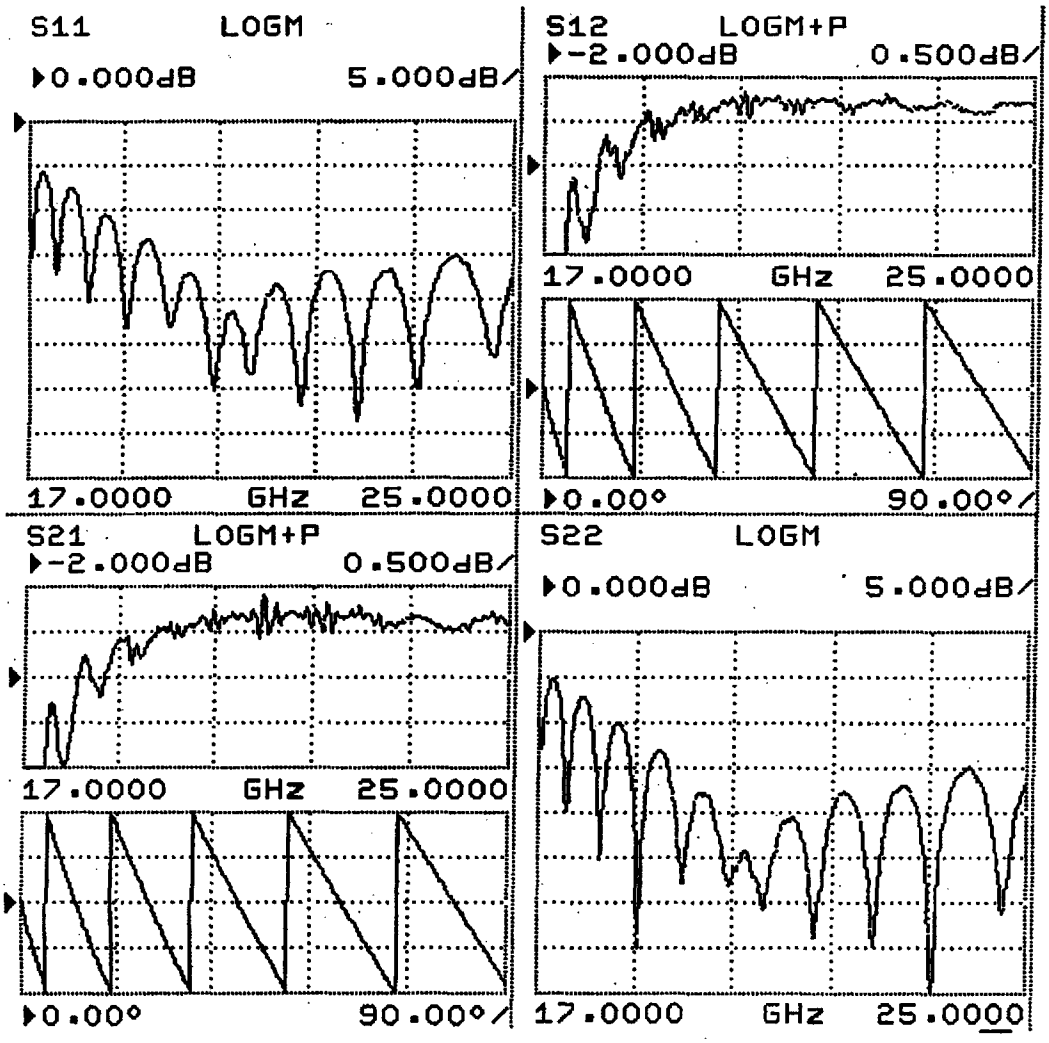

Figure 72. Short non-radiating LWG S-parameters

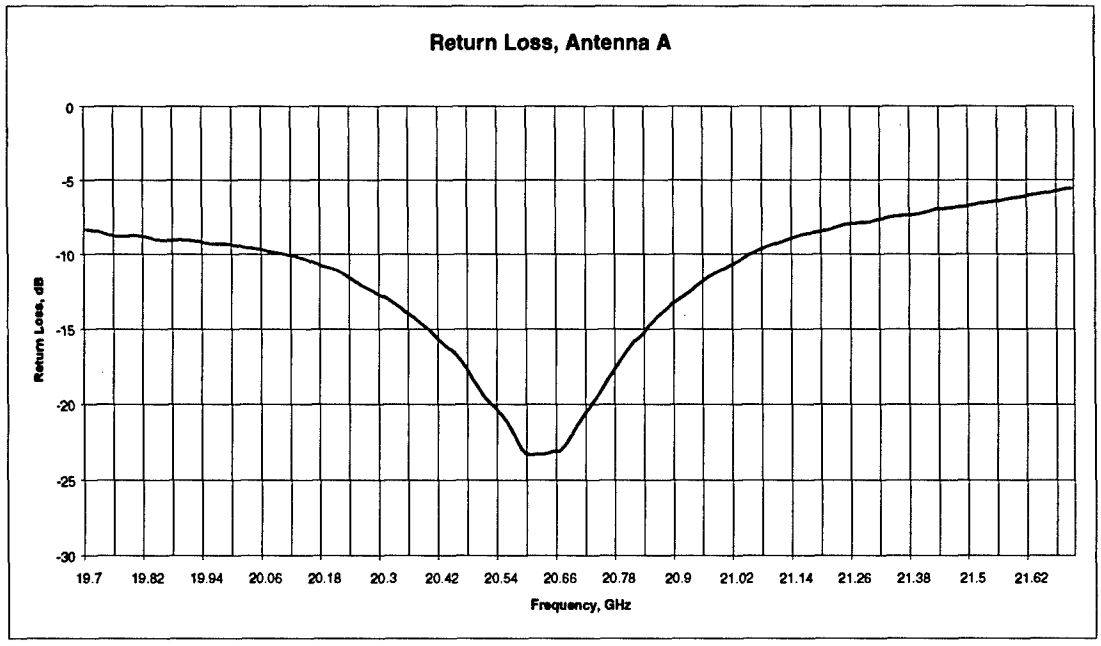

Figure 73. Antenna A Return Loss

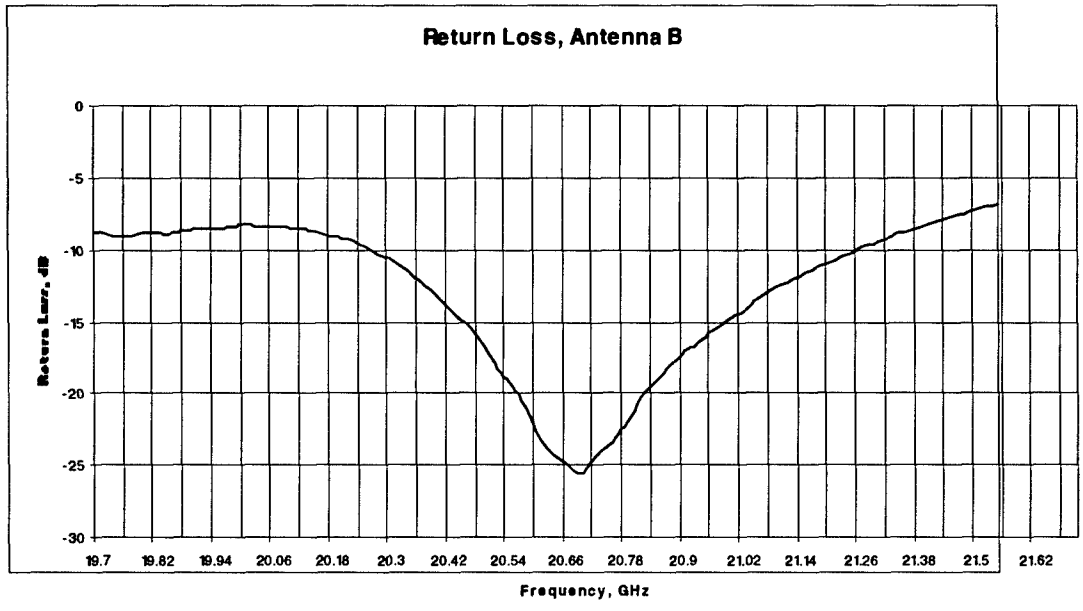

Figure 74. Antenna B Return Loss

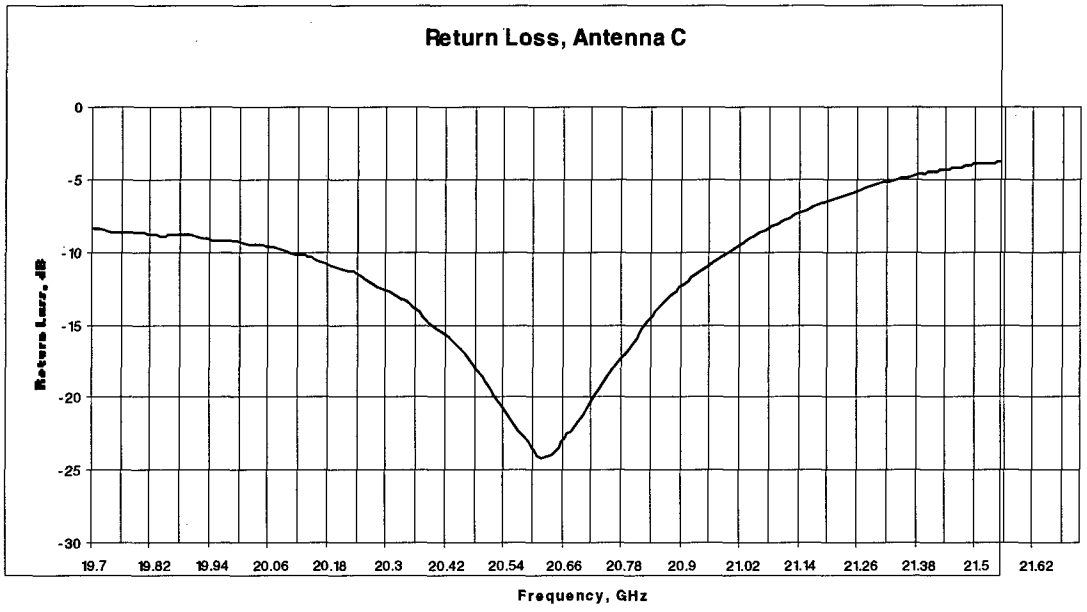

Figure 75. Antenna C Return Loss

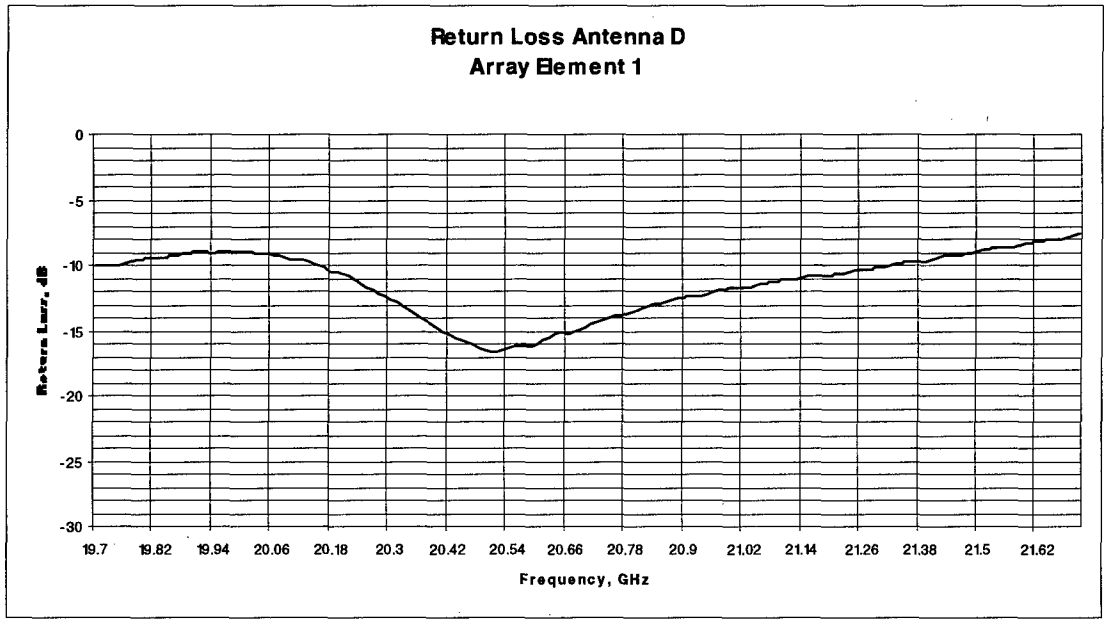

Figure 76. Array Element 1 Return Loss

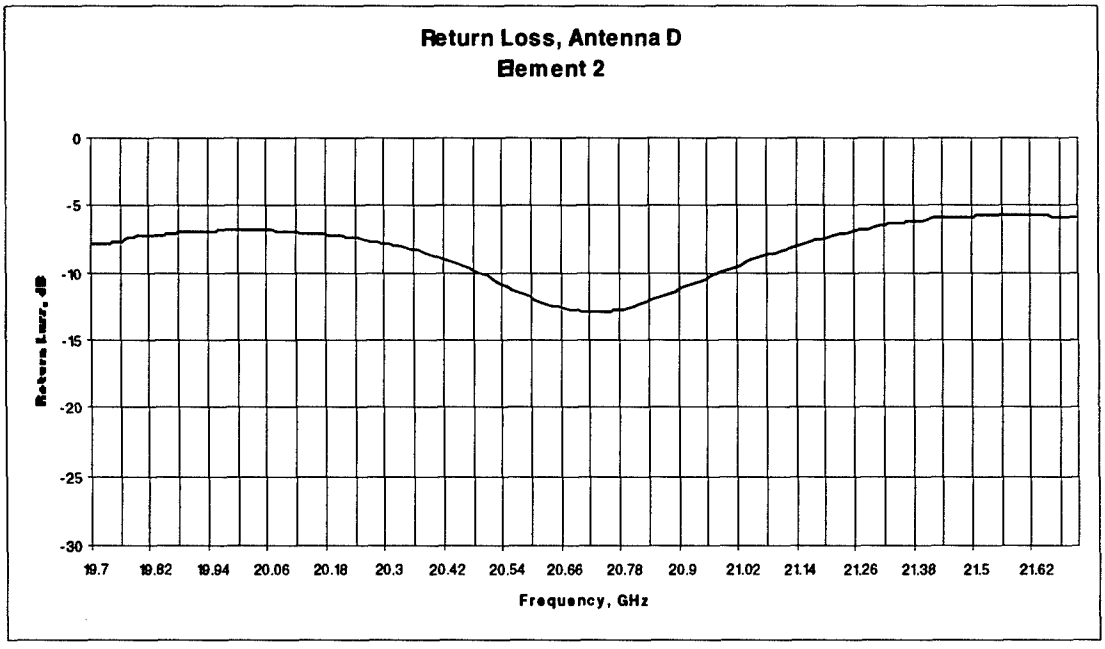

Figure 77. Array Element 2 Return Loss

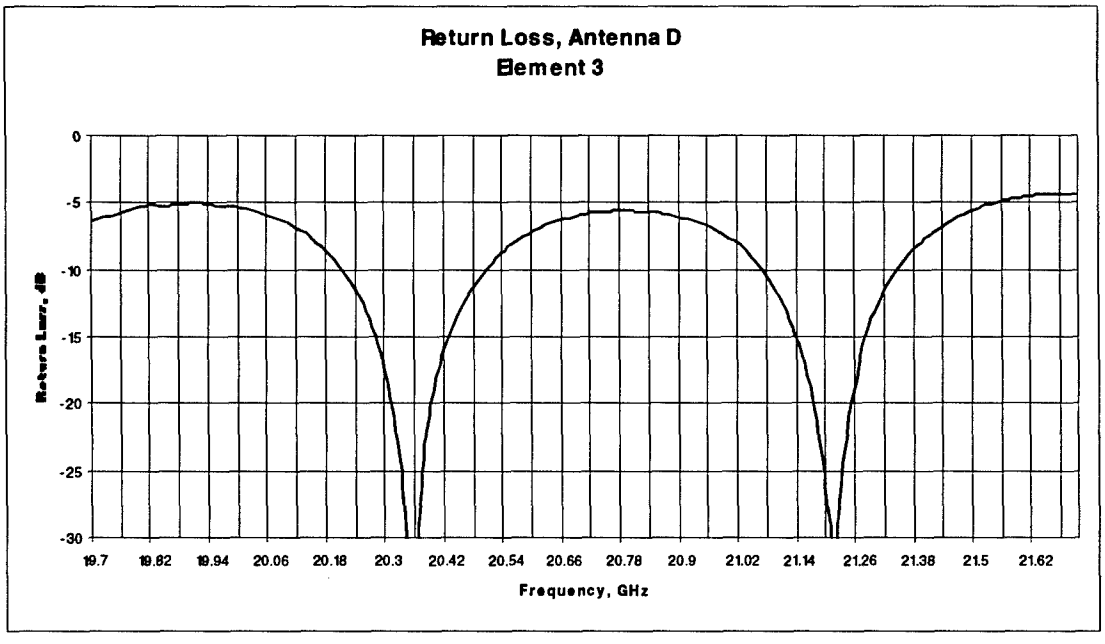

Figure 78. Array Element 3 Return Loss

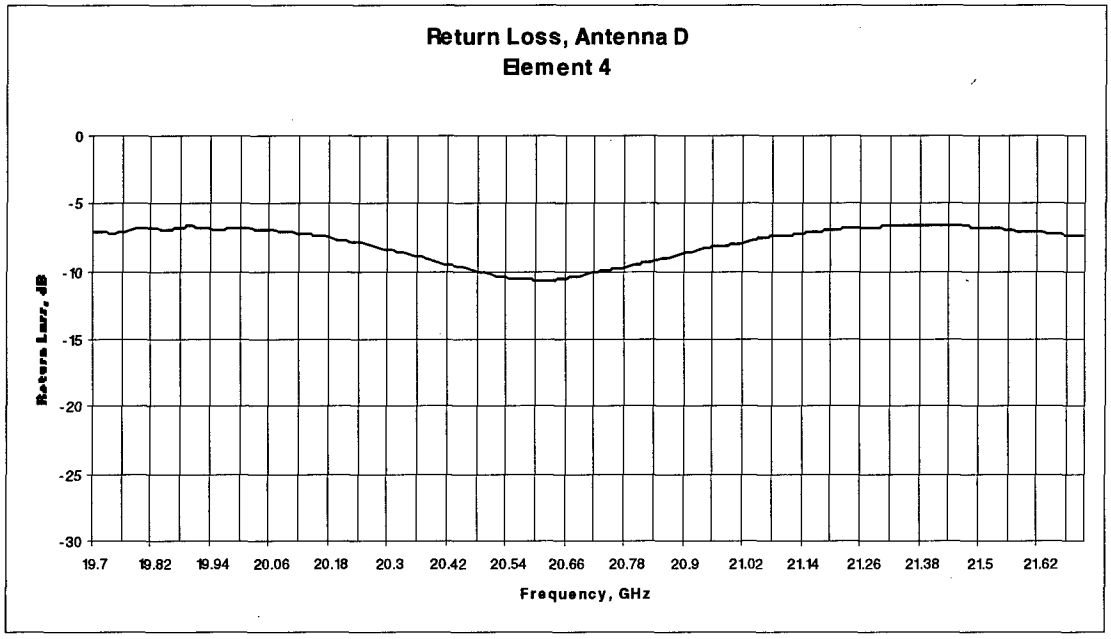

Figure 79. Array Element 4 Return Loss

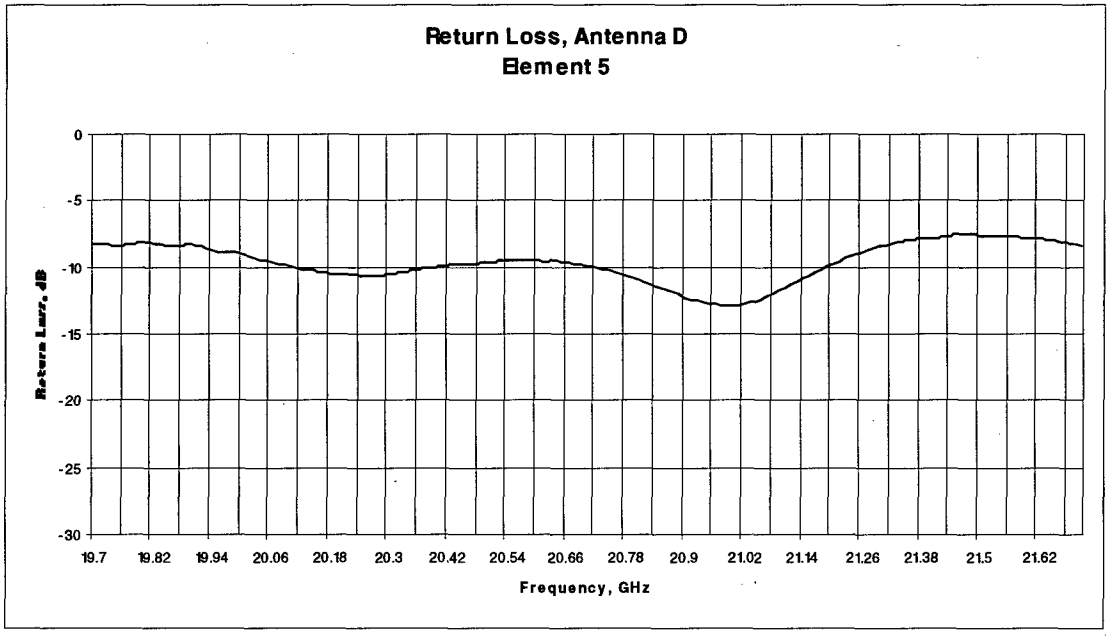

Figure 80. Array Element 5 Return Loss

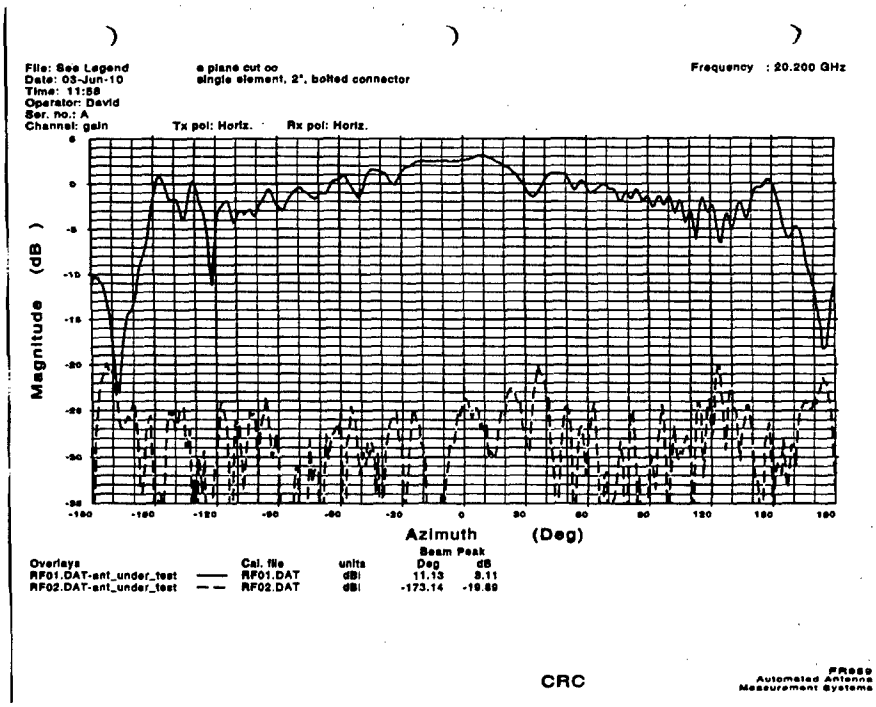

Figure 81. Antenna A E-Plane Co- and Cross-polarisation (---) 20.2 GHz

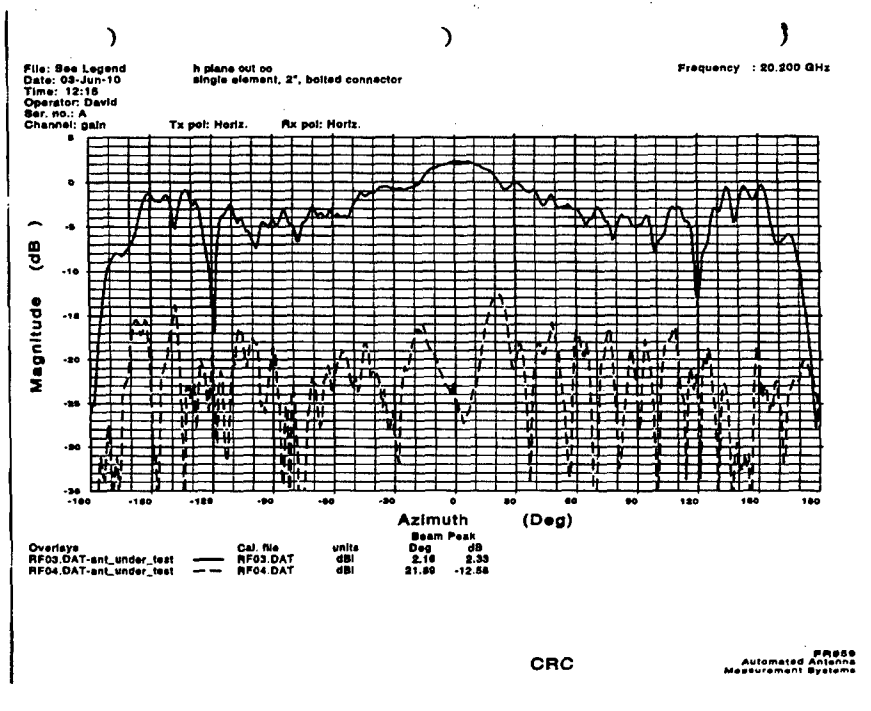

Figure 82. Antenna A H-Plane Co- and Cross-polarisation (---) 20.2 GHz

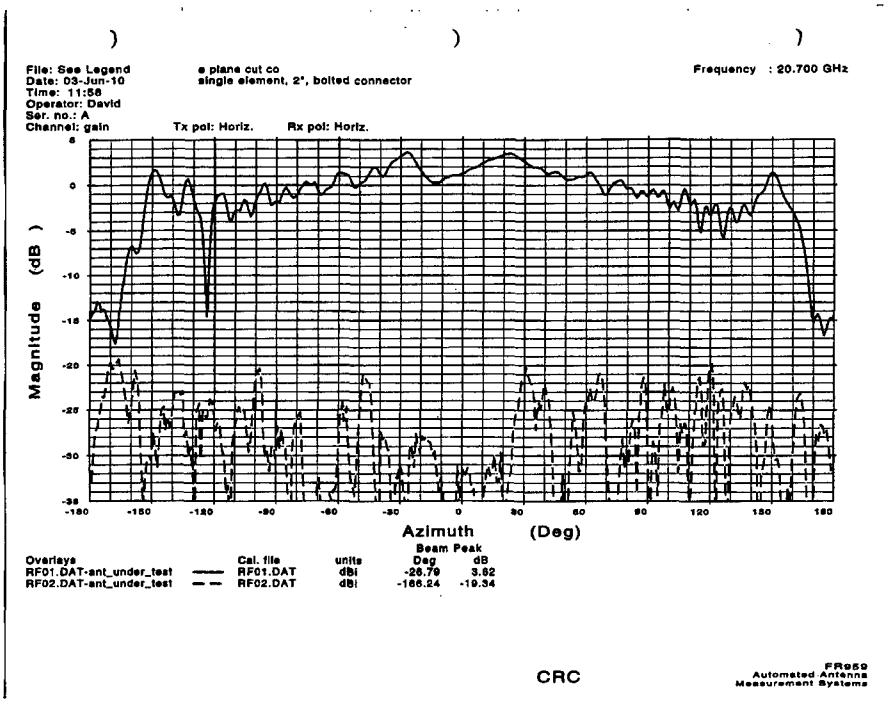

Figure 83. Antenna A E-Plane Co- and Cross-polarisation (---) 20.7 GHz

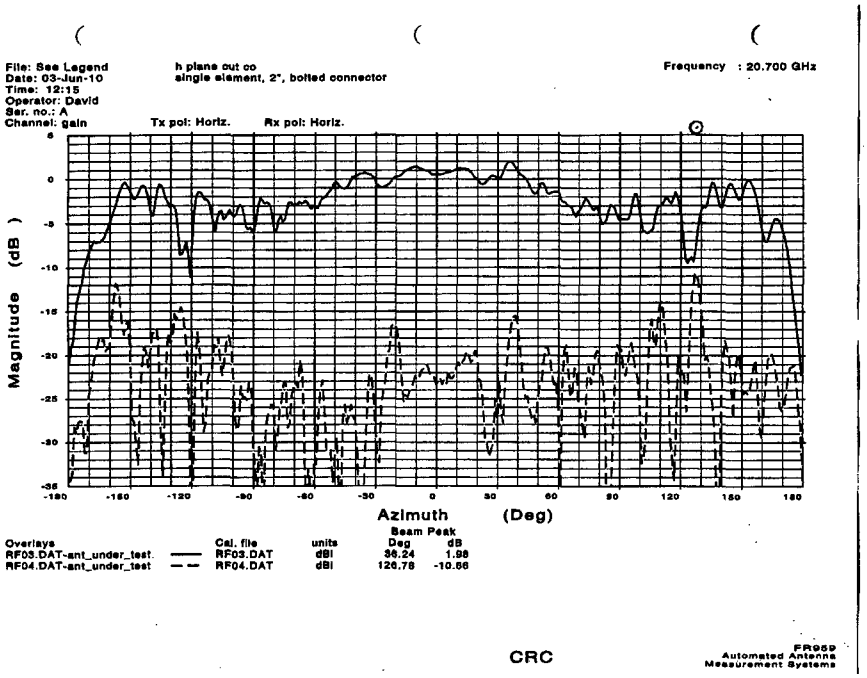

Figure 84. Antenna A H-Plane Co- and Cross-polarisation (---) 20.7 GHz

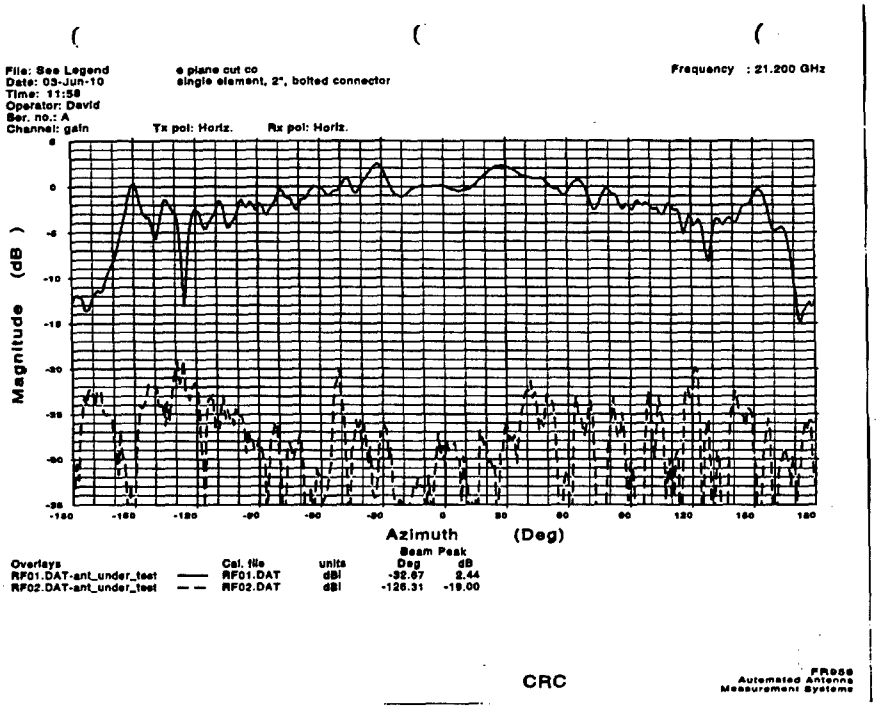

Figure 85. Antenna A E-Plane Co- and Cross-polarisation (—) 21.2 GHz

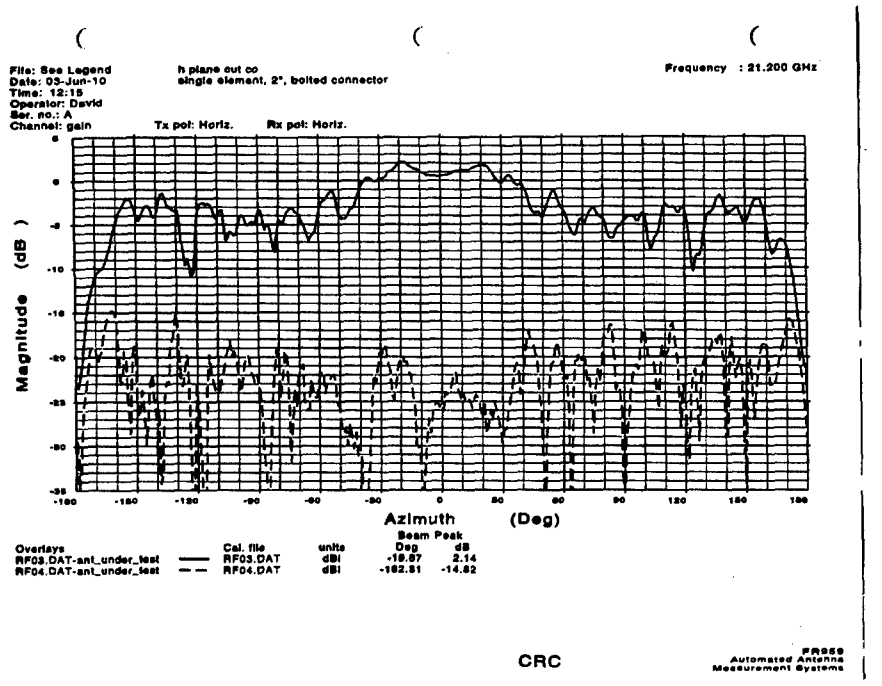

Figure 86. Antenna A H-Plane Co- and Cross-polarisation (—) 21.2 GHz

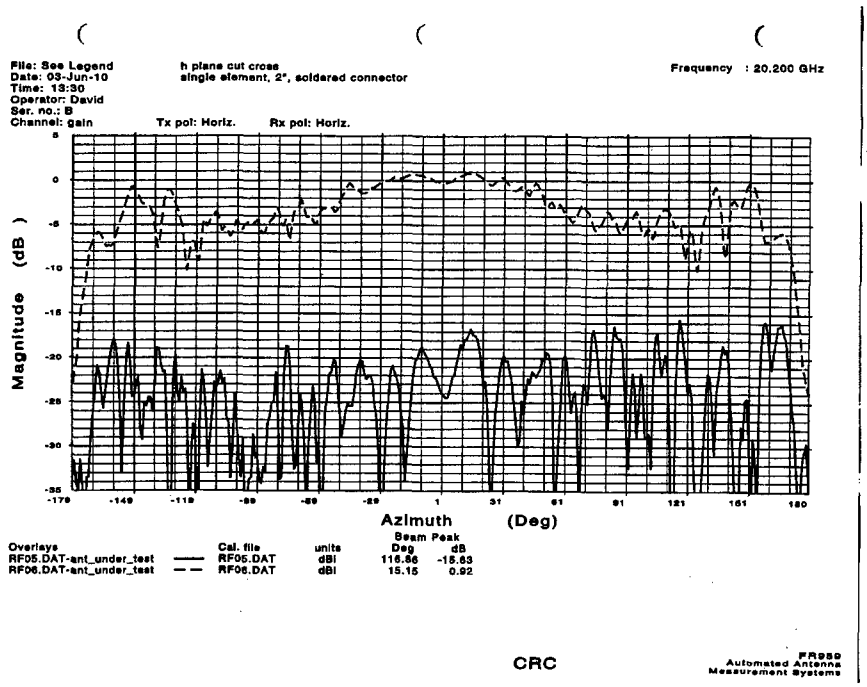

Figure 87. Antenna B H-Plane Co- (---) and Cross-polarisation 20.2 GHz

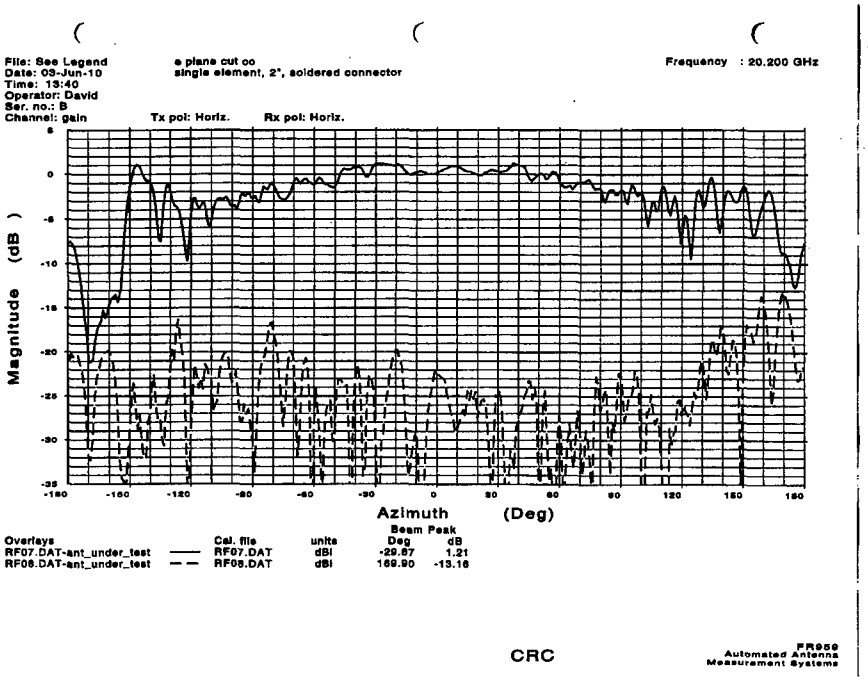

Figure 88. Antenna B E-Plane Co- and Cross-polarisation (---) 20.2 GHz

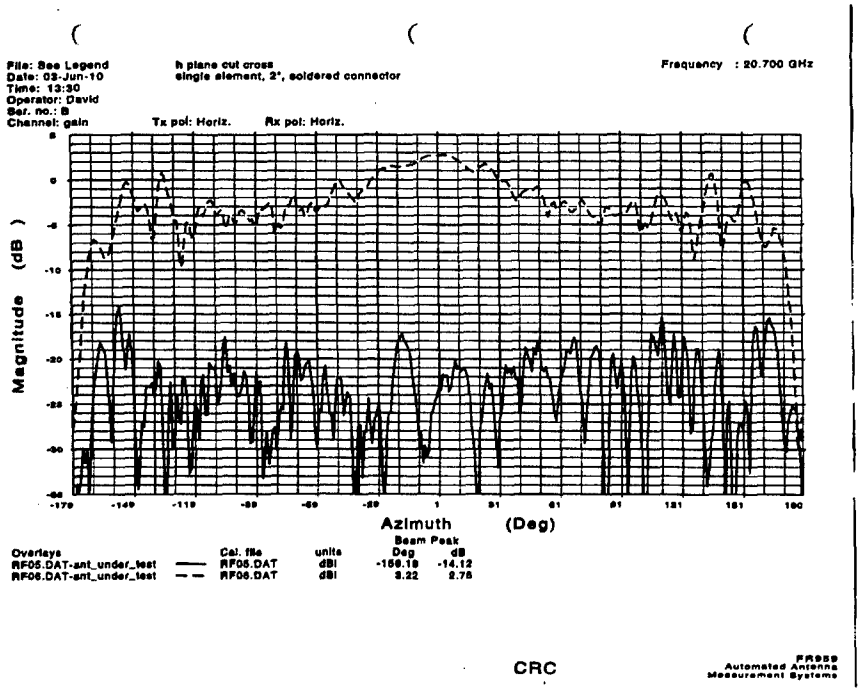

Figure 89. Antenna B H-Plane Co- (---) and Cross-polarisation 20.7 GHz

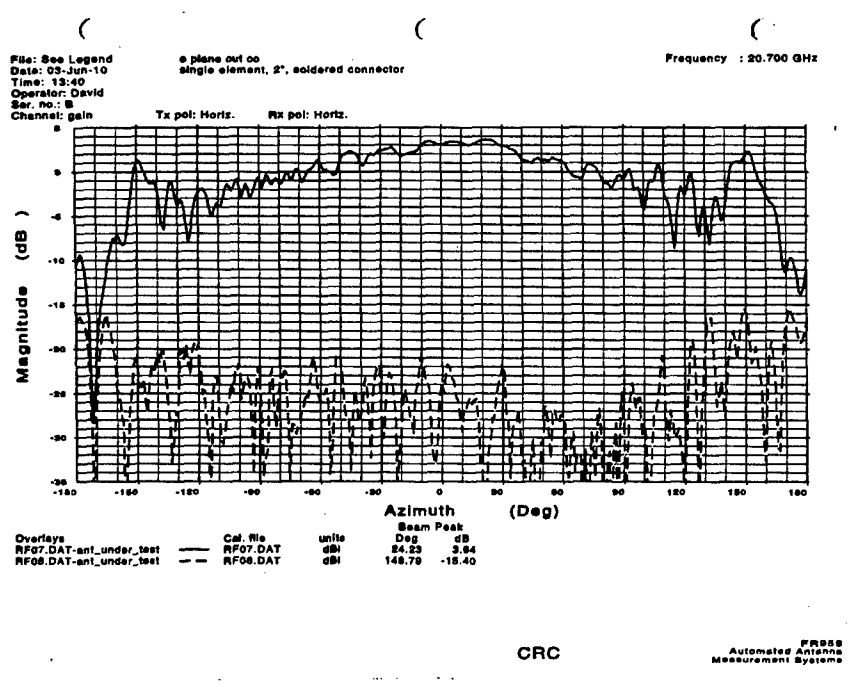

Figure 90. Antenna B E-Plane Co- and Cross-polarisation (---) 20.7 GHz

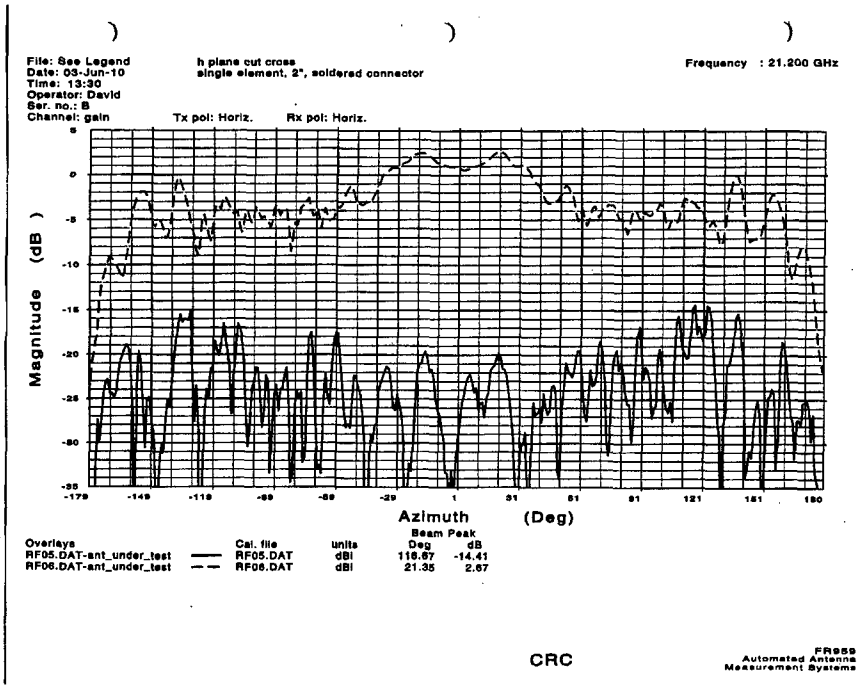

Figure 91. Antenna B H-Plane Co- (---) and Cross-polarisation 21.2 GHz

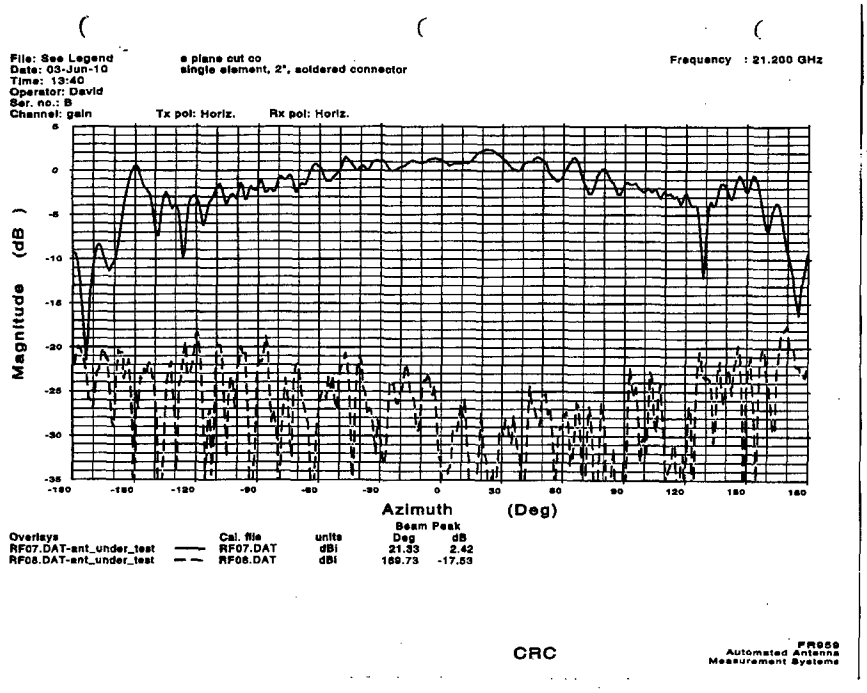

Figure 92. Antenna B E-Plane Co- and Cross-polarisation (—) 21.2 GHz

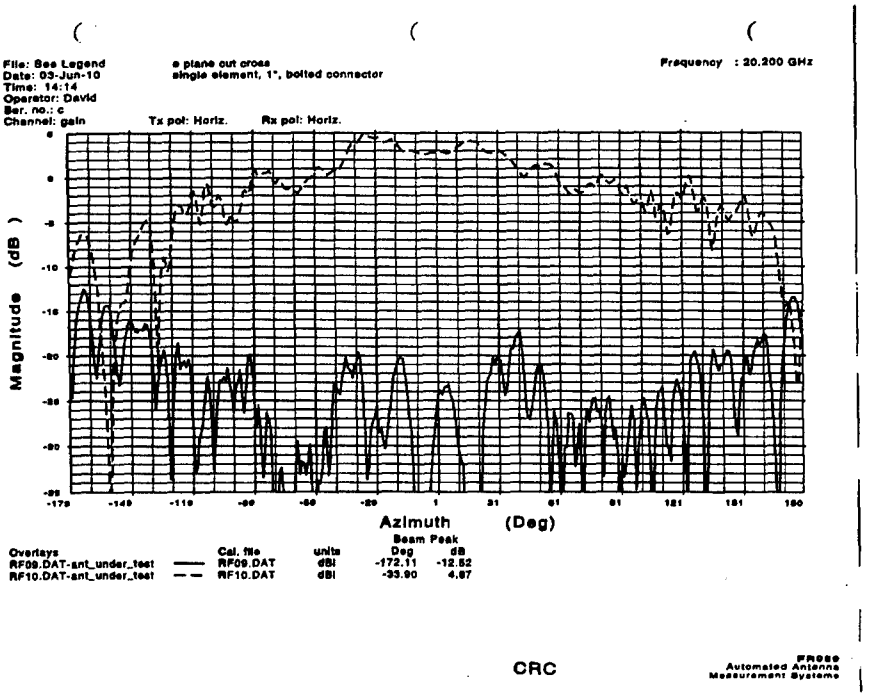

Figure 93. Antenna C E-Plane Co- (—) and Cross-polarisation 20.2 GHz

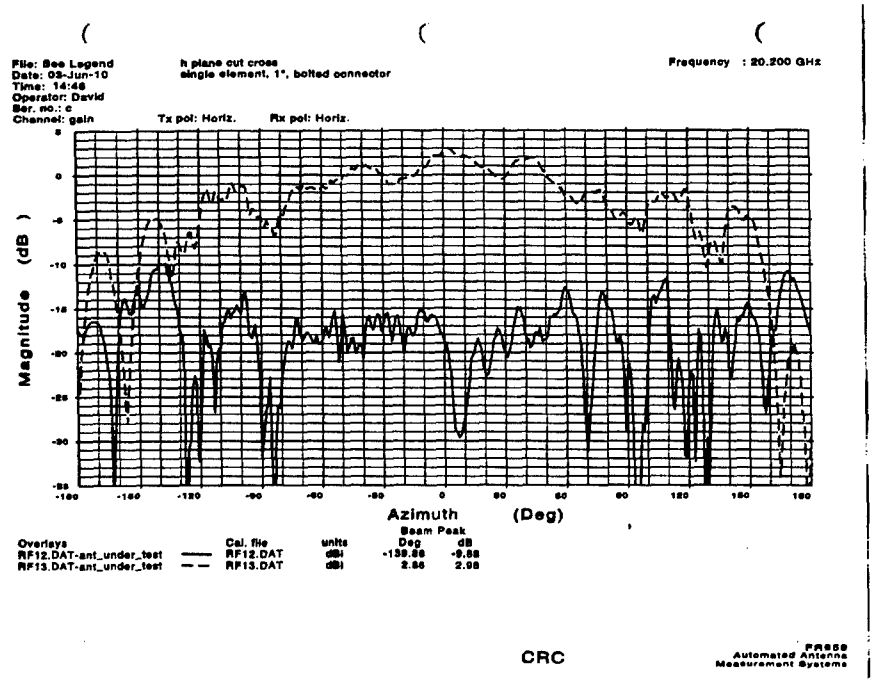

Figure 94. Antenna C H-lane Co- (—) and Cross-polarisation 20.2 GHz

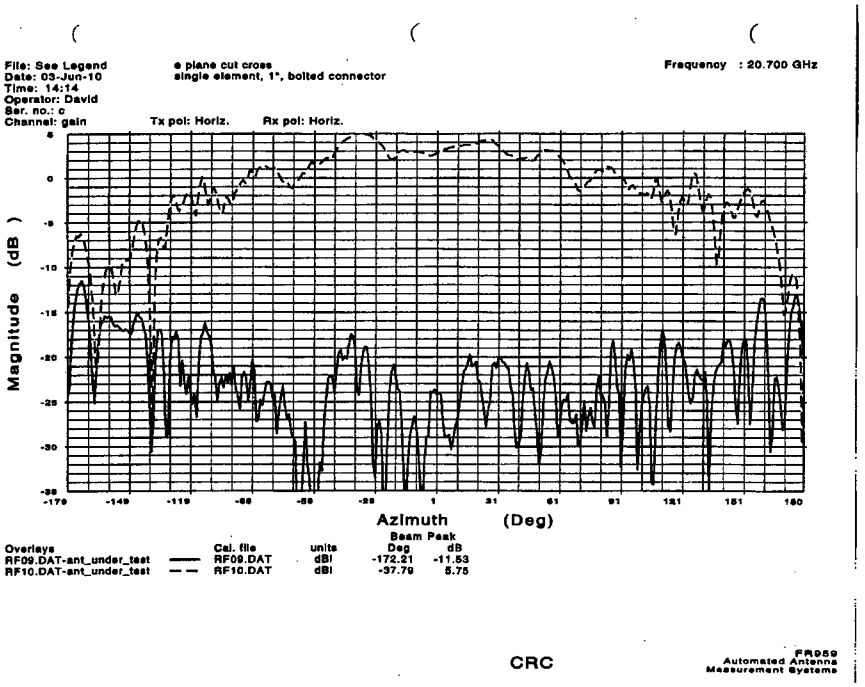

Figure 95. Antenna C E-Plane Co- (---) and Cross-polarisation 20.7 GHz

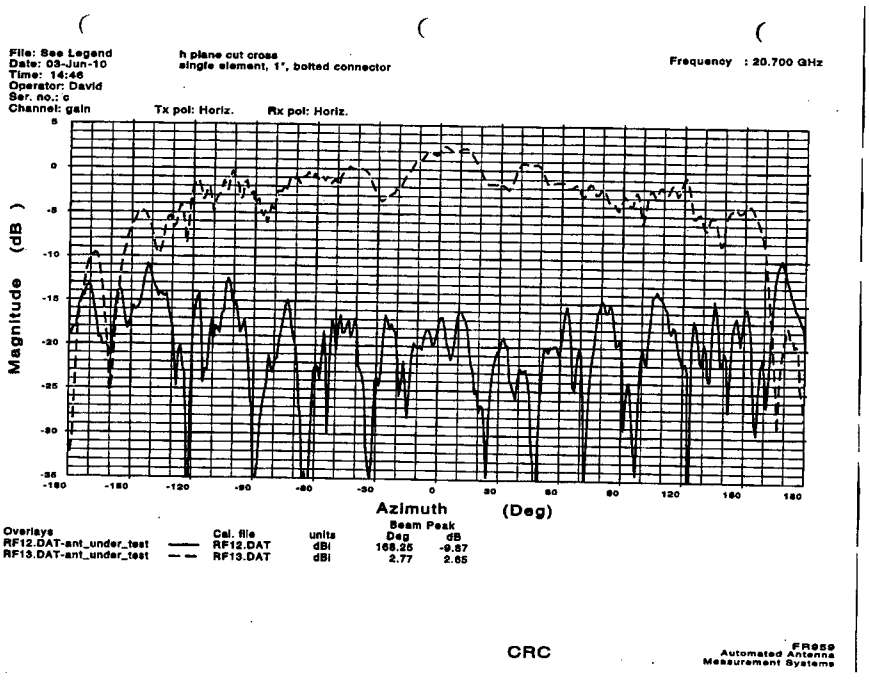

Figure 96. Antenna C H-Plane Co- (---) and Cross-polarisation 20.7 GHz

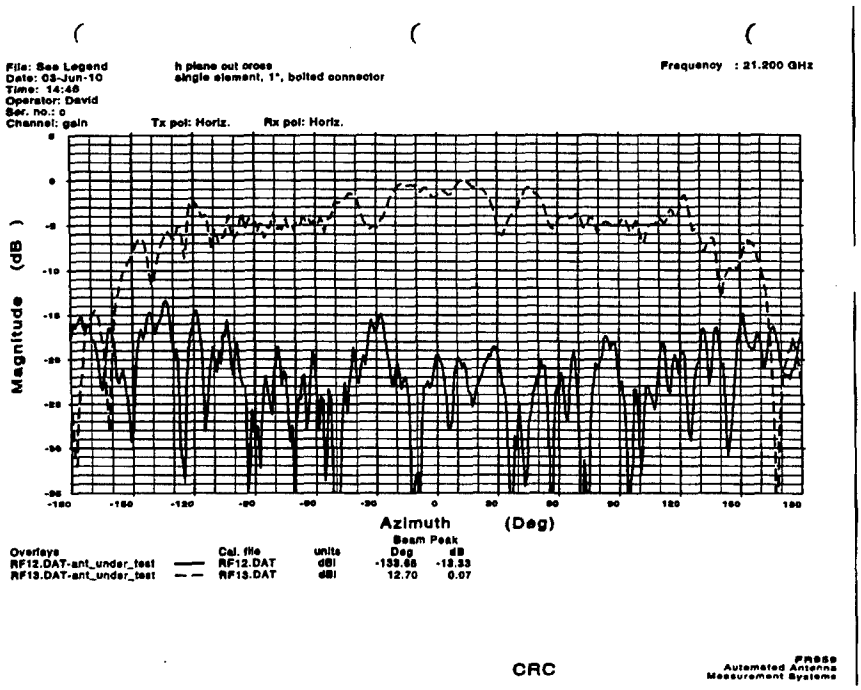

Figure 97. Antenna C H-Plane Co- (---) and Cross-polarisation 21.2 GHz

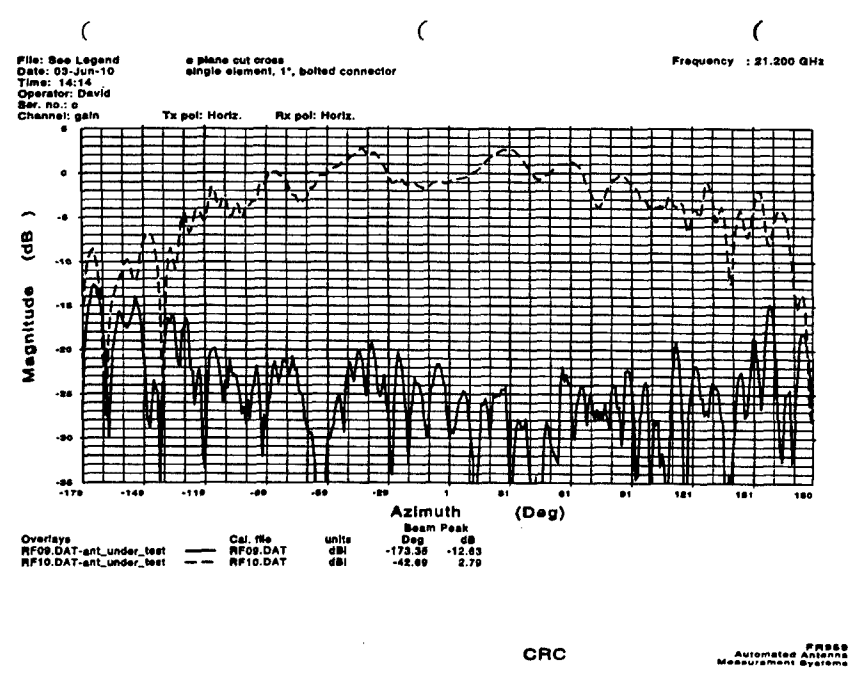

Figure 98. Antenna C E-Plane Co- (---) and Cross-polarisation 21.2 GHz

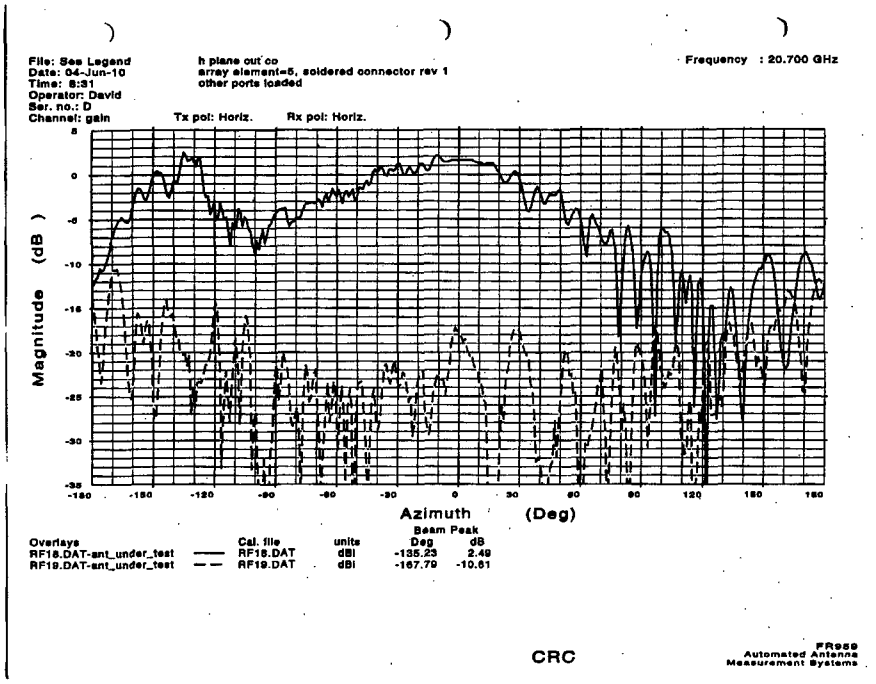

Figure 99. Array Element 1 H-Plane Co- and Cross-polarisation (---) 20.7 GHz

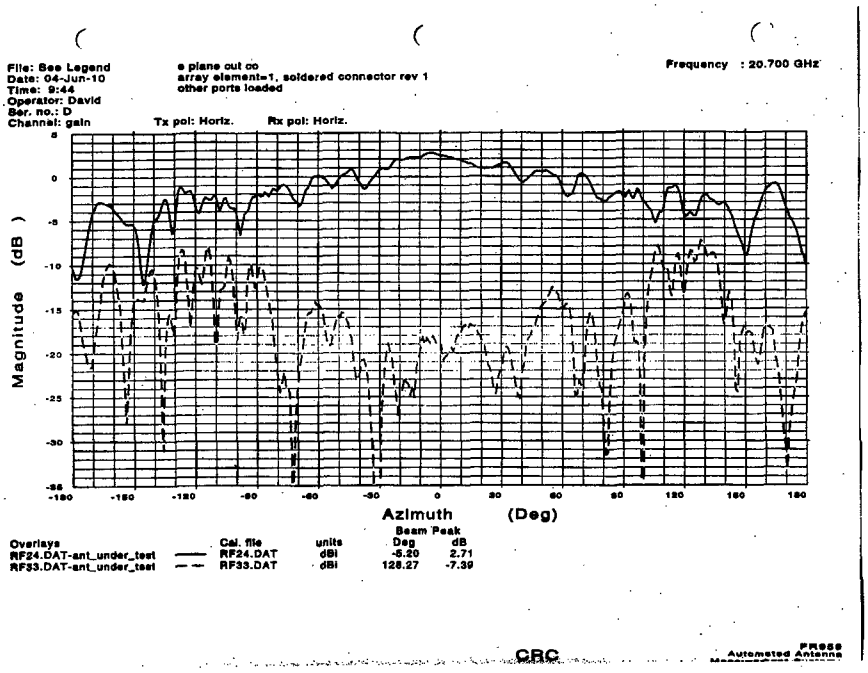

Figure 100. Array Element 1 E-Plane Co- and Cross-polarisation (---) 20.7 GHz

7.4. Appendix D - Prototype specifications and dimensions

The Figures below contain the actual specifications provided to CRC for the fabrication of the various LWG prototypes.

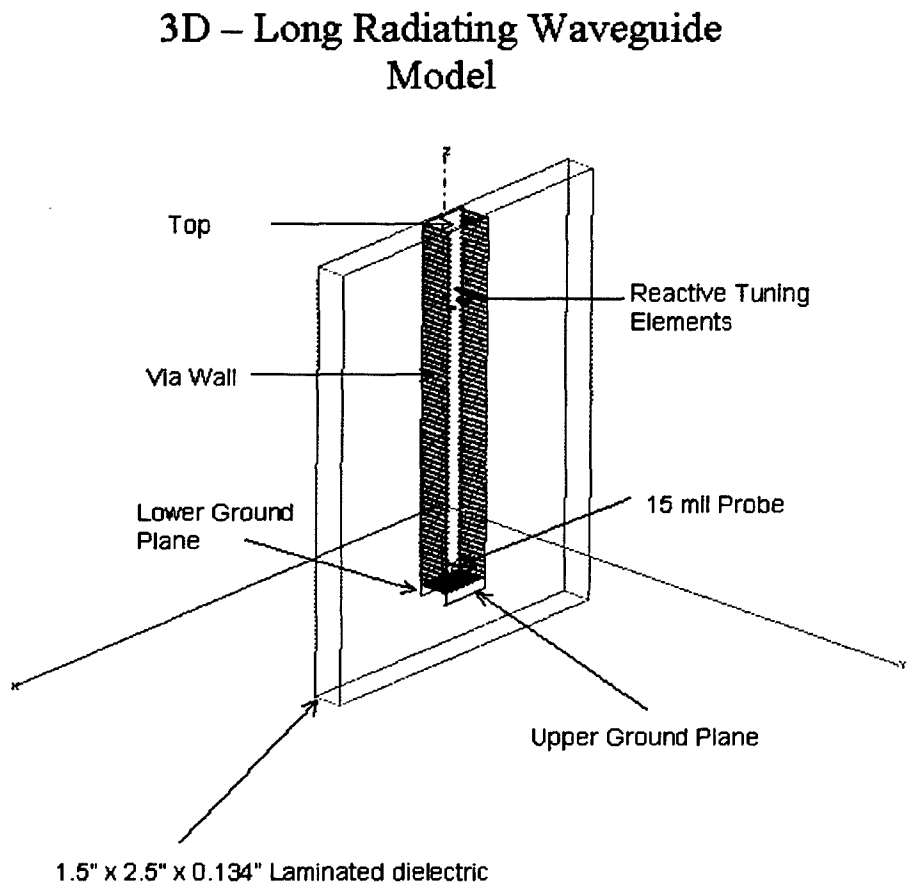

1

Figure 101. Long Radiating LWG Model

Long Radiating Waveguide with Upper Ground Plane

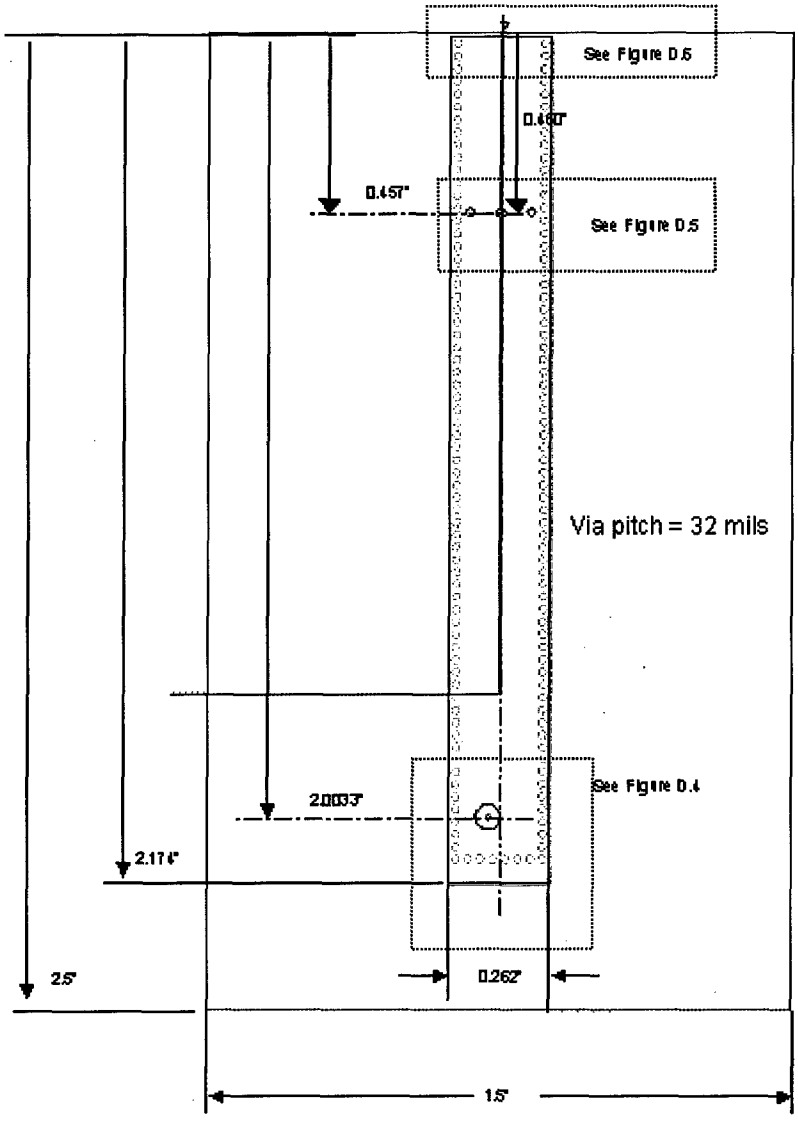

2

Figure 102. Long Radiating LWG Upper Ground Plane

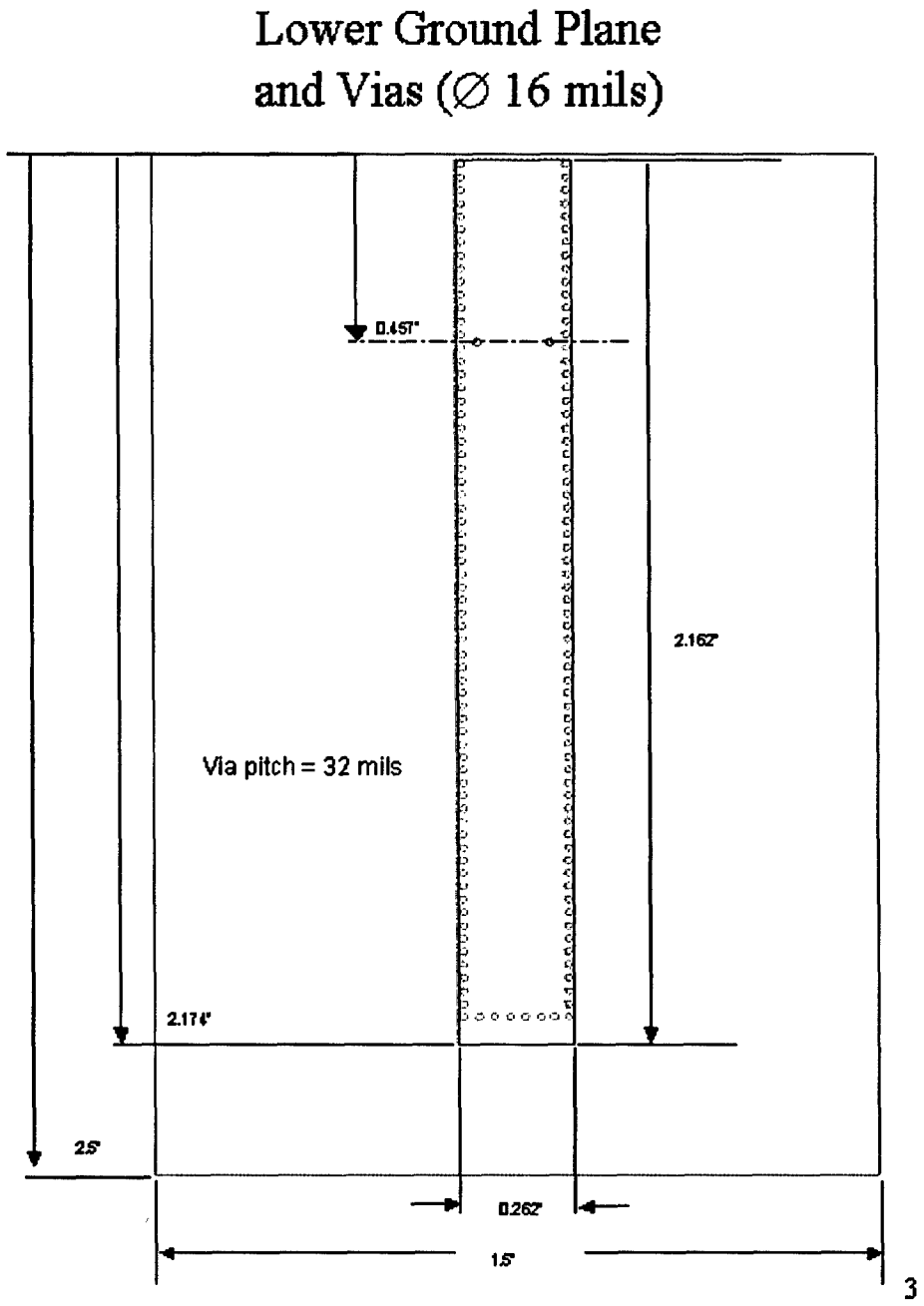

Figure 103. Lower Ground Plane

Figure D.4
Upper Ground Plane with Coaxial Probe

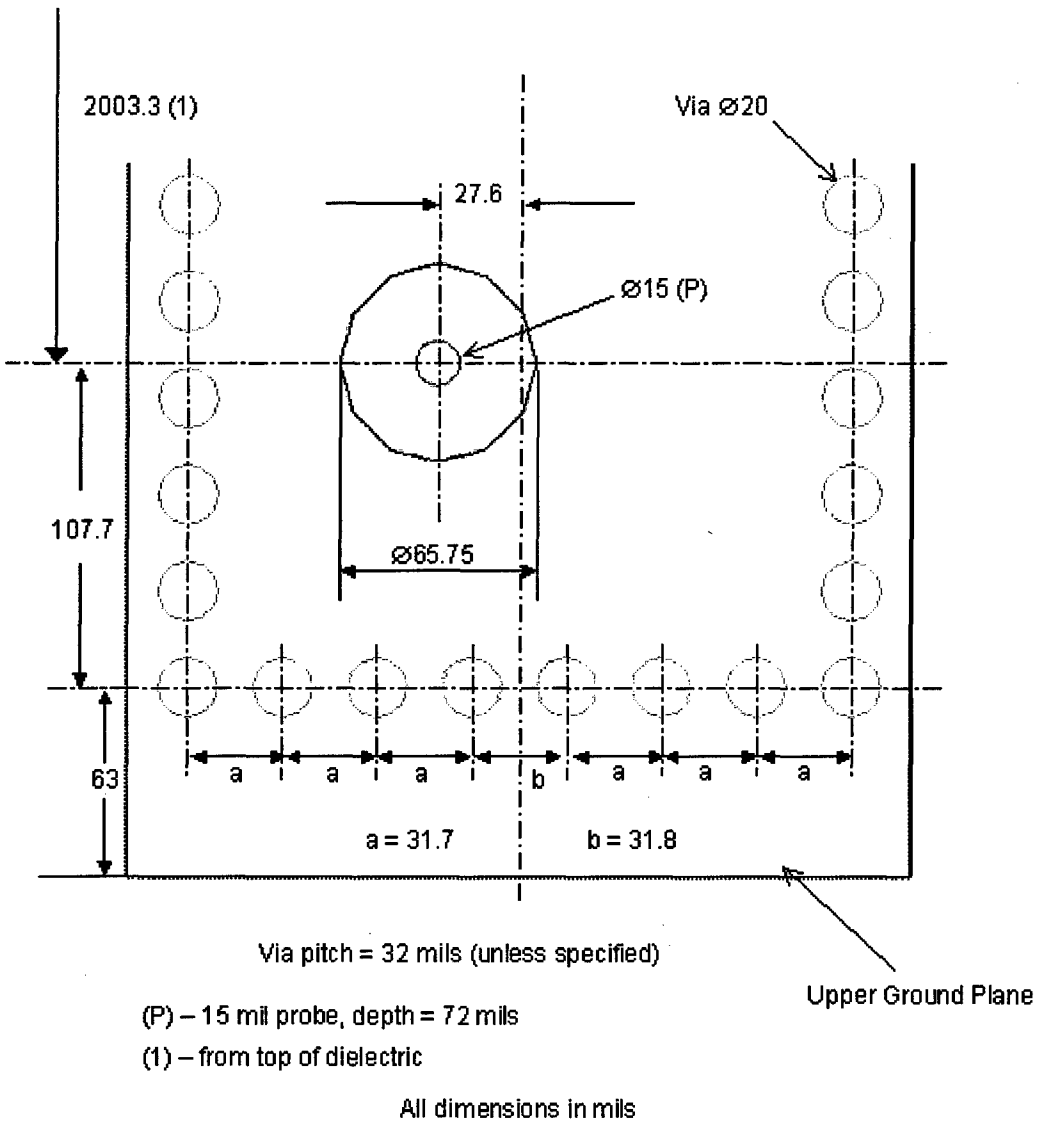

4

Figure 104. Upper Ground Plane with Coaxial Probe

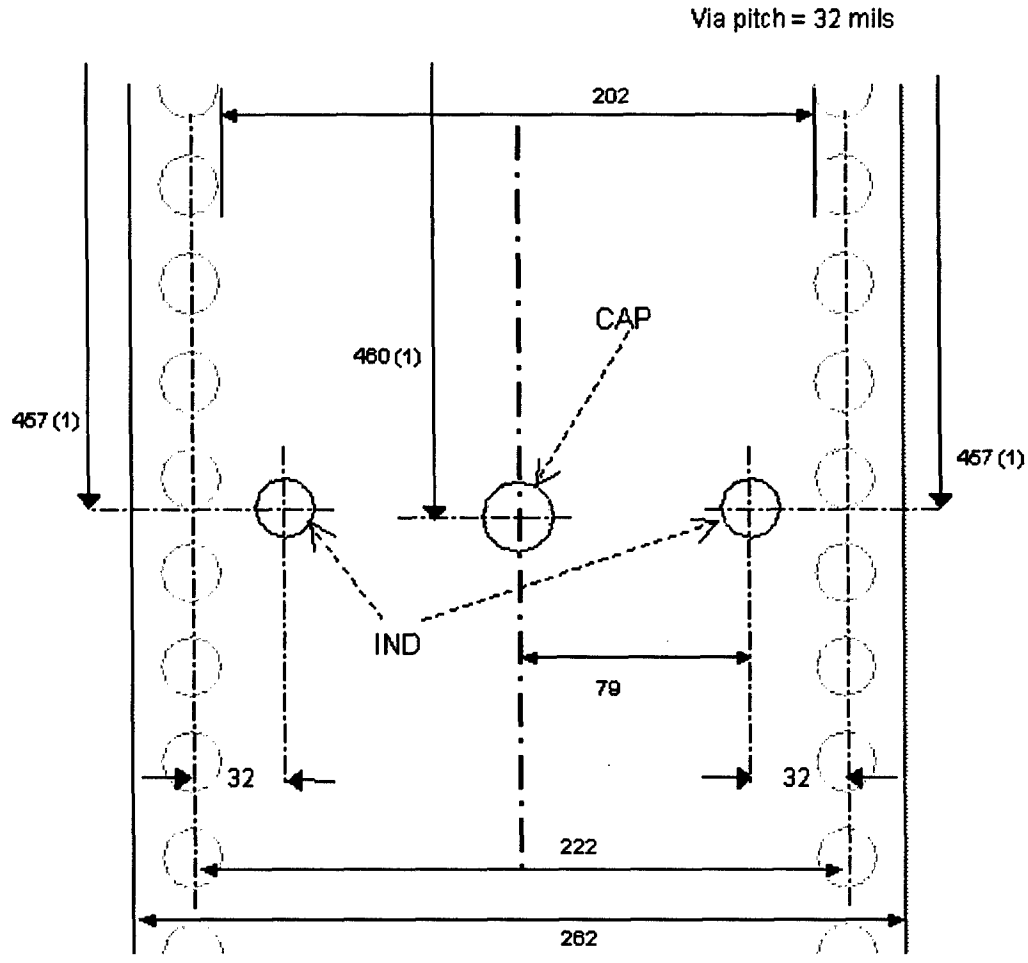

CAP ø 24, depth 49.6 mil
IND ø 20 via

All dimensions in mils

(1) Measured from the top of the dielectric

5

Figure 105. Aperture Matching Components

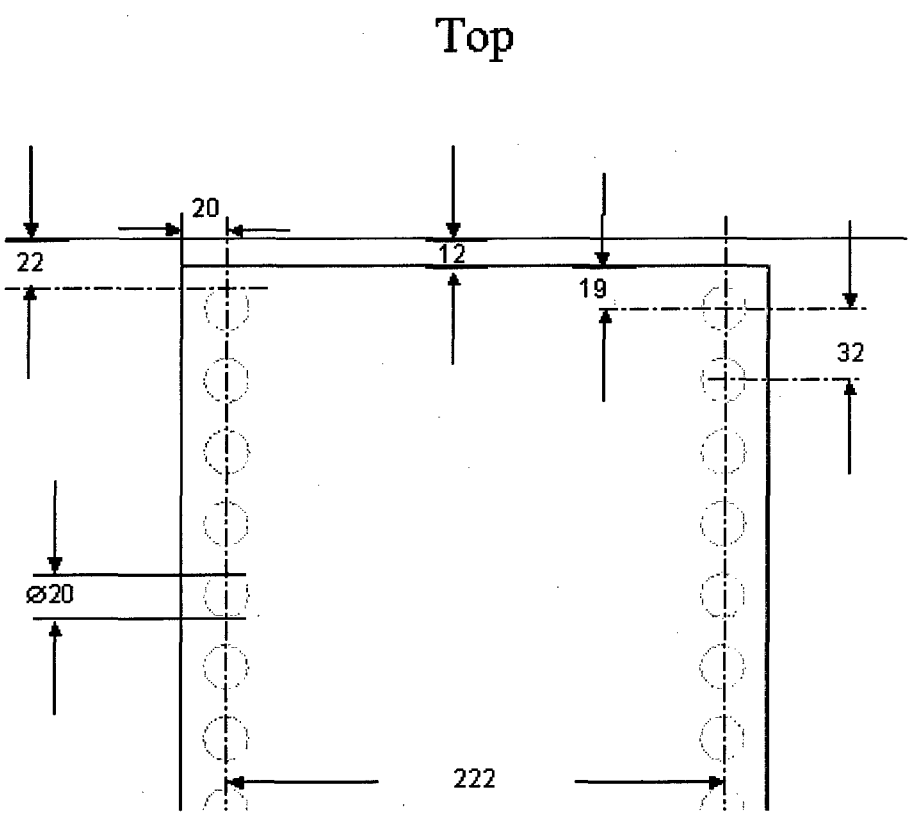

Figure 106. Radiating Edge

Blind Vias
Long Radiating Waveguide

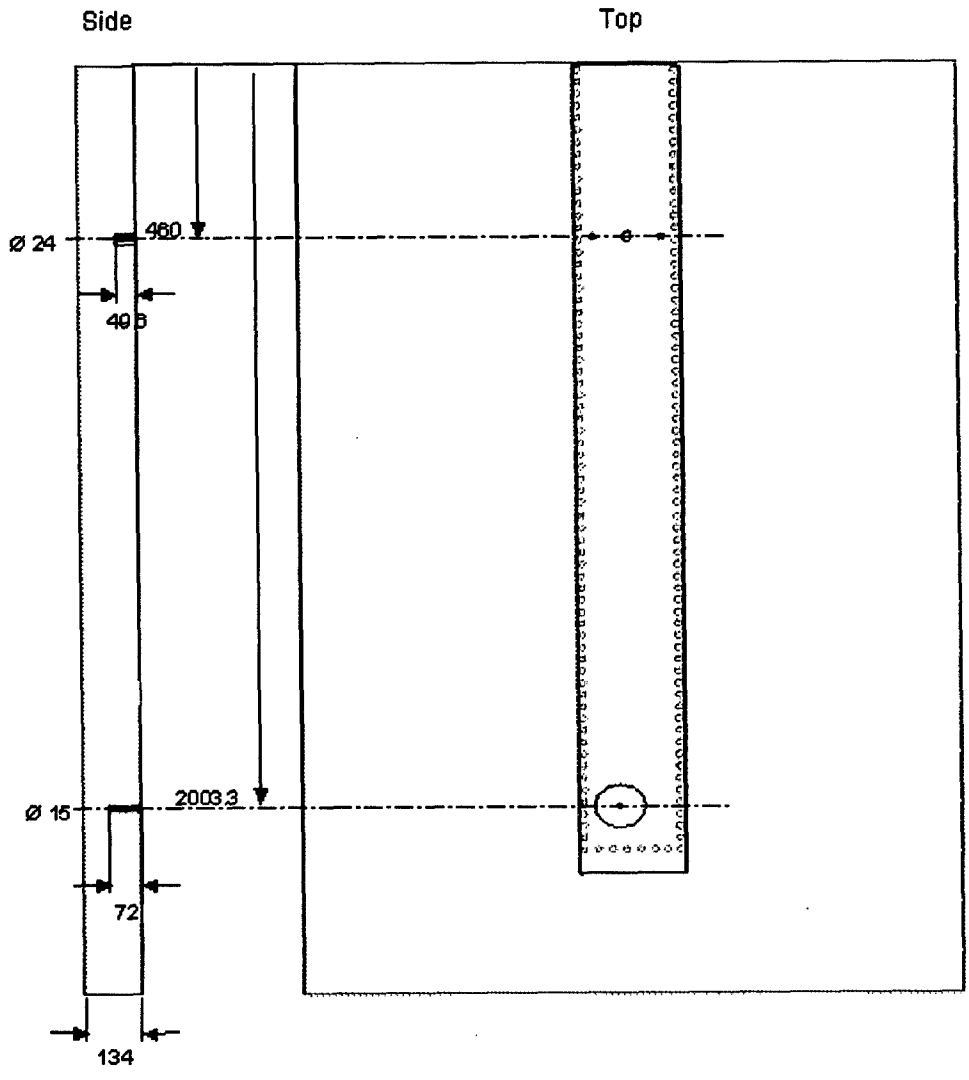

All dimensions in mils

Figure 107. Blind Vias

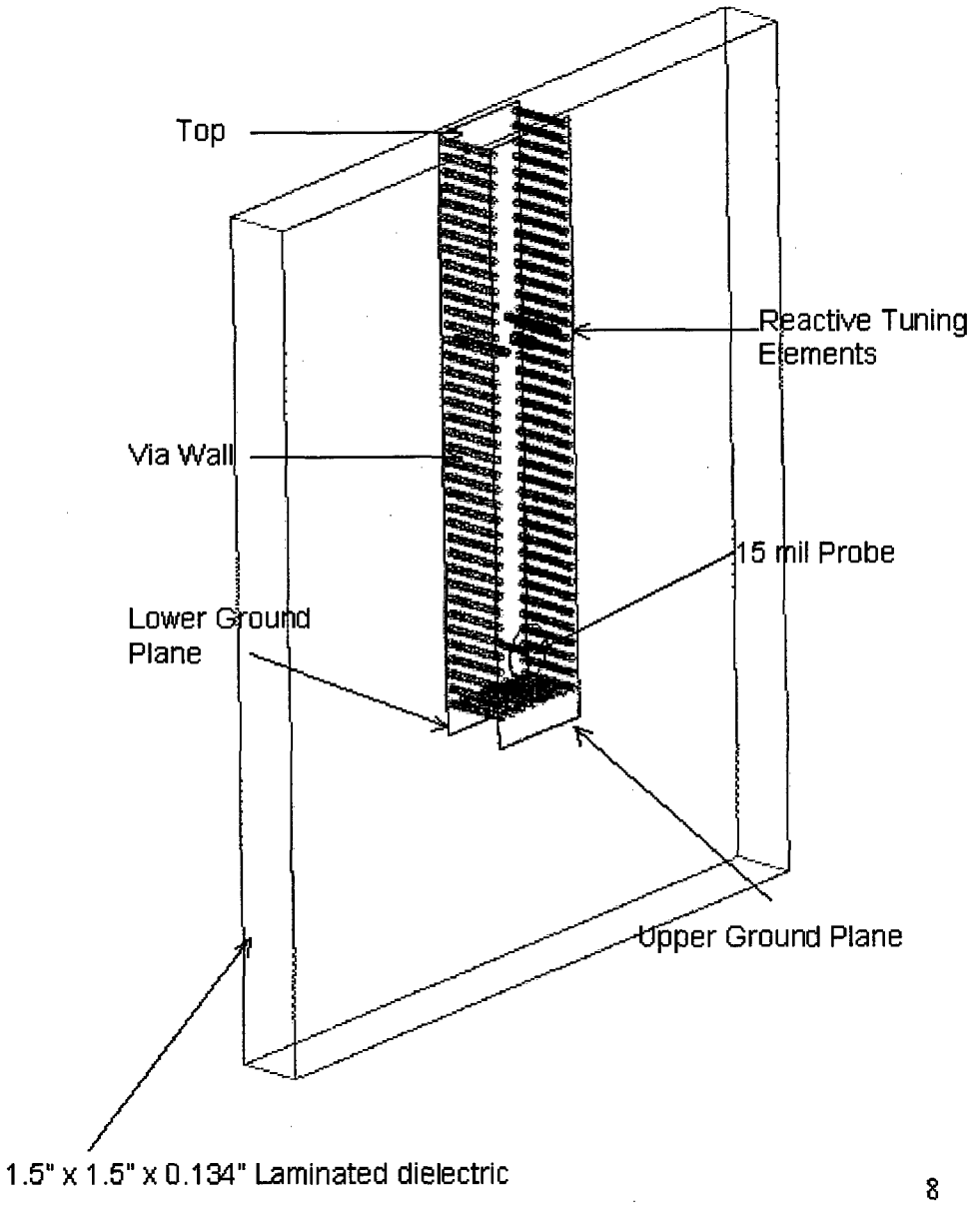

Figure 108. Short Radiating LWG

Short Radiating Waveguide
Upper Ground Plane

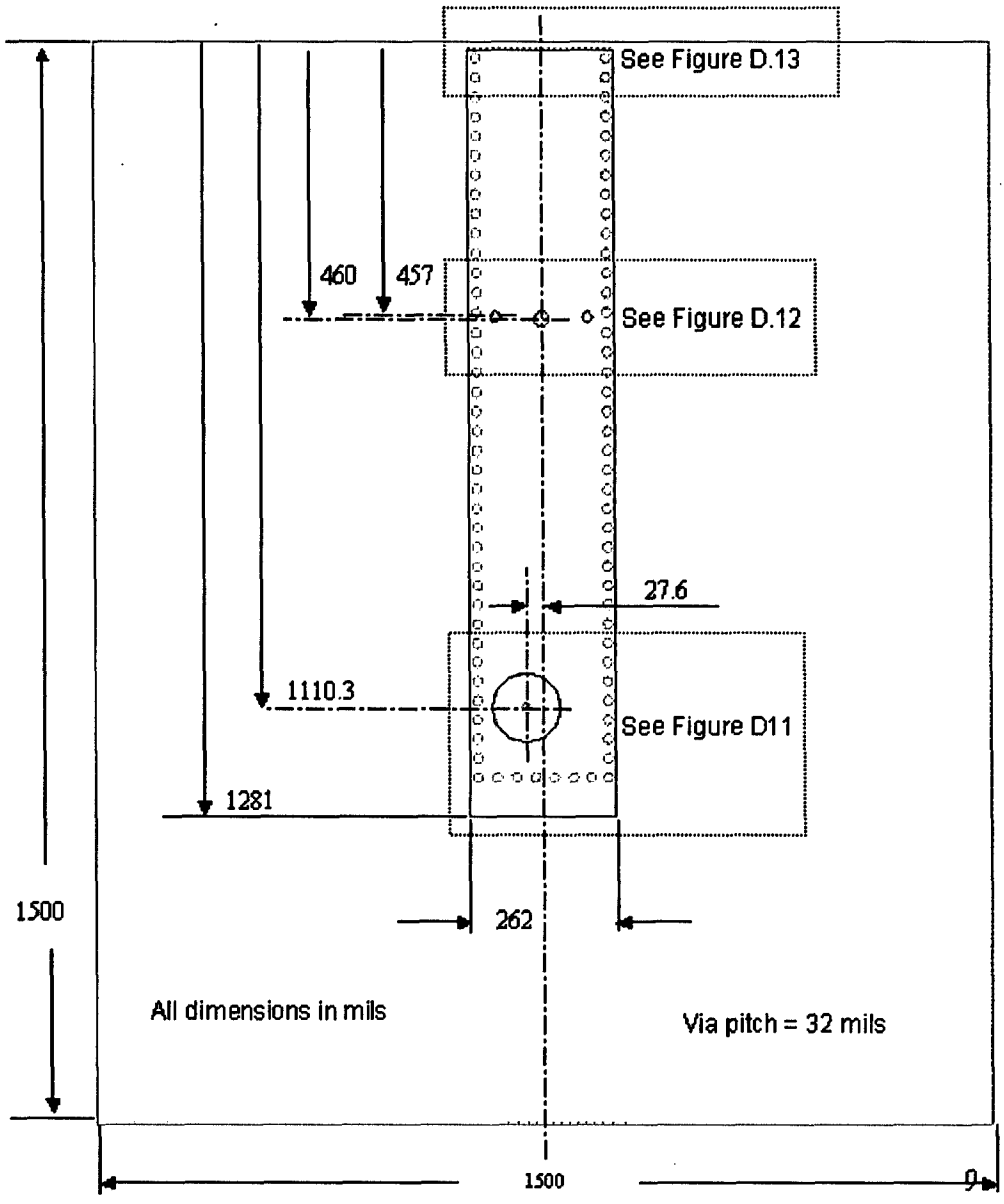

Figure 109. Short Radiating LWG Upper Ground Plane

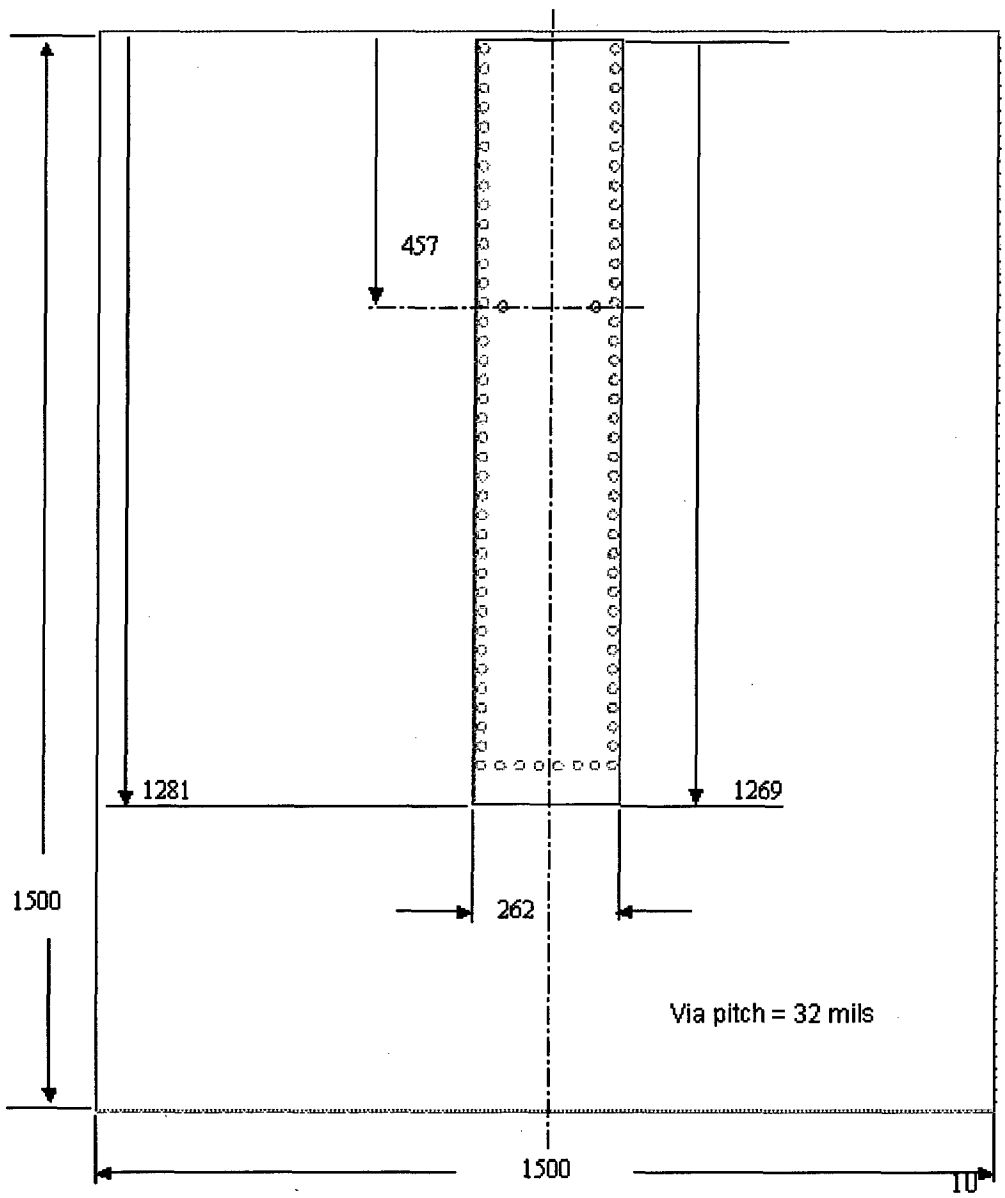

Figure 110. Lower Ground Plane and Vias

Figure D.11
Upper Ground Plane with Coaxial Probe

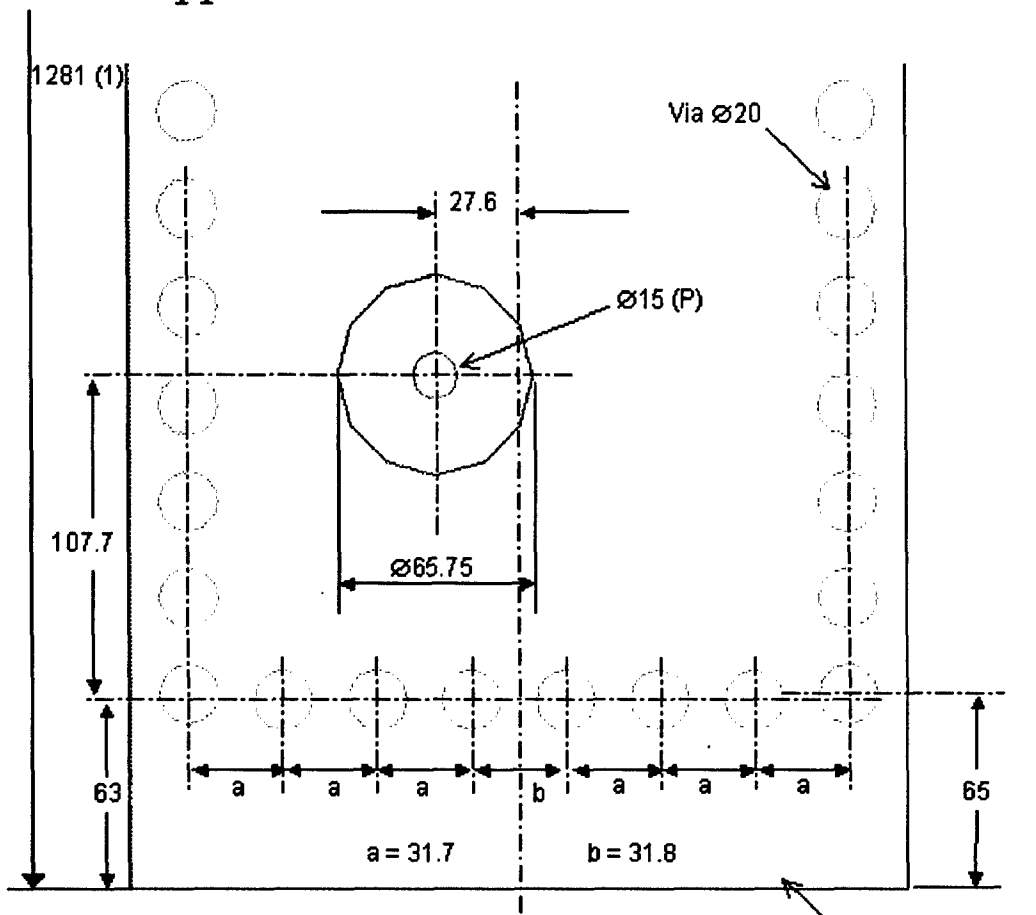

(P) – Ø15 mil probe, depth = 72 mils

(1) Measured from front of dielectric

All dimensions in mils

11

Figure 111. Upper Ground Plane with Coaxial Probe

Figure D.12

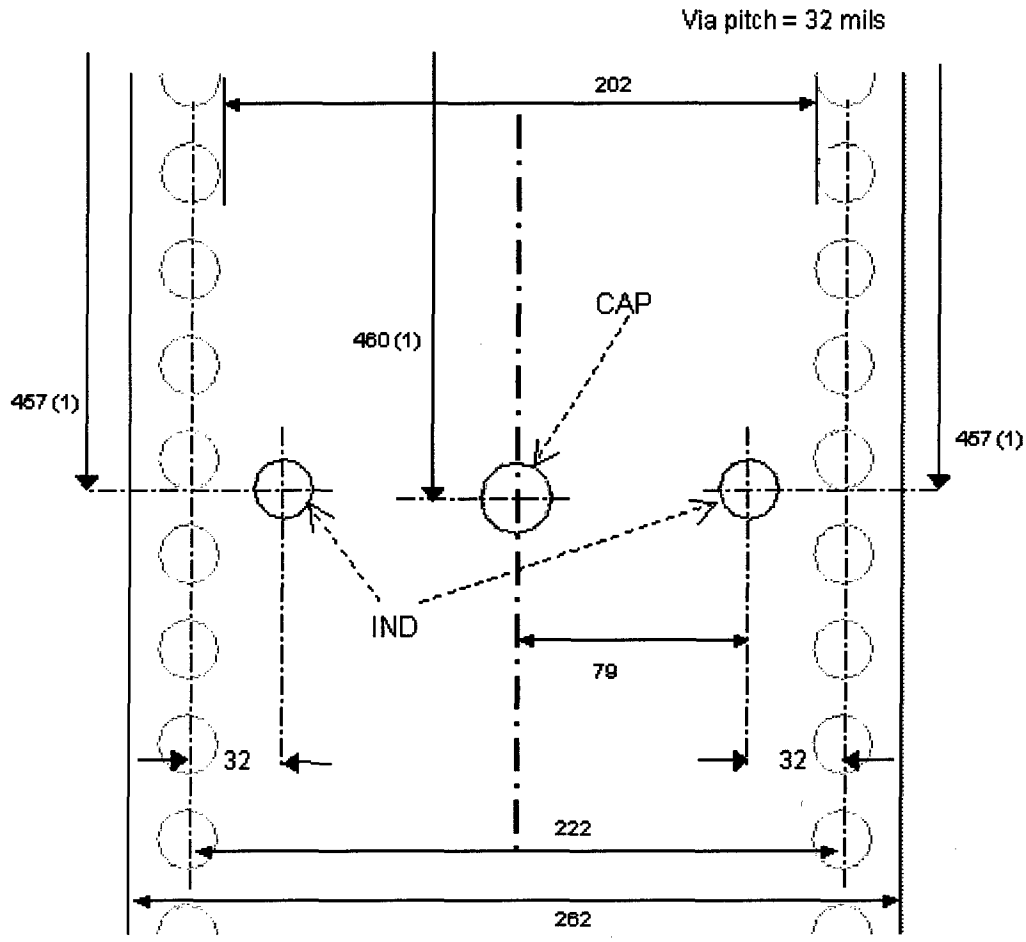

CAP ø 24, depth 49.6 mil
IND – ø 20 via

All dimensions in mils

(1) Measured from the top of the dielectric

12

Figure 112. Aperture Matching Components

Figure D.13
Top

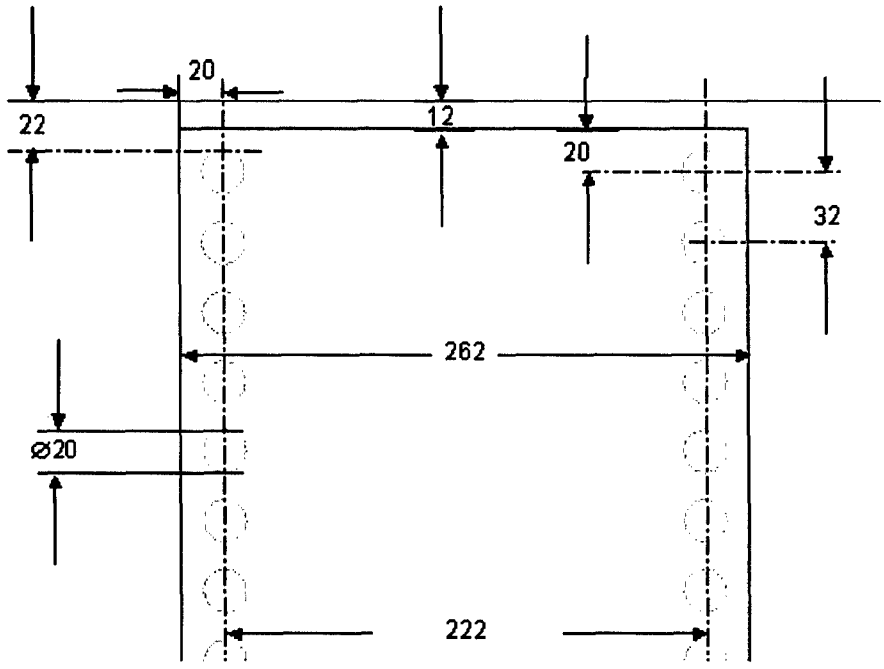

Via pitch = 32 mils

All dimensions in mils

13

Figure 113. Radiating Edge

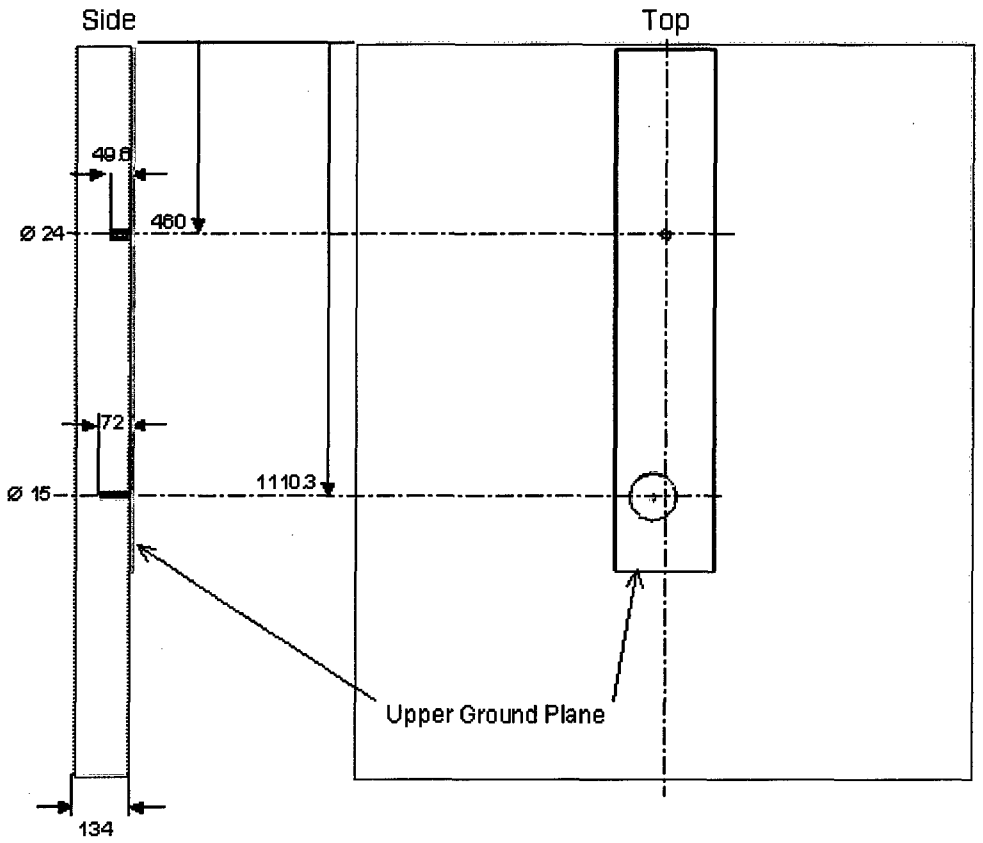

Figure 114. Short Radiating LWG Blind Vias

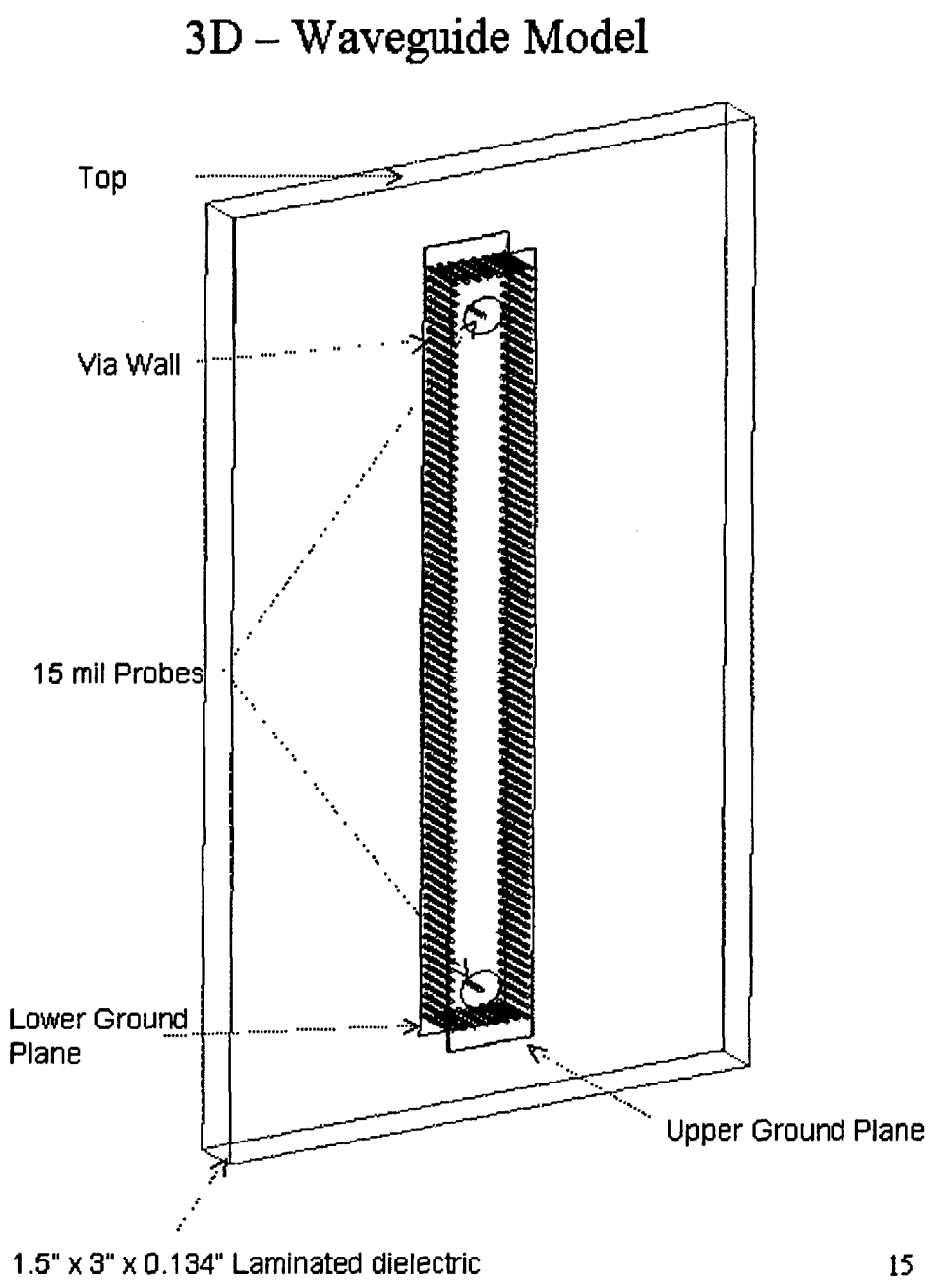

Figure 115. Non-Radiating LWG

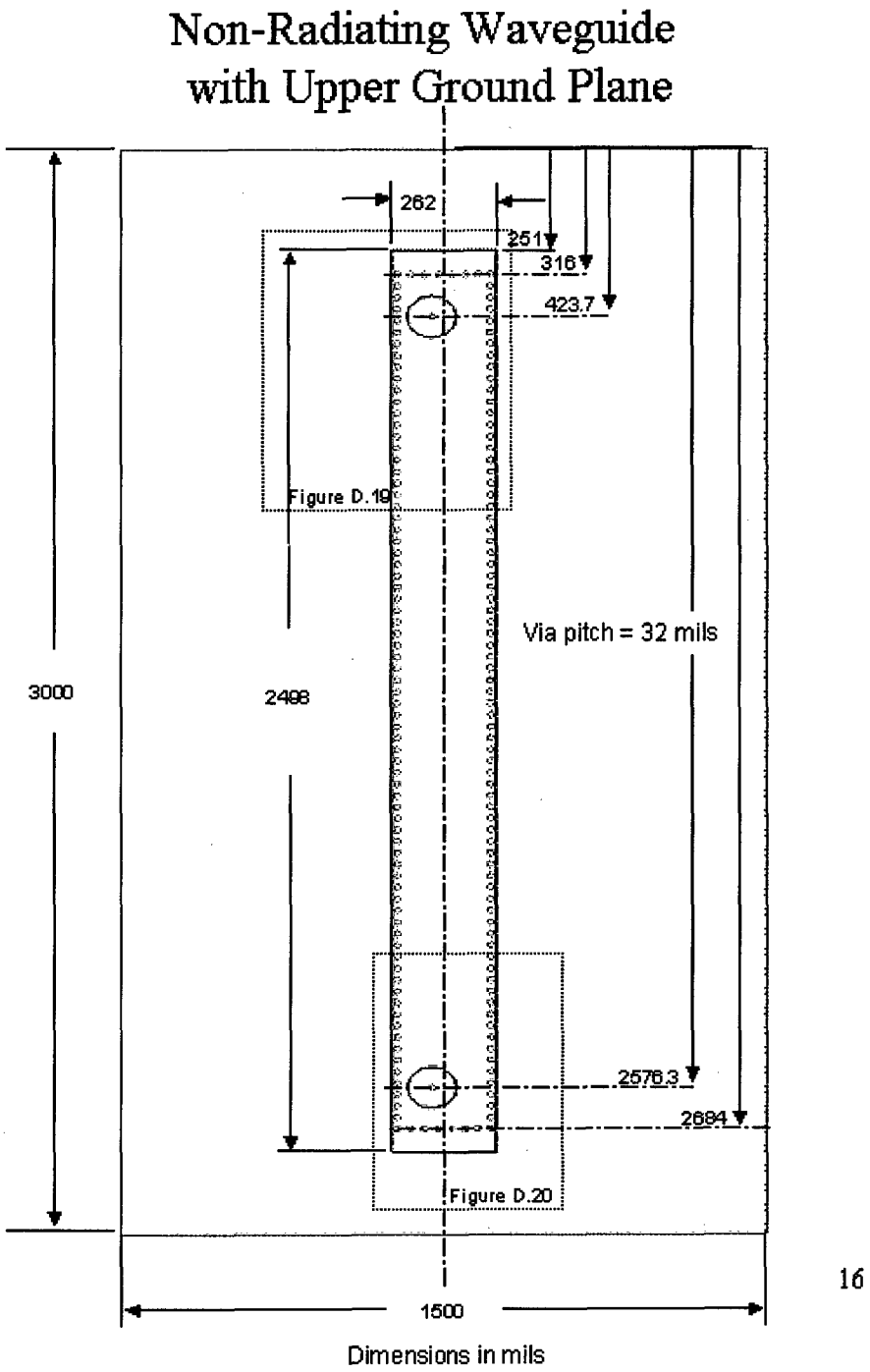

Figure 116. Non-Radiating LWG Upper Ground Plane with Vias

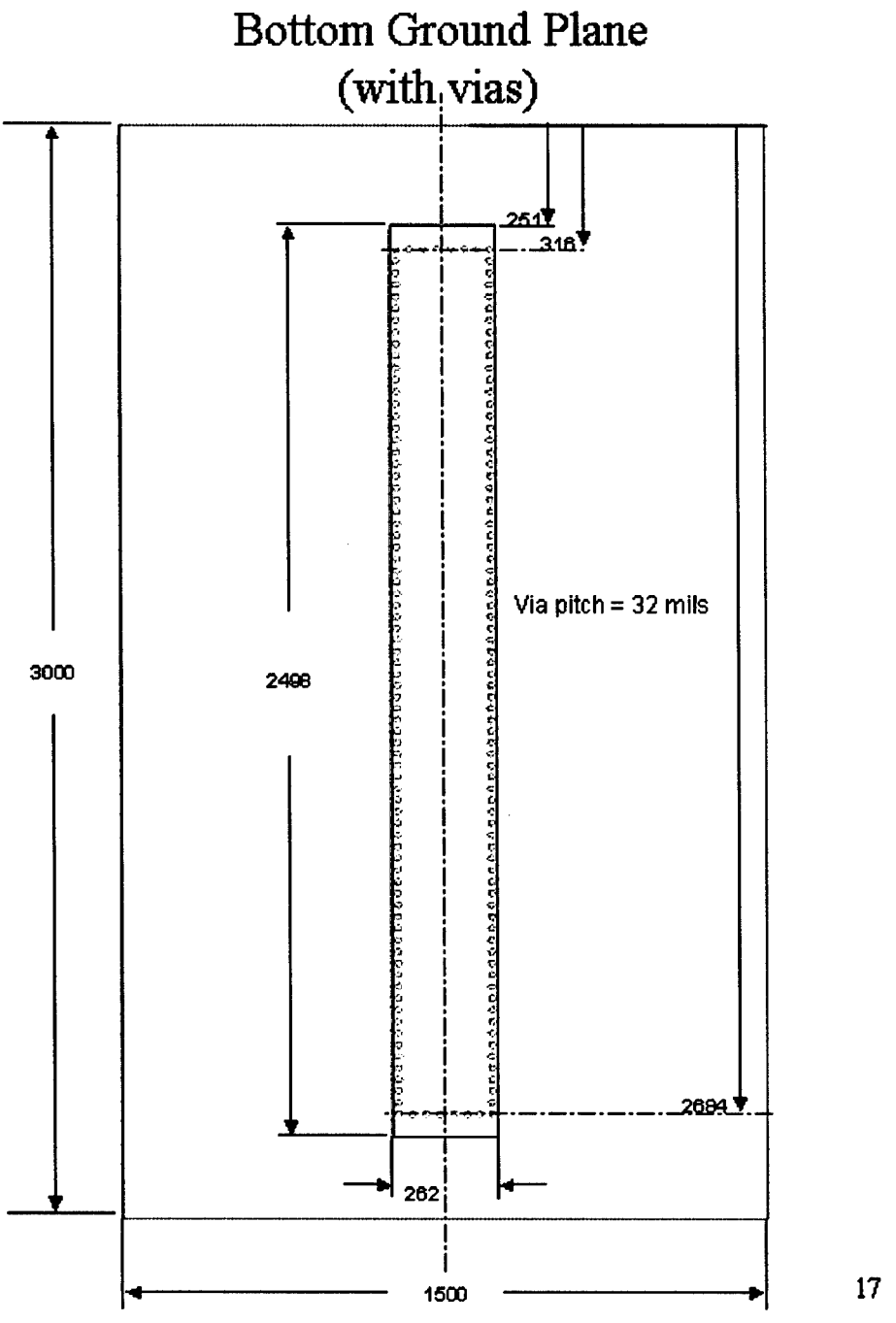

Figure 117. Bottom Ground Plane with Vias

Non-Radiating Waveguide Blind Vias

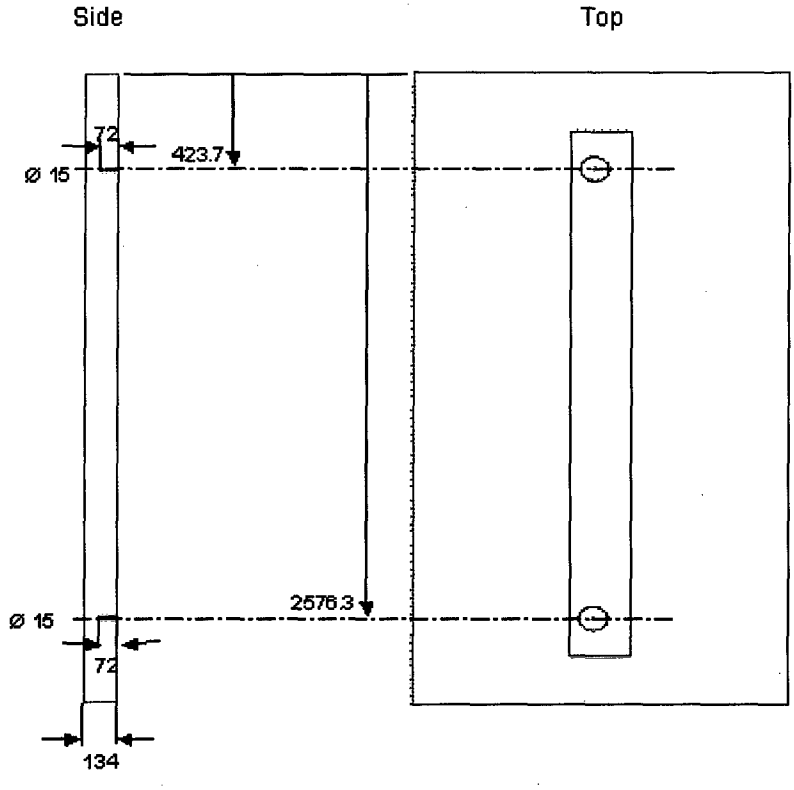

18

Figure 118. Non-Radiating LWG Blind Vias

Figure D.19
Top Upper Ground Plane with Coaxial Probe

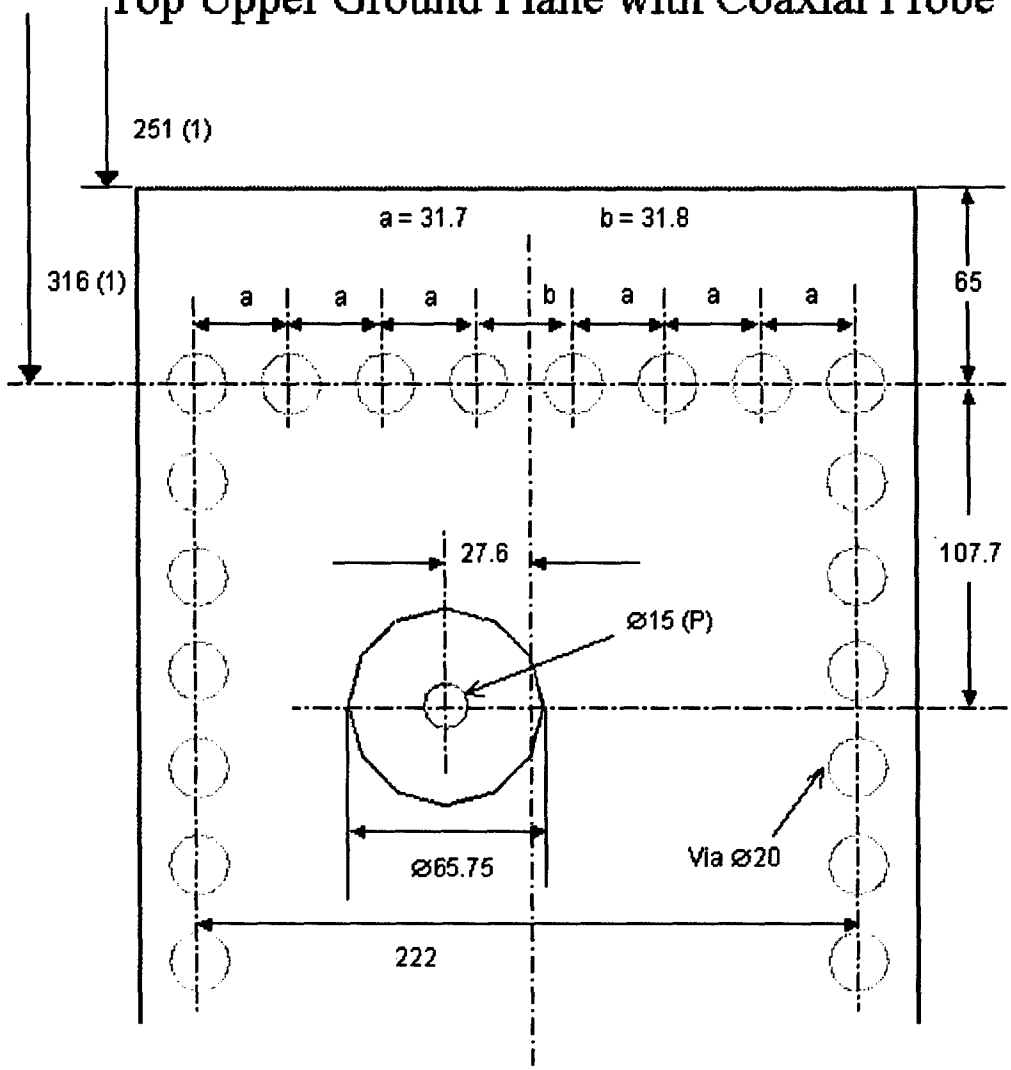

Via pitch = 32 mils (unless specified)

(P) – 15 mil probe, depth = 72 mils

(1) – from top of dielectric

All dimensions in mils

19

Figure 119. Front Coaxial Transition

Figure D.20
Upper Ground Plane with Coaxial Probe

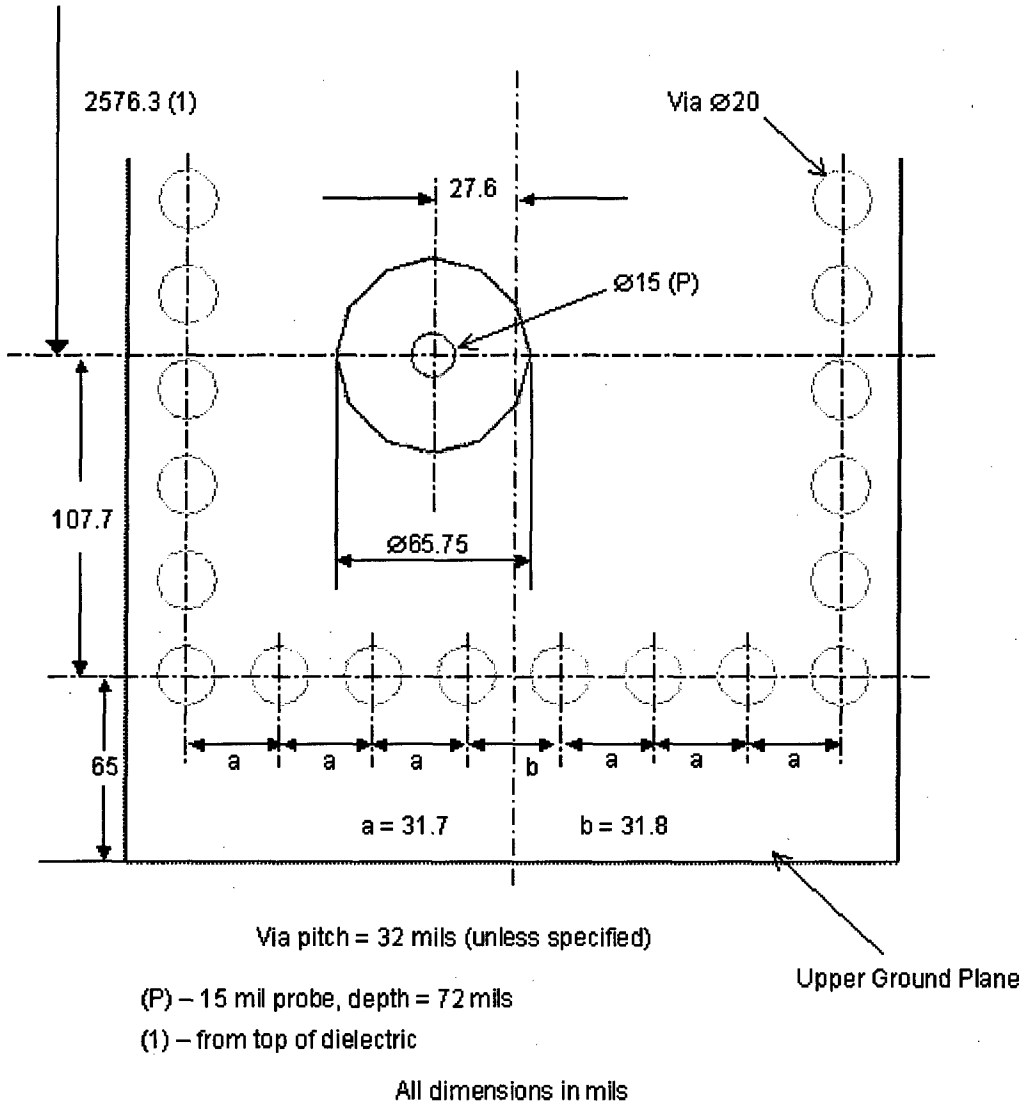

Figure 120. Back Coaxial Transition

List of symbols/abbreviations/acronyms/initialisms

DND	Department of National Defence
RMC	Royal Military College of Canada
3D	Three Dimensional
A	Electric Potential
a	Rectangular Waveguide Width
ADP	Antenna Directivity Pattern
AEHF	Advanced Extremely High Frequency
AGP	Antenna Gain Pattern
b	Rectangular Waveguide Height
$\overline{B}$	Normalized Susceptance
CF	Canadian Forces
CRC	Communication Research Centre
d	Via Pitch (centre to centre)
$D(\phi,\theta)$	Directivity
dB	decibels
DTV	Digital Television
E	Electric field (bold denotes a vector)
EHF	Extremely High Frequency
EM	Electromagnetic

EMT	Electromagnetic Theory
f	Frequency (cycles/second)
F	Magnetic Potential
FEM	Finite Element Method
fm	Fundamental Frequency
GHz	Gigahertz
H	Magnetic Field (bold denotes a vector)
HFSS	High Frequency Structure Simulator
HPBW	Half Power Beamwidth
j	$\sqrt{-1}$
J	Electric Current Density
k	wave number in radians/metre ($k = \omega\sqrt{\mu\varepsilon}$)
LTCC	Low Temperature Co-Fired Ceramic
LWG	Laminated Waveguide
M	Magnetic Current Density
MHz	Megahertz
MIC	Microwave Integrated Circuit
mil	one thousandth of an inch (1 mil = 25.4 □m)
mm	millimetre
MMIC	Monolithic Microwave Integrated Circuit
PCB	Printed Circuit Board
PEC	Perfect Electric Conductor
r	radial distance from source
R_0	Radiation Resistance

RWG	Rectangular Waveguide
S11	reflection coefficient
S21	transmission coefficient
SHF	Super High Frequency
SWR	Standing Wave Ratio
TE	Transverse Electric
TEM	Transverse Electromagnetic
TM	Transverse Magnetic
U (ϕ,θ)	Radiation Intensity
VNA	Vector Network Analyzer
Z	Impedance (Ohms)
Z_0	Characteristic Impedance
Z_l	Load Impedance
Z_{PI}	RWG impedance (power-current formulation)
$\overline{Y}$	Normalized Admittance
$\overline{Z}$	Normalized Impedance

θ	angle measurement from z-axis
ϕ	angle measurement in x-y plane from x-axis
α	attenuation constant in Nepers/metre
$\varnothing$	diameter
Ω	Ohm
μ	permeability
ε	permittivity

β	phase constant in radians/metre
γ	propagation constant ($\gamma=\alpha+j\beta$)
η	intrinsic Impedance
Γ	reflection coefficient
λ_g	guided wavelength
λ_o	wavelength in free space
δ	skin depth
σ	conductivity
ε_r	relative dielectric constant

DOCUMENT CONTROL DATA

(Security classification of title, body of abstract and indexing annotation must be entered when the overall document is classified)

1. ORIGINATOR (the name and address of the organization preparing the document. Organizations for whom the document was prepared, e.g. Establishment sponsoring a contractor's report, or tasking agency, are entered in section 8.)

Defence R&D Canada- Ottawa
Department of National Defence
Ottawa, ON Canada K1A 0Z4

2. SECURITY CLASSIFICATION (overall security classification of the document, including special warning terms if applicable)

UNCLASSIFIED

3. TITLE (the complete document title as indicated on the title page. Its classification should be indicated by the appropriate abbreviation (S,C or U) in parentheses after the title.)

Study of a waveguide antenna implemented in laminated material (U)

4. AUTHORS (Last name, first name, middle initial)

J. O. Litzenberger, M. Clénet, G. A. Morin, Y. M. M. Antar

5. DATE OF PUBLICATION (month and year of publication of document)	6a. NO. OF PAGES (total containing information. Include Annexes, Appendices, etc.)	6b. NO. OF REFS (total cited in document)
December 2002	xiv + 134	37

7. DESCRIPTIVE NOTES (the category of the document, e.g. technical report, technical note or memorandum. If appropriate, enter the type of report, e.g. interim, progress, summary, annual or final. Give the inclusive dates when a specific reporting period is covered.)

DRDC Ottawa Technical Report

8. SPONSORING ACTIVITY (the name of the department project office or laboratory sponsoring the research and development. Include the address.)

9a. PROJECT OR GRANT NO. (if appropriate, the applicable research and development project or grant number under which the document was written. Please specify whether project or grant)	9b. CONTRACT NO. (if appropriate, the applicable number under which the document was written)
5ck18	

10a. ORIGINATOR'S DOCUMENT NUMBER (the official document number by which the document is identified by the originating activity. This number must be unique to this document.)	10b. OTHER DOCUMENT NOS. (Any other numbers which may be assigned this document either by the originator or by the sponsor)
DRDC Ottawa TR 2002-132	

11. DOCUMENT AVAILABILITY (any limitations on further dissemination of the document, other than those imposed by security classification)

(X) Unlimited distribution
( ) Distribution limited to defence departments and defence contractors; further distribution only as approved
( ) Distribution limited to defence departments and Canadian defence contractors; further distribution only as approved
( ) Distribution limited to government departments and agencies; further distribution only as approved
( ) Distribution limited to defence departments; further distribution only as approved
( ) Other (please specify):

12. DOCUMENT ANNOUNCEMENT (any limitation to the bibliographic announcement of this document. This will normally correspond to the Document Availability (11). However, where further distribution (beyond the audience specified in 11) is possible, a wider announcement audience may be selected.)

Full unlimited announcement

13. ABSTRACT (a brief and factual summary of the document. It may also appear elsewhere in the body of the document itself. It is highly desirable that the abstract of classified documents be unclassified. Each paragraph of the abstract shall begin with an indication of the security classification of the information in the paragraph (unless the document itself is unclassified) represented as (S), (C), or (U). It is not necessary to include here abstracts in both official languages unless the text is bilingual).

This document presents the investigation of a novel end-fire antenna implemented in laminated material. This study is related to the development of a phased array for the AEHF Military Satellite Communication Systems. This work includes theoretical analysis, computation of the developed models and measurement of the realised prototypes at 20.7GHz. The antenna element consists of a radiating rectangular waveguide. As a laminated dielectric material, like LTCC material, is supporting the antenna, the vertical walls need to be formed with vias of specific pitch. An effective coaxial-to-waveguide transition has also been developed to feed the radiating element. The results show that this laminated waveguide can be used as an integrated radiating element in the AEHF band for military satellite communications. A five-element array has also been prototyped. Although the results show low mutual coupling between the elements, additional work needs to be carried out to improve the array radiation characteristics.

14. KEYWORDS, DESCRIPTORS or IDENTIFIERS (technically meaningful terms or short phrases that characterize a document and could be helpful in cataloguing the document. They should be selected so that no security classification is required. Identifiers such as equipment model designation, trade name, military project code name, geographic location may also be included. If possible keywords should be selected from a published thesaurus. e.g. Thesaurus of Engineering and Scientific Terms (TEST) and that thesaurus-identified. If it is not possible to select indexing terms which are Unclassified, the classification of each should be indicated as with the title.)

antenna
waveguide
laminated material
multi-layer material
LTCC
array
coaxial-to-waveguide transition